CUMENTATION PAGE

Form Approved OMB No. 0704-0188

1b RESTRICTIVE MARKINGS	
2a. SECURITY CLASSIFICATION AUTH	3. DISTRIBUTION/AVAILABILITY OF REPORT: Approved for public release; distribution unlimited
2b. DECLASSIFICATION/DOWNGRADI SCHEDULE	
4. PERFORMING ORGANIZATION REPO UMBER(S): VPI-AOE-173	5. MONITORING ORGANIZATION REPORT NUMBER(S)

6a. NAME OF PERFORMING ORGANIZATION: Aerospace and Ocean Engineering Department	6b. OFFICE SYMBOL (If applicable)	7a. NAME OF MONITORING ORGANIZATION: Office of Naval Research, Fluid Dynamics Program
6c. ADDRESS (City, State, and ZIP Code): Virginia Polytechnic Institute and State University, Blacksburg, VA. 24061		7b. ADDRESS (City, State, and ZIP Code): 800 N. Quincy St., Arlington, VA 22217
8a. NAME OF FUNDING/SPONSORING ORGANIZATION: Defense Advanced Research Projects Agency	8b. OFFICE SYMBOL (If applicable)	9. PROCUREMENT INSTRUMENT IDENTIFICATION NUMBER: N00014-89-J-1275
8c. ADDRESS (City, State, and ZIP Code): Submarine Technology Program, 1400 Wilson Blvd, Arlington, VA 22209		10. SOURCE OF FUNDING NUMBERS

PROGRAM ELEMENT NO.	PROJECT NO.	TASK NO	WORK UNIT ACCESSION NO

11. TITLE (Include Security Classification)
Measurements of Surface Shear Stresses Under a Three-Dimensional Turbulent Boundary Layer Using Oil-Film Laser Interferometry

12. PERSONAL AUTHOR(S)
K. G. Ailinger and R. L. Simpson

13a. TYPE OF REPORT	13b. TIME COVERED	14. DATE OF REPORT (Year, Month, Day)	15. PAGE COUNT
Technical	FROM 12/1/88 TO 11/30/89	1990 April 1	128

16. SUPPLEMENTARY NOTATION

17. COSATI CODES			18. SUBJECT TERMS (Continue on reverse if necessary and identify by block number)
FIELD	GROUP	SUB-GROUP	Skin friction measurement technique, Three-dimensional boundary layers
13	10	01	
14	02		

19. ABSTRACT (Continue on reverse if necessary and identify by block number)

Measurements of surface shear stress magnitude and direction are reported for a three-dimensional, pressure driven, turbulent boundary layer around a wing body junction. Measurements were made using a dual-beam oil film laser interferometer at 56 locations.

An iterative procedure was developed which increased the precision of the data extracted from the data records. Skin friction directions computed using a least square error fit were compared to angles obtained from surface oil flows, hot wire anemometry, and LDV measurements. Also, the magnitude of the skin friction coefficients were compared to independently obtained skin friction coefficients. The data agreed to within experimental error outside the effects from the vortex legs present along the side of the wing-body. No accurate data was available for quantitative comparison under the effects of the vortex, but the magnitudes followed the qualitative trends expected. This method failed badly in the region of large three-dimensional effects and requires further study in this area of application.

20. DISTRIBUTION/AVAILABILITY OF ABSTRACT	21 ABSTRACT SECURITY CLASSIFICATION
☒ UNCLASSIFIED/UNLIMITED ☐ SAME AS RPT ☐ DTIC USERS	None
22a NAME OF RESPONSIBLE INDIVIDUAL	22b TELEPHONE (Include Area Code) / 22c OFFICE SYMBOL

DD Form 1473, JUN 86 — Previous editions are obsolete

SECURITY CLASSIFICATION OF THIS PAGE
UNCLASSIFIED

Table of Contents

List of Tables

List of Illustrations

Nomenclature

A	Interference signal amplitude
$C(x)$	Product of fringe number and time, $C(x) = N_{eff}t_{eff}$
C_f	Skin friction coefficient, $C_f = \frac{\tau}{q_\infty}$
$C_{x'}$	Skin friction coefficient component in x' direction
$C_{z'}$	Skin friction coefficient component in z' direction
dt	Time origin error
$\frac{\partial p}{\partial x}$	Pressure gradient
e	Error on product of fringe number and time
f	Lens focal length
h	Oil film thickness
h_λ	Change in thickness corresponding to pathlength change of one wavelength
i_i	Data record element
k	Zero crossing number

n_o	Index of refraction in oil
n	Normal coordinate
N	Fringe number
q_∞	Dynamic pressure, $q_\infty = \frac{\rho U_\infty^2}{2}$
Re_θ	Reynolds number based on momentum thickness
s	Streamwise coordinate
t	time
T	Maximum wing thicknes, 7.17cm
T_o	Temperature of air flow
T_{nom}	Nominal temperature for oil viscosity
u	Velocity component in x' direction
u_F	Particle velocity on oil-air interface
U_{ref}	Undisturbed freestream velocity
w	Velocity component in z' direction
x_0	Leading edge of oil film
x	Direction of measurement
x', y', z'	Cartesian coordinates (reference points defined in figure 1)
α	Direction of flow with respect to the x'-axis
α_d	Measurement direction with respect to the x'-axis
α_{vis}	Flow direction measured from oil flow visualization
$\alpha_{w/u}$	Flow direction measured from hot-wire and LDV data
β	Error in oil film leading edge
γ	Angle between measurement direction and flow direction

ε	Pressure gradient correction factor
θ_i	Laser beam incidence angle, in air
θ_o	Laser beam incidence angle, in oil
λ_{air}	Laser wavelength in air
λ_o	Laser wavelength in oil
μ	Oil viscosity
μ_{nom}	Nominal oil viscosity
ρ	Density of air
τ	Shear stress or skin friction at oil-air interface
τ'	Corrected shear stress

Subscripts

0	Relating to the oil film leading edge
1	"Upstream" laser beam location
2	"Downstream" laser beam location
eff	Effective (computed) value
o	Property of the oil
∞	Free stream flow values

1.0 INTRODUCTION

Fluid flowing over a surface creates a shear stress which acts on that surface according to Newton's Law of Viscosity. If this shear stress, referred to as skin friction, is known over the entire surface, it can be integrated over the surface to determine the skin friction component of the total drag acting on that surface. The other major drag component, referred to as pressure drag or form drag, is due to the boundary layer effect on the pressure distribution and also depends on the shape and orientation of a body in a flow.

Due to the importance of skin friction in determining the total drag on such surfaces as aircraft, ship hulls, etc., many methods have been devised to measure this parameter. The most direct method is the floating beam balance which measures the force exerted by the flow over a small area of the test section. However, it is very sensitive to misalignment of the test area with respect to the surrounding surface and to pressure gradients, and is generally complicated, time consuming, and expensive to use. Other methods are based on near-wall velocity-

profile similarity assumptions or property analogies. For example, in the well known "Law of the Wall", the similarity velocity profile scales on the wall shear stress and can be used to determine the skin friction from measured velocity profiles. Similarly, the analogy between heat transfer and skin friction is often exploited to provide a means of measurement using heated metal films. These are just a few of the more popular techniques. All of these methods, however, are either difficult to use, expensive, intrusive, or indirect and depend on assumptions or analogies. Thus, the search continued for a direct, inexpensive, nonintrusive method which can be easily implemented.

Tanner and Blows (1976) developed such a method known as Oil Film Laser Interferometry based on standard oil lubrication theory and laser interferometry. Although the method was both inexpensive and non-intrusive, it was very time consuming. Monson and Higuchi (1981), Monson, Driver, and Szodruch (1981), and Monson (1984) simplified the method and reduced the time necessary to obtain the data. Applying it to a variety of complex flows produced results in good agreement with those obtained by traditional methods. They also developed equations to measure an unknown oil viscosity by using this method with gravity as the only force on the oil. Westphal (1985,1986) further improved the method by automating the data reduction procedure. In addition, he investigated several parameters and set up guidelines for determining bad data records. In subsequent studies, Kim and Settles (1988) applied the method to supersonic flow past a wedge and Cooke (1988) applied the method to three-dimensional flow past a wing-body junction with pressure gradients.

This study continues Cooke's study by employing oil-film laser interferometry to investigate air flow around a wing-body junction and includes an exploration of skin friction behind the tail and in areas around a line of low shear. The wing is composed of a 3:2 elliptical nose and a NACA 0020 tail mounted at zero angle of attack (Figure 1). The momentum thickness Reynolds number for the conditions in this study was $Re_\theta = 6700$ based on the undisturbed freestream velocity $U_{ref} = 27.7 m/s$ and the momentum thickness of the approach boundary layer 15.1cm upstream of the wing leading edge. The surface oil flow visualization in Figure 2 illustrates the primary features of the flowfield. The flow includes a three-dimensional, pressure-driven, turbulent boundary layer, which is symmetric about the wind tunnel centerline, and is dominated by a horseshoe vortex formed around the nose of the wing (Devenport and Simpson, 1988b). This vortex brings high momentum flow down along the side of the wing, into the test wall boundary layer and out away from the model. A line of low shear develops at the outer edge of the horseshoe vortex due to the effect of the upward flow of the vortex at this location (Devenport and Simpson, 1988a). Figure 3 shows the probability density functions of the U component velocity fluctations measured in the vicinity of the vortex upstream of the nose of the wing at $x'/T = -0.20$. The double-peaked probability density functions near the wall indicate that the vortex is subject to intense, large-scale, low-frequency unsteadiness. Exact details of this unsteadiness are currently unknown. This particular flow has been the subject of intense investigation by several researchers at Virginia Polytechnic Institute and State University. Surface pressure

fluctuations, hot wire and laser Doppler anemometer velocity measurements, and flow visualizations have been obtained (Agarwal and Simpson, 1989, Devenport and Simpson, 1988a, 1988b, 1990).

In this thesis, the basic principles of oil lubrication theory and light interference will be discussed as they apply to the measurement of skin friction. An historical development of the oil film laser interferometer technique will follow. The hardware and procedure used in this study will then be discussed, followed by an analysis of the final results and major sources of error. Conclusions and recommendations will then be presented.

2.0 THEORY

Oil-film laser interferometry was developed from two basic principles -- oil lubrication theory and laser interferometry. Both principles were well known and accepted within the scientific community long before Tanner and Blows (1976) combined them to measure skin friction.

Oil lubrication theory states that a thin oil film will flow over a smooth surface under the action of the shear stress created by air flowing over the surface. Squire (1962) developed the basic equations for oil flowing under the action of a shear stress. In a two dimensional, laminar airflow with a constant shear stress and no shear gradients, pressure gradients, or surface curvature, the oil film will assume a linear profile (Figure 4). Starting with Newton's Law of Viscosity

$$\tau = \mu \frac{\partial u}{\partial y} \Big|_{y=0} \tag{1}$$

and noting that, for the linear profile

$$\frac{\partial u}{\partial y} = \frac{u_F - 0}{h - 0} \tag{2}$$

and

$$u_F = \frac{x - x_0}{t} \tag{3}$$

where t is the time it would take an oil particle to travel from x_0 to x at speed u_F, Tanner and Blows (1976) derived the simple relation between the shear stress and the time dependent oil-film thickness at a given location, x, for such a flow

$$\tau = \mu \frac{x - x_0}{h(t,x)t} \tag{4}$$

The measurement location, x, and the oil-film leading edge, x_0, are fixed for a particular run and can be accurately measured. The time of flowing, t, can be measured directly or calculated from the data record; the latter method alleviates several problems and will be discussed later. The oil viscosity as a function of temperature can be obtained from the manufacturer's equation. Thus, if the time dependent oil-film thickness can be accurately determined, the time-averaged shear stress over the area between x and x_0 can be obtained from equation (4).

The time dependent oil film thickness can be measured accurately using a laser interferometer. This is accomplished by directing a laser beam onto an oil film flowing over a partially reflective glass surface as depicted in Figure 5. Part of the laser beam is specularly reflected from the air-oil interface B, resulting in

beam BE, and the remainder of the beam is transmitted into the oil film as beam BC. A similar reaction occurs at the oil-surface interface C, creating beams CD and CJ. At the oil-air interface, part of beam CD is transmitted as beam DF and part is reflected. This process will continue, but due to losses from the multiple reflections, beams other than BE and DF can be neglected. Since BE and DF are parallel and coherent, they interfere with each other, and the resulting interference pattern is detected by the receiving optics. As the oil film thins due to the action of the shear stress acting upon it, the differences in path length between beams BE and DF decrease. This path length difference changes the relative phases of beams BE and DF at parallel wavefronts causing the intensity of the combined beams to vary as a sinusoid with a decaying period (Figure 6). As the oil film continues to thin, the path length difference goes through full interference cycles -- varying from maximum constructive interference through maximum destructive interference and back to maximum constructive interference. This cycle, referred to as one "fringe," corresponds to a change in the path length difference of one laser wavelength. Note that, due to a difference in indices of refraction between the air and the oil, the wavelength of the laser in the oil differs from the wavelength in air according to the relation

$$\lambda_o = \frac{\lambda_{air}}{n_o} \tag{5}$$

When light travelling in a medium with refractive index n_1 encounters an interface with a material of refractive index n_2 where $n_2 < n_1$ both transmission and reflection occur, but the phase of the reflected beam is shifted 180°. If

$n_2 > n_1$, then no phase shift occurs. Note that the phase of the transmitted beam is never shifted, regardless of n_1 and n_2.

None of the reflections which result in beams BE and DF cause a phase change. Therefore, when the difference in path length between beams BE and DF is an integral number of wavelengths, a constructive maximum will occur. The path length difference, Δl, is (refer to Figure 5 for geometry and notation)

$$\Delta l = n_o(BCD) - BI \tag{6}$$

However, ID and BH represent successive positions of the same wavefront (Jenkins and White, 1957). Therefore, the beams HD and BI contain the same number of wavelengths

$$n_o(HD) = BI \tag{7}$$

and the path length difference becomes

$$\Delta l = n_o(BCH) + n_o(HD) - BI = n(BCH) \tag{8}$$

By extending DC until it intersects a vertical line through B, and noting that GC = BC due to equal angles of incidence and reflection at point C, the final form of the path length is

$$\Delta l = n_o(GC + CH) = n_o(GH) = n_o[2h\cos(\theta_o)] \tag{9}$$

As stated previously, a maxima will occur when the path length difference is an integral multiple of wavelengths

$$m\lambda = 2n_o h \cos\theta_o \qquad m = 1,2,3,... \tag{10}$$

Thus, a change in the path length of λ_0 corresponds to a change in oil film thickness of

$$h_\lambda = \frac{\lambda}{2n_o \cos\theta_o} \tag{11}$$

where

$$\theta_o = \sin^{-1}\left[\frac{\sin\theta_i}{n_o}\right] \tag{12}$$

This change in height is referred to as a thickness change of one "fringe." By recording the interference level as a function of time and allowing the oil film to thin to less than one fringe in height, the height of the oil film at any time can be computed by simply counting the fringes backward (peaks labeled as "N =" in Figure 6) beginning with the final fringe, to the desired time. The height of the oil film at that time is simply the number of interference fringes, N (referred to as the fringe number), times the "fringe thickness," h_λ ($h(t_i, x) = h_\lambda N_i$). Thus, the oil lubrication equation becomes

$$\tau = \mu \frac{x - x_0}{h_\lambda N t} \tag{13}$$

Since, h_λ, $x - x_0$, μ, and τ are constant for a given test run, the product of fringe number, N, and time, t, must also be a constant, $C(x)$, at a given location.

$$C(x) = constant = Nt \tag{14}$$

Note that most interferometers reflect one of the interfering beams off of a stationary reference and measure the change in distance of the test surface often to less than one micron. Thus, interferometers are generally very sensitive to vibration of the test surface. However, the system used to measure thinning of an oil film is relatively insensitive to vibrations of the test surface since the interference occurs due to the distance between the oil-air interface and the oil-surface interface. Thus, if the test surface is shifted upward a small amount during vibration, the oil film will also be shifted upward by the same amount. While this changes the actual distance travelled by the laser beams from the laser to the receiving optics, it will not affect the path length difference which is what causes the interference to occur.

3.0 HISTORICAL DEVELOPMENT

The first oil film laser interferometer, designed and built by Tanner and Blows (1976), consisted of a He-Ne laser beam directed through a beamsplitter to create two laser beams a fixed distance apart; this distance was measured directly. A drop of oil was then placed on the test section and the beams were directed onto the test section where the upstream beam was visually positioned at the oil drop's leading edge, x_0. Thus, only the downstream beam was used to measure the thinning of the oil film. For this reason, it is referred to as a single beam system. The photodetector output from the receiving optics was initially monitored on a strip chart recorder, and the positively sloped zero crossings were read off manually to denote the interference fringes. Note that, using the positively sloped zero crossings to identify the fringes yields fringe numbers which will be integers plus 1/4 (i.e. 1.25, 2.25, etc.) as a result of equation (10). Later, an analog fringe-detection circuit and computer were used to identify the zero crossings.

Two separate data reduction methods were applied to this single beam system. First, the oil was allowed to thin to less than one fringe, as mentioned earlier, and an effective time of flowing was computed using a best fit to equation (14). (For clarity, when the time or fringe number is calculated instead of being measured directly, an "eff" subscript will be used to denote an effective quantity as opposed to a measured quantity.) This procedure resulted in very long test runs--some as long as 60 minutes. As an alternative, the time of flowing was referenced to the time the wind tunnel was started, and the effective fringe numbers, N_{eff} were calculated from equation (14). This allowed for shorter test runs since the oil did not have to thin to less than one fringe. However, this method underpredicts the actual time of flowing due to the initial slope of the oil film. This time discrepancy was shown to be $\frac{\mu}{\alpha\tau}$ where α is the initial slope of the oil film leading edge (Tanner and Blows, 1981), and was computed to be typically between 2 seconds and 5 seconds for the specific flow conditions studied.

Tanner's method had several drawbacks that prevented its widespread use. First, it often entailed very long test runs -- especially for low shear flows. Second, visually locating the oil film leading edge was found to be a difficult task in practice and the leading edge was also subject to move slightly due to oil spreading after it had been located with the upstream laser beam and before the wind tunnel was started. Furthermore, the effective flow time of the oil differs from the length of time the wind tunnel is operating due to transient effects and the initial slope of the leading edge of the oil drop.

Monson and Higuchi (1981) were able to eliminate the major problems with Tanner's system by positioning both beams downstream of the leading edge and using both to record data. Monson perpendicularly polarized the two beams and separated the signals they carried with polarizing filters. Since both beams were used to obtain data, this is referred to as a dual-beam system. The time of the signal peaks, instead of the positively sloped zero crossings used by Tanner and Blows (1976), were used to denote the fringe numbers to eliminate difficulties arising from any drift in the mean signal level. Therefore, Monson and Higuchi's fringe numbers were integers. Noting that τ (taken as an average over the area between the two beams), μ, and x_0 are identical for both beams, the leading edge position can be eliminated algebraically by solving one of the following equations for x_0 and substituting it into the other.

$$\tau = \mu \frac{x_1 - x_0}{h_\lambda N_{eff1} t_{eff1}} \tag{15}$$

$$\tau = \mu \frac{x_2 - x_0}{h_\lambda N_{eff2} t_{eff2}} \tag{16}$$

After simplification, Monson's equation for a dual-beam laser interferometer becomes

$$\tau = \mu \frac{x_2 - x_1}{h_\lambda (N_{eff2} t_{eff2} - N_{eff1} t_{eff1})} \tag{17}$$

Thus, the distance between the two laser beams is required, but the leading edge need not be located. Also, Monson ran each individual test run only long enough to identify 20 "good" fringes (smooth, easily identifiable, etc.) on the downstream beam, recording his output on a strip-chart recorder. He then developed equations to calculate the effective time based upon the elapsed time for 20 fringes on the downstream beam to occur, and for the fringe numbers for each beam based on the elapsed time for 10 fringes from each beam to occur (Monson and Higuchi, 1981). This considerably reduced the time necessary to obtain the data, eliminated all the problems related to locating the leading edge of the oil film, and allowed the time origin to be computed without having to let the oil film thin to less than one fringe.

Monson and coworkers applied their dual beam system to a wide variety of flows and derived equations and correction terms for various flow conditions. They showed that if the direction of measurement (denoted by an imaginary line connecting the two laser beams) were different than the actual direction of the skin friction, the interferometer system would measure the component of skin friction in the direction of measurement. In addition, they derived first order correction terms for shear gradients, pressure gradients, linear temperature gradients, and body forces. Up to this point in the development of the Oil Film Laser Interferometer, "bad" data records were rejected subjectively upon visual inspection of the strip-chart recorder output. Uneven signal visibility and obvious noisiness were considered the main reason for rejection of bad data records.

Murphy and Westphal (1985) and Westphal and Bachalo (1986) were the next to improve the system. They obtained a more equal signal visibility between the two beams than Monson by spatially resolving the laser beams. However, Westphal's most important contribution was to automate the data reduction procedure. Instead of using a strip chart recorder, he converted the photodetector output, using an analog-to-digital converter, to a digital signal which was stored directly on a computer hard disk. He wrote FORTRAN routines to identify fringes from the data record and a two-variable least squares error minimization routine to obtain the best fit to equation (14). He defined the effective time and fringe numbers as

$$N_{eff} = N_0 - k \tag{18}$$

$$t_{eff} = t_0 + t_k \tag{19}$$

where k is the chronological fringe number within the data record (see Figure 6), t_k is the time of the k^{th} positively sloped zero crossing referenced to the beginning of the data record, N_0 is a constant to give the actual height, in h_i's, and t_0 is the time origin or effective time of oil flowing. Note that, if transient effects and the initial slope of the oil film leading edge are negligible, t_0 is identical to the time the wind tunnel was started. The error minimization routine iterates on N_0 and t_0 to find the minimum normalized rms error of the constant $C(x)$

$$e = \frac{\sqrt{\overline{(C^2)} - (\overline{C})^2}}{\overline{C}} \tag{20}$$

It is important to note that previously, N_{eff} and t_{eff} were calculated using only two or three distinct, widely spaced fringes. Using the power and speed of the computer, Westphal used all of the fringes to calculate N_{eff} and t_{eff}. In addition, Westphal computed a time origin t_0 from each data record, thus producing two values for the time origin. Since the time origin is a property of the entire oil flow, it is independent of the measurement location (x_1 or x_2). Realizing this, Westphal determined that if the difference exceeded a certain level, then at least one of the data records was "bad." The criterion he established for rejection was

$$dt = \frac{| t_{01} - t_{02} |}{t_{eff}(\text{at k} = 1)} > .02 \qquad (21)$$

Westphal also established a maximum allowable error on the constant $C(x)$ for each beam, defined in equation (20). This criterion limited the error to $e < .004$; if either beam failed to meet this requirement, the data record was considered unacceptable. In practice, he found most good runs to have $e < .003$. These rejection criteria were based upon a maximum allowable error of $\pm$ 5% on the final skin friction result for a single run. This accounted for variations in oil viscosity, beam separation measurements $(x_2 - x_1)$, etc. These criteria will produce a result within a $\pm$ 5% uncertainty only for a two dimensional, laminar flow with no pressure or shear gradients and no gravitational effects such as the flow Westphal studied.

It is important to note here that Westphal (1986) defines the variable λ_o to be one wavelength in the oil (which is correctly defined in equation (5)), but

then gives an equation for a thickness variation (referred to here as h_λ) of the oil film corresponding to a change of one λ_o and uses the same variable name, λ_o, for this change in height. However, his subsequent analysis is consistent with the definition of λ_o as the change in height. For clarity, h_λ is used in this study.

Cooke (1988) applied Oil-Film Laser Interferometry to flow past a wing body junction. He used the programs written by Westphal (1986) combined with a linear pressure gradient correction term developed by Monson, Driver, and Szodruch (1981). He determined the skin friction as if no pressure gradient existed, and then modified the result as follows

$$\tau' = \frac{\tau}{1 - \varepsilon} \tag{22}$$

where

$$\varepsilon = \frac{\lambda N_{effB}}{2n_o \tau \cos \theta_o} \cdot \frac{\partial p}{\partial x} \tag{23}$$

Murphy and Westphal (1985) showed that for sufficiently thin oil films (less than 20 microns), this system would measure the time-averaged shear stress in a three-dimensional flow. For oil films thicker than 20 microns, they showed that surface waves may appear at the oil-air interface depending on the particular flow conditions.

Cooke did not actually measure both the magnitude and direction of this shear stress in his experiments. Instead, he pre-determined the direction of flow from surface oil flow patterns produced by earlier researchers working on the

same flow. Knowing the flow angle, he aligned the laser beams with the direction of flow and measured the skin friction magnitude. He also experimented with various scanning devices which could take data at several closely spaced data points, but did not find an acceptable device. He also experimented with measuring the oil-film thickness from below the test section. This requires the thickness of the glass plate to be measured and subtracted from the thickness measured with the oil on the test section. His final decision was to use a dual-beam system mounted above the test section. The system was placed on a wooden frame which surrounded the wind tunnel but was not in contact with it. This eliminated the possibility of transmitting vibrations from the wind tunnel motor to the interferometer system.

With the exception of Cooke, this method had only been applied to well understood flows such as two-dimensional flows, axisymmetric flows, flows with one-dimensional pressure gradients, etc. Cooke applied this method to a complex three-dimensional flow, but relied upon surface oil flow visualizations to determine the flow angles and then aligned the laser beams with the flow.

For the situation in which the flow angle is unknown, Monson, Driver, and Szodruch (1981) derived an important result for two dimensional flow. Figure 7 illustrates the geometry and notation used to derive the flow angle and shear stress for this situation. For a constant shear stress and constant oil viscosity (i.e. constant temperature), the oil lubrication equations at points (x'_1, z'_1) and (x'_2, z'_2) (refer to Figure 7 for notation and geometry) are

$$\tau = \frac{\mu(s_1 - s_{01})}{h_1 t_1} \tag{24}$$

$$\tau = \frac{\mu(s_2 - s_{02})}{h_2 t_2} \tag{25}$$

Since the flow direction is unknown, the streamwise variables, s_0 , s_1, and s_2 must be solved for in terms of the measurement direction variables x_0, x_1, and x_2

$$s_1 - s_{01} = \frac{x_1 - x_0}{\cos \gamma} \tag{26}$$

$$s_2 - s_{02} = \frac{x_2 - x_0}{\cos \gamma} \tag{27}$$

Substituting into eqautions (21) and (22) and eliminating x_0 as previously done yields

$$\tau = \frac{\mu(x_2 - x_1)}{h_2 t_2 - h_1 t_1} \cdot \frac{1}{\cos \gamma} \tag{28}$$

Thus, the total shear τ is unknown since γ is unknown, but $\tau_x = \tau \cos \gamma$ which gives the final result

$$\tau_x = \frac{\mu(x_2 - x_1)}{h_2 t_2 - h_1 t_1} \tag{29}$$

Thus, oil-film laser interferometry measures the component of the shear stress in the direction of an imaginary line connecting the laser beams on the test surface

(known as the measurement direction). It is very important that the initial line of oil be placed perpendicular to the measurement direction as will be shown in Chapter 7.

In this thesis, measurements were initially taken in the x and $-z$ directions (using the nomenclature of Figure 1) so the measurements in each direction could be combined vectorially to obtain the magnitude and direction of the shear stress at each point. However, when the angle between the flow and the x-axis was less than approximately 20° and the laser interferometer was aligned in the -z direction, the oil did not flow over both data beams (see Figure 8). Therefore, data could not be obtained in the $-z$ direction, and the angles and magnitudes of the actual shear stress could not be determined.

Since both principal axis directions could not be used, measurements were taken in three directions far enough apart to provide acceptable spatial resolution. Data were obtained at 0°, −45°, and −60° with respect to the wind tunnel axis. Note that measurements in only two directions are sufficient to obtain the skin friction magnitude and direction. Measurements in the third direction were included to provide redundancy. The rejection criteria developed by Westphal ($e < .004$) were applied to this data and most good runs were observed to have $e < .003$ for each beam, in agreement with his findings.

4.0 APPARATUS

All the experiments from this study were done in the VPI&SU Low-Speed Boundary-Layer Wind Tunnel (Figure 9). The tunnel is an open circuit tunnel with a rectangular test section 8m long x .91m wide x .26m high (over the central portion). Air is taken into a centrifugal blower through a filter. Upstream of the test section is a fixed-setting damper, a plenum, a honeycomb section, seven screens, and a 4:1 contraction ratio nozzle which leads to the test section. In the absence of the wing, a nearly zero pressure gradient exists in the test section. At the inlet to the test section, the flow is uniform to within .5% in the spanwise direction and 1% in the vertical direction with a .2% turbulence intensity at 27m/s. The flow is tripped as it enters the test section by a .63cm step, and is accelerated to test speed by a further 1.5:1 contraction produced by the shape of the upper wall. The wind tunnel is the same as that used by Cooke (1988).

The upper wall of the wind tunnel is made of plexiglas reinforced with aluminum channel. The side tunnel walls are made of glass and lined internally

with 6.4mm thick plexiglas plates. When the wing is mounted in the test section, the plexiglas liners near the wing are removed to minimize the effects of blockage induced pressure gradients. This effectively widens the test section by 12.7mm in the area between a location 330mm upstream of the leading edge of the wing and 203mm downstream of the trailing edge of the wing. These distances were chosen to make the side walls follow, very approximately, a streamline produced by the wing in an unbounded flow. The corners produced by the removal of the plexiglas liners are taped over adhesive tape to reduce added turbulence and recirculation due to the surface discontinuity. The streamlines followed by the side walls were calculated using two-dimensional potential flow theory.

The floor of the test section is made of 19mm thick fin-form plywood. The area immediately surrounding the permanent wing mount has been cut away so different materials may by used for the actual test surface. The test area inserts used in this study consist of two parts. The first is made of 3/4″ finished plywood secured flush with the surrounding floor by countersunk bolts located at the edges. A cutout section with a 1/2″ lip holds the second piece -- a 1/4″ thick Denton Vacuum MLBS-30 partially reflective glass plate. The glass plate, chosen by Cooke to match the intensity of the interfering beams, has a 30% reflective coating on the test side. Cooke took data only in front of the wing, using the plywood insert shown in Figure 10(a) The present study investigated positions in front, along the side, and behind the wing. Therefore, two additional plywood inserts were constructed, with cutouts as shown in Figures 10(b) and 10(c).

The wing used in this study consists of a 3:2 elliptical nose upstream of the maximum thickness and a NACA 0020 tail. The maximum thickness is 7.17 cm, the chord is 30.48 cm, and the height of the wing is 22.9 cm. This height allowed for a 3.7 cm gap between the top of the wing and the wind tunnel roof to prevent the formation of a junction vortex at the top of the wing. Such a vortex could have interfered with the flow further downstream on the test wall. Sandpaper strips (120 grade) located 10 mm upstream of the maximum thickness ensured a constant turbulence transition point on the wing surface.

The plywood insert and glass plate were secured flush with the surrounding tunnel floor and the wing was bolted to a permanent mount in the tunnel floor. The wing was mounted with its leading edge 1.39m downstream of the tunnel throat and its chord parallel to the tunnel centerline. Small gaps between the inserts and the surrounding floor were covered with Scotch brand "Magic Mending" tape to provide a smooth surface continuity.

A wooden frame was constructed around the wind tunnel to support the laser assembly. On top of this structure, Cooke secured the laser assembly such that it was directly above the test location. In order to provide access to the additional downstream locations investigated in this study, Cooke's structure was extended two and a half feet in the streamwise direction (see Figure 11 for the final structure). With Cooke's setup, the time required to move between locations was about 45 minutes. This large relocation time occurred because the laser assembly had to be physically picked up and moved, carefully re-aligned with the flow direction, and clamped in place. To reduce this relocation time, a movable

platform was mounted on top of the wooden structure on a rail system (Figure 12). The movable platform could slide along the rails in the streamwise (top set of rails) and spanwise (bottom set of rails) directions, thus allowing the laser assembly mounted on top of the movable platform to be relocated without changing the alignment angle. This was done by attaching two parallel metal angles to the bottom of the platform. These angles subsequently fit into an additional set of oppositely oriented angles with the same spacing, forming a set of rails. Another, orthogonally oriented pair of angles was bolted to the bottom of the first set of rails and fit into a pair of angles rigidly mounted atop the wooden frame.

To allow for easy rotation of the laser assembly with respect to the platform, a 1/2″ thick "U-shaped" aluminum piece was attached to the laser assembly base plate. One inch holes were drilled in both the platform and the U-shaped fixture, and a 1″ bolt through both holes firmly attached the laser assembly to the movable platform. The laser beams were aligned with the three different measurement directions in a similar manner. Three 1/4″ holes in the platform, when aligned with a 1/4″ hole in the laser assembly base plate, oriented the laser beams at 0° , 45°, or 60° with respect to the wind tunnel centerline. Wheels mounted to the underside of the laser assembly base plate further simplified the rotation.

The platform was made of 3/4″ birch plywood with a 1/4″ aluminum plate affixed to the corner with a 1″ bolt to provide additional strength. Two 90° arcs cut through the platform and aluminum plate gave the laser beams clear access

to the test section at any angle between 0° and 90° with respect to the tunnel centerline. Figure 13 shows the movable platform mounted on the rail system above the wooden frame. Figure 14 shows the author applying oil to the test surface and depicts the relative positions of the wooden frame, rail system, movable platform, and laser assembly with respect to the wind tunnel.

The basic laser interferometer system used was that developed by Cooke. Figure 15 shows the laser assembly from the side and Figure 16 shows the laser assembly looking down the optical rail axis. Two parallel optical rails were firmly mounted on a common 1/4" aluminum base plate, and all optical components were mounted and aligned on these rails. A Spectra Physics Model 105-1 5 mW He-Ne laser ($\lambda = 6328$Å) was mounted such that lateral and vertical adjustments could easily be made. The laser beam paths shown in Figure 17 are described as follows. The laser beam first passes through a beam expander and focusing assembly consisting of a 20X objective lens and an output lens with a focal length f = 301mm. This assembly is mounted on the same optical rail as the laser beam. The beam is then reflected from a plane mirror, mounted on the same optical rail as the laser, to the beamsplitter, a 6mm thick optical window, which is mounted on the second optical rail. The two beams are then directed down to the test surface via an adjustable plane mirror. Although the beamsplitter creates a pathlength difference which prevents both beams from being simultaneously focused on the test surface, this difference is not crucial. Rather, focal lengths were adjusted such that the laser beams have approximately the same diameter at the test surface -- one focused slightly above the test surface and the other

focused the same distance below it. The returning beams are reflected from a plane mirror similar to the one used for locating the beams on the test surface, and are then re-focused through a convex lens with focal length f = 401mm. These focused beams are split spatially by two plane mirrors mounted 90 degrees apart, and are again reflectd to finally impinge on United Detector Technology silicon PiN-10DP photodiodes operating in photovoltaic mode. The photodiode amplifier circuits were the same as those used by Cooke (1988). The spot size of the laser beams on the photodiodes was controlled by an adjustable iris. The iris opening used in these experiments was approximately 1.5mm to 2mm.

Each photodiode signal was amplified to approximately 2.5 volts and subsequently offset to allow bi-polar analog-to-digital conversion. This offset adjustment was calibrated through use of a voltmeter while in complete darkness (lights and laser turned off). The voltmeter responded too slowly to be useful during data acquisition. A Krohn-Hite model 3202 fourth order Simple RC filter was operated in the low-pass mode at a cutoff frequency of 20 Hz to eliminate noise from vibration of the tunnel motor, etc. The signal was monitored in real time on an oscilloscope; data acquisition was initiated when interference variations were detected. A Data Translation DT 2801-A analog-to-digital converter board installed in an IBM PC XT operating at 10 Hz recorded the digital signal to a computer floppy disk for later analysis. Figure 18 shows a block diagram of the components as they were set up for this study.

The oil used was Dow Corning 200 fluid (manufactured by Dow Corning Corporation, Midland, MI), a 50 centi-Stoke nominal viscosity silicone oil with a

nominal temperature of 25° Celsius. The oil was chosen based on Cooke's recommendation for the shear levels involved. The temperature was monitored from a thermometer attached to the inside of the test section approximately two feet downstream of the tail of the model. The manufacturer's equation for oil viscosity-temperature dependence was used to determine the oil viscosity for each run

$$\mu(T_o) = \frac{\mu_{nom}}{e^{.0146(T_o - T_{nom})}} \tag{30}$$

5.0 PROCEDURE

A transparency with the measurement locations was attached to the bottom of the glass plate to assist in positioning the laser beams in the proper location (Figure 19). The laser beams were positioned such that the measurement location (marked on the transparency) was directly between the two, since the average shear stress between the two beams is actually measured. The laser and the lights were turned off and the zero level for the photodetectors was set to -1.25 volts. The laser was then turned on and fine adjustments were made to the receiving optics alignment.

The beam spacing was then measured directly by placing a piece of paper on the test section and measuring the distance between the upstream edges of the laser beams with a caliper. These measurements were accurate to .05 mm. The beam spacing used in these experiments was 4.35mm. The test section and surrounding area were then cleaned using commercial glass cleaner and lens paper. The oil was kept in a syringe to protect it from dust while still allowing

easy application. The oil was applied from the syringe to the edge of a taped razor blade (the tape was to prevent scratching the reflective surface of the glass plate). The razor blade was then pressed down on the test section between one and two beam spacings ahead of the upstream beam, creating a line of oil perpendicular to the measurement direction. The tunnel was then started. Once the tunnel reached operating conditions, the dynamic pressure ($q_\infty = \frac{1}{2}\rho U_{ref}^2$) was measured using a pitot-static tube mounted in the wind tunnel throat. The temperature was also recorded; it was normally between 24°C and 26°C. When the intensity of the downstream beam, viewed in real time on an oscilloscope, reached a smooth oscillation, the lights in the lab were turned off (to prevent the photodetectors from picking up stray light) and the computer program, OILAD32 (see Appendix A) , which recorded the data to a computer disk was begun. The amount of time between when the tunnel reached the designated dynamic pressure and when the beginning of the data recording was typically between one and two minutes. When the data was finished recording, the lights were turned on and the initial temperature was verified.

Figures 20, 21, 22, and 23 are examples of typical raw data records obtained using this method. Figures 24 and 25 (upstream and downstream data records for the same test run) show an example of a data record that cannot be reduced. The most likely reason for the signal degradation in Figure 25 is that the receiving optics gradually shifted over the test run due to vibration.

6.0 DATA REDUCTION

Several different data reduction methods were tried in searching for the best. The first method was the same as that used by Cooke. Cooke recorded data in a fashion similar to the procedure mentioned previously and used Westphal's data reduction codes, modified to account for the pressure gradient, to reduce the data he obtained. Although the error criterion determined by Westphal produced results within $\pm 5\%$ uncertainty only for his simpler flow, his criteria were also applied to this flow.

The second method used the derivative of the oil film height with respect to time to determine the skin friction since the time rate of change of the oil-film height is the directly measured quantity. Rearranging equation (1) to isolate the height

$$h = \frac{\mu x}{\tau t} \tag{31}$$

and taking the derivative of the oil film height with respect to time yields

$$\frac{\partial h}{\partial t} = -\frac{\mu x}{\tau t^2} \tag{32}$$

Since $\frac{\partial h}{\partial t}$ is inherently negative for an oil film thinning under the action of a shear stress, multiplying through by -1 and taking the logarithm of each side yields a linear equation

$$\log\left(-\frac{\partial h}{\partial t}\right) = \log\left(\frac{\mu x}{\tau}\right) - 2\log(t) \tag{33}$$

$$y = b + mx \tag{34}$$

By evaluating $\frac{\partial h}{\partial t}$ as a backward finite difference and substituting $h = h_i N$, discrete values can be determined for $\log\left(-\frac{\partial h}{\partial t}\right)$ and $\log(t)$. Thus the equation is in the form of a straight line with slope -2. Using a linear least squares fit, the constant term, $\log\left(\frac{\mu x}{\tau}\right) = b$, and the related uncertainties for each beam were determined. The slopes for most data records were between -2 and -2.2. The errors on the constant terms were about 3% on average. Solving for the skin friction and eliminating x_0 as before, the final equation becomes

$$\tau = \mu \frac{[x^2 - 10^{(b1-b2)}x_1]}{10^{b1} - 10^{b2}} \tag{35}$$

The values of the constants $b1$ and $b2$ were fairly close, thus their position in the denominator makes the skin friction very sensitive to these values. In addition, by taking 10 to the power of $b1$ and $b2$, any errors associated with these

constants are increased accordingly and degrade the usefulness of the calculated skin friction. This process results in an unacceptably high uncertainty of as much as 50% on the final result.

The third method was actually a modification of the first method. It was realized that more information could be obtained from each data record. Most notably, the negatively sloped zero crossings were used. These points were not used in the calculation of $C(x)$ and therefore can be used to obtain another value of $C(x)$ and shear stress using data from the same test run. In addition, the data was shifted up by .1 rms of each signal and the positive and negative zero crossings were used to calculate two more values of the shear stress. The data was then shifted down from the original level by .1 rms of each signal and the process was repeated. Thus, it was possible to obtain six values of the skin friction from a single test run, which translated into 18 possible independent values of skin friction at every location, in each of the three directions.

Applying the third method produced large amounts of scatter among the skin friction values. In fact, measurements taken at the same location and in the same direction varied so much that any effort to combine them with measurements in other directions at the same location sometimes resulted in uncertainties on the final values in excess of 100%.

The fourth and final method extended the third method, using another piece of physical information, to reduce the scatter among the skin friction values calculated at a given point in a given direction. In reviewing the output from the reduction program and seeking a method of reducing the uncertainty of the

results, a pattern between the magnitude of the skin friction and the time origin error, dt, within each run was ascertained. Many plots were made of skin friction magnitude versus dt at a given location and angle. Figures 26, 27, and 28 are typical of these plots. The data points from each individual run are connected with straight lines. For the large majority of test runs, the magnitude of the skin friction component is almost a linear function of dt within each run. Different test runs at the same angle do not fit onto the same line, or even necessarily have slopes of the same sign. However, in well over half of the locations viewed, if the lines formed by connecting the values from each test run were extended to $dt = 0$, the values converged.

It was realized that, since the time origin is a property of the particular flow, and therefore independent of x_1 or x_2, the time origin for each beam should be identical. Westphal's program included the option to either input the time origin for each beam, or to allow the program to calculate the time origin for each beam. By varying the number of zeroes used from each beam, it was normally possible to obtain a time origin error within the stated criteria ($dt < .02$). In fact, in most cases, it was possible to obtain dt values less than .01. Once this had been accomplished by interactively iterating on the number of zeroes for each beam, an average of the upstream and downstream beam time origins was input as the time origin for each beam. Thus, the time origin was forced to be the same for each beam and the time origin error was identically zero. This process usually required between 3 and 5 iterations. If the errors on the constants $C(x_1)$ and $C(x_2)$ were still below the acceptable level ($e < .004$), then the skin friction values

computed were used in determining the magnitude and direction of the skin friction at that location. A typical example of this iteration process is shown in Table 1.

The first column of Table 1 gives the number of zeroes used from the upstream beam / downstream beam. The second column shows the skin-friction coefficients obtained in the first reduction iteration. The top line, denoted "0 =", is the reduction using the positive sloped zero crossings. The second line, denoted "M =", is the value obtained by subtracting .1 of the signal rms from the average signal intensity and using the positive sloped zero crossings. The third line, denoted "P =", is the value obtained by adding .1 of the signal rms value to the signal average and using the positive sloped zero crossings. In the next three lines, the first letter again denotes the value used for the signal mean and calculated the skin friction using the negative sloped zero crossings.

In Table 1, part (a), the data records (upstream and downstream beams) were reduced using 20 zero crossings from each beam and the time origins were calculated by the computer to obtain a best fit to equation (14). Note that the lowest value of the skin friction coefficient was .00175 and the highest value was .00187. Also, some of the time origin errors (dt) were above the acceptable limit of .02. Therefore, the data were reduced again using 10 zero crossings on the upstream beam. The output is shown in Table 1, part (b). Again, the computer was allowed to calculate individual time origins for each skin friction coefficient. Reducing the data using these parameters produced time origin errors within the acceptable limits. Therefore, 10 zero crossings were used on the upstream beam

and 20 zero crossings were used on the downstream beam. The time origin was fixed at 75.5 (the average value) for each beam for the final run. Using these parameters produced the output in part (c). Notice that the maximum difference in the skin friction coefficient values for the final run is much less than 1% of the skin friction coefficient. This method increases the precision of the skin friction coefficient, but not necessarily the accuracy. It is possible that another combination of the number of zero crossings used from each beam could also produce an acceptable, but different, skin friction coefficient.

Once all of the individual data records had been reduced with $dt = 0$, factors such as the uncertainty in the angle between the oil-film leading edge and the measurement direction, and the effects of non-zero shear gradients had to be accounted for.

The analysis at the end of Chapter 3, in which equation (29) was developed for unknown flow angles, was based on the perpendicularity of the initial oil line and the measurement direction. Since the oil line was applied to the surface by hand, this angle could not be precisely ensured. The effects of errors in angular position may be determined through an analysis of Figure 29. This figure depicts an oil flow with an unknown direction γ with respect to the measurement direction and an oil line which deviates from being perpendicular to the measurement direction by an angle β. The distance travelled by an oil particle from the leading edge to point x_1 is $s_1 - s_{01}$ and the distance to x_2 is $s_2 - s_{02}$. Thus, the basic shear stress equations are

$$\tau' = \frac{\mu(s_1 - s_{01})}{h_1 t_1} = \frac{\mu[(x_1 - x_0)\cos\gamma + (x_1 - x_0)\sin\gamma\tan(\gamma - \beta)]}{h_1 t_1} \tag{36}$$

$$\tau' = \frac{\mu(s_2 - s_{02})}{h_2 t_2} = \frac{\mu[(x_2 - x_0)\cos\gamma + (x_2 - x_0)\sin\gamma\tan(\gamma - \beta)]}{h_2 t_2} \tag{37}$$

Eliminating x_0 as before and reducing yields

$$\tau' = \frac{\mu(x_2 - x_1)}{h_2 t_2 - h_1 t_1}\left[\frac{1}{1 + \tan\gamma\tan\beta} \cdot \frac{1}{\cos\gamma}\right] \tag{38}$$

and

$$\tau'_x = \tau'\cos\gamma = \tau_x\left[\frac{1}{1 + \tan\gamma\tan\beta}\right] \tag{39}$$

where τ_x is the shear stress component in the measurement direction calculated from equation (17) and τ' is the total shear stress (with correction for angle β).

However, β is an unknown error angle so the total shear stress cannot be computed. The effect of this error factor increases as the angle between the measurement direction and the flow angle, γ increases. When the measurement angle and flow angle coincide ($\gamma = 0$) the error factor is 1.0, and therefore the angle β has no effect. Since this effect was not considered until after the data had been obtained, the uncertainty in the angle β was not minimized. However, under normal conditions (i.e. sitting at a desk), the error in this angle is less than $\pm$ 1° if care is taken. However, for purposes of data reduction, this error was assumed to be less than $\pm$ 3° to account for the limited working space in the wind

tunnel while applying the oil (see Figure 14). The uncertainty due to this angle was included in the data reduction program LS.FOR.

The geometry for the shear gradient analysis (see Figure 7) is similar to that for the misalignment angle, β, analysis. In all previous analyses, the shear stress was assumed to be constant and was denoted simply as τ. Since the shear stress is now assumed to be variable, τ_1 and τ_2 are used to represent the shear stresses at points (s_1, n_1) and (s_2, n_2), respectively.

$$\tau'_1 = \frac{\mu(s_1 - s_{01})}{h_1 t_1} \tag{40}$$

$$\tau'_2 = \frac{\mu(s_2 - s_{02})}{h_2 t_2} \tag{41}$$

Furthermore, expanding the shear stress in a Taylor series about point (s_1, n_1) yields

$$\tau' = \tau'_1 + \frac{\partial \tau}{\partial x'}(x' - x'_1) + \frac{\partial \tau}{\partial z'}(z' - z'_1) + \ldots \tag{42}$$

Keeping only the first order terms, writing the above equation for $\tau(s_2, n_2) = \tau_2$ and substituting for τ_1 and τ_2 from equations (40) and (41) yields

$$\frac{\mu(s_2 - s_{02})}{h_2 t_2} = \frac{\mu(s_1 - s_{01})}{h_1 t_1} + \frac{\partial \tau}{\partial x'}(x'_2 - x'_1) + \frac{\partial \tau}{\partial z'}(z'_2 - z'_1) \tag{43}$$

Making the following geometrical substitutions

$$s_1 - s_{01} = \frac{x_1 - x_0}{\cos \gamma} \tag{44}$$

$$s_2 - s_{02} = \frac{x_2 - x_0}{\cos \gamma} \tag{45}$$

$$x'_2 - x'_1 = (x_2 - x_1) \cos \alpha_d \tag{46}$$

$$z'_2 - z'_1 = (x_2 - x_1) \sin \alpha_d \tag{47}$$

Solving for x_0, substituting into equations (40) and (41), and multiplying each by $\cos \gamma$ to obtain the shear stress component in the direction of measurement x yields

$$\tau'_{1x} = \frac{\mu(x_2 - x_1)}{h_2 t_2 - h_1 t_1} \left[1 - \frac{(h_2 t_2) \cos \gamma}{\mu} \left(\frac{\partial \tau}{\partial x'} \cos \alpha_d + \frac{\partial \tau}{\partial z'} \sin \alpha_d \right) \right] \tag{48}$$

$$\tau'_{2x} = \frac{\mu(x_2 - x_1)}{h_2 t_2 - h_1 t_1} \left[1 - \frac{(h_1 t_1) \cos \gamma}{\mu} \left(\frac{\partial \tau}{\partial x'} \cos \alpha_d + \frac{\partial \tau}{\partial z'} \sin \alpha_d \right) \right] \tag{49}$$

However, the laser beams were positioned such that the data point was midway between the two beams. Thus, since only the linear terms were retained in the Taylor series expansion, the value of the shear stress at the data point is taken as the average of τ_1 and τ_2

$$\tau'_x = \tau_x \left[1 - \frac{h_1 t_1 + h_2 t_2}{2} \frac{\cos \gamma}{\mu} \left(\frac{\partial \tau}{\partial x'} \cos \alpha_d + \frac{\partial \tau}{\partial z'} \sin \alpha_d \right) \right] \tag{50}$$

Rearranging equations (15) and (16) as follows

$$h_1 t_1 = h_\lambda N_{eff1} t_{eff1} = \frac{\mu(x_1 - x_0)}{\tau} \tag{51}$$

$$h_2 t_2 = h_\lambda N_{eff2} t_{eff2} = \frac{\mu(x_2 - x_0)}{\tau} \tag{52}$$

shows that the constants $h_1 t_1$ and $h_2 t_2$ are proportional to the distance from each of the beams to the leading edge of the oil film. Thus, the effects of non-zero shear gradients can be minimized by keeping the distance from the upstream beam to the leading edge $(x_1 - x_0)$ as small as possible. This minimization, however, is limited by the fact that x_1 must be far enough away from x_0 to obtain sufficient fringes for data reduction. Westphal (1986) recommends using at least 10 fringes for the upstream beam calculations. Decreasing the distance between the beams $(x_2 - x_1)$ also reduces the distance between the downstream beam and the oil film leading edge, which reduces the effect of non-zero shear gradients. Therefore, the minimum laser beam separation required to maintain spatial resolution should be used.

If the locations at which data were taken composed an orthogonal grid, the shear gradients could be obtained through an iterative procedure. However, since this was not the case, a method was needed to determine the shear gradients with the given data. Noting that $(\frac{\partial \tau}{\partial x'} \cos \alpha_d + \frac{\partial \tau}{\partial z'} \sin \alpha_d)$ from equation (50) represents the shear gradient in the direction of measurement $(\frac{\partial \tau}{\partial x})$, an approximation of the shear gradient can be obtained from the data records.

Referring to the linear oil-film profile in Figure 4, the following result may be obtained via similar triangles at time t_1

$$\frac{h_2(t_1) - h_1(t_1)}{x_2 - x_1} = \frac{h_2(t_1)}{x_2 - x_0} = \frac{h_1(t_1)}{x_1 - x_0} \tag{53}$$

where h_1 and h_2 are the heights of the oil film at x_1 and x_2 at the same time. The easiest time to determine the height of the oil film is at one of the zero crossings, but the upstream and downstream beams do not cross the zero axis at the same times. Therefore, the height of the upstream beam was determined at one of its zero crossings, and the height of the downstream beam was found by linear interpolation at the same time. Once h_1 and h_2 are known, the distances $x_1 - x_0$ and $x_2 - x_0$ can be determined from equation (53). Thus, the shear at the upstream and downstream locations can be determined as follows

$$\tau_1 = \frac{\mu(x_1 - x_0)}{h_1 t_1} \tag{54}$$

$$\tau_2 = \frac{\mu(x_2 - x_0)}{h_2 t_2} \tag{55}$$

The shear gradient was then taken as

$$\frac{\partial \tau}{\partial x} = \frac{\tau_2 - \tau_1}{x_2 - x_1} \tag{56}$$

Having reduced the individual data records and accounted for uncertainty on these values, the skin friction values that met the error criteria were combined

to give the magnitude and direction using program LS.FOR (Appendix C). Program LS combines the acceptable skin friction measurements in a least square error fit of the data to obtain the x' and z' components of the skin friction coefficient. Each of these skin friction coefficients should satisfy the following equation

$$C_{m,i}(\alpha_{d,i}) = C_{x'} \cos \alpha_{d,i} + C_{z'} \sin \alpha_{d,i} \tag{57}$$

$C_{x'}$ and $C_{z'}$ were subsequently chosen to minimize the square of the errors

$$S = \sum_{i=1}^{9} (C_{m,i} - C_{x'} \cos \alpha_{d,i} - C_{z'} \sin \alpha_{d,i})^2 = minimun. \tag{58}$$

To obtain the values of $C_{x'}$ and $C_{z'}$ which yield a minimum for S, the partial derivatives of S with respect to $C_{x'}$ and $C_{z'}$ were set equal to zero

$$\frac{\partial S}{\partial C_{x'}} = 0 = \sum_{i=1}^{9} (-C_{m,i} \cos \alpha_{d,i} + C_{x'} \cos^2 \alpha_{d,i} + C_{z'} \cos \alpha_{d,i} \sin \alpha_{d,i}) \tag{59}$$

$$\frac{\partial S}{\partial C_{z'}} = 0 = \sum_{i=1}^{9} (-C_{m,i} \sin \alpha_{d,i} + C_{x'} \cos \alpha_{d,i} \sin \alpha_{d,i} + C_{z'} \sin^2 \alpha_{d,i}) \tag{60}$$

With the following definitions

$$A = \sum_{i=1}^{9} \cos^2 \alpha_{d,i} \tag{61}$$

$$B = \sum_{i=1}^{9} \cos \alpha_{d,i} \sin \alpha_{d,i} \tag{62}$$

$$D = \sum_{i=1}^{9} \sin^2 \alpha_{d,i} \tag{63}$$

$$E = \sum_{i=1}^{9} C_{m,i} \cos \alpha_{d,i} \tag{64}$$

$$F = \sum_{i=1}^{9} C_{m,i} \sin \alpha_{d,i} \tag{65}$$

these equations may be written in matrix notation

$$\begin{bmatrix} A & B \\ B & C \end{bmatrix} \begin{Bmatrix} C_{x'} \\ C_{z'} \end{Bmatrix} = \begin{Bmatrix} E \\ F \end{Bmatrix} \tag{66}$$

The values of $C_{x'}$ and $C_{z'}$ which best fit the data $C_{m,i}$ are then given by

$$C_{x'} = \frac{DE - BF}{AD - B^2} \tag{67}$$

$$C_{z'} = \frac{AF - BE}{AD - B^2} \tag{68}$$

These components were then combined to give the magnitude and direction of the skin friction coefficient

$$C_f = \sqrt{C_{x'}^2 + C_{z'}^2} \tag{69}$$

$$\alpha = \tan^{-1}\left(\frac{C_{z'}}{C_{x'}}\right) \tag{70}$$

6.1 *Uncertainty Analysis*

Program LS averaged all six values from a single run together and computed 95% uncertainty bounds on the averaged value from each run. Thus, for the general case in which there were three test runs taken in each of the three measurement directions, LS first computed nine skin friction coefficients along with their uncertainties. Then the uncertainty in each measurement due to the leading edge perturbation angle β was added to the original uncertainty by taking the square root of the sum of the squares. This produced nine skin friction coefficients and their related uncertainties -- C_{m_i} and δC_{m_i}, $i = 1,2,...,9$. The least squares fit was

then performed as described above to obtain $C_{x'}$ and $C_{z'}$. These values were considered the "baseline" values.

To determine the uncertainty in $C_{x'}$ and $C_{z'}$ due to each of the individual measurements, the first value was perturbed by an amount equal to its uncertainty

$$C'_{m,1} = C_{m,1} + \delta C_{m,1} \tag{71}$$

and the least square error fit was performed again. The differences between the $C_{x'}$ and $C_{z'}$ obtained from the perturbed calculation and the baseline case were taken as the uncertainties in $C_{x'}$ and $C_{z'}$ due to the uncertainty in the first measured skin friction coefficient $C_{m,1}$. Each of the remaining eight values were similarly perturbed to obtain the uncertainties in $C_{x'}$ and $C_{z'}$ due to the uncertainty in each of the original values $C_{m,i}$ These nine uncertainties were then combined with the least square error S, by taking the square root of the sum of the squares to produce the final uncertainties on $C_{x'}$ and $C_{z'}$ of $\delta C_{x'}$ and $\delta C_{z'}$, respectively. For comparisons in Table 2, the magnitude and angle were necessary, and thus the uncertainties needed to be expressed in terms of the magnitude and angle. Therefore, $\delta C_{x'}$ and $\delta C_{z'}$ were combined as follows to obtain δC_f and $\delta\alpha$

$$\delta C_f = \sqrt{\left(\frac{\partial C_f}{\partial C_{x'}}\right)^2 (\delta C_{x'})^2 + \left(\frac{\partial C_f}{\partial C_{z'}}\right)^2 (\delta C_{z'})^2} \tag{72}$$

where

$$\frac{\partial C_f}{\partial C_{x'}} = \frac{C_{x'}}{\sqrt{C_{x'}^2 + C_{z'}^2}} \tag{73}$$

from equation (69), and

$$\frac{\partial C_f}{\partial C_{z'}} = \frac{C_{z'}}{\sqrt{C_{x'}^2 + C_{z'}^2}} \tag{74}$$

from equation (69)

$$\delta\alpha = \sqrt{\left(\frac{\partial \alpha}{\partial C_{x'}}\right)^2 (\delta C_{x'})^2 + \left(\frac{\partial \alpha}{\partial C_{z'}}\right)^2 (\delta C_{z'})^2} \tag{75}$$

where

$$\frac{\partial \alpha}{\partial C_{x'}} = \frac{-C_{z'}}{C_{x'}^2 + C_{z'}^2} \tag{76}$$

from equation (70), and

$$\frac{\partial \alpha}{\partial C_{z'}} = \frac{C_{x'}}{C_{x'}^2 + C_{z'}^2} \tag{77}$$

from equation (70).

6.2 *Curve fitting method*

An alternative method for reducing the data was developed based on curve fitting the entire data record. This method uses every element in the data record, instead of only using the zero-crossings or signal peaks, to obtain the skin friction. Knowing that the intensity of the returning laser beams varies sinusoidally as a function of the oil film height and that a change in height of h_λ corresponds to one period, the intensity may be written as

$$i_i = A \sin\left(\frac{2\pi h}{\lambda} + \phi \right) \tag{78}$$

where A is the amplitude of the signal. As $t \to \infty$, $h \to 0$, and $\frac{i_i}{A} \to 1$. Thus, $\phi = \frac{\pi}{2}$ and the expression for the intensity becomes

$$\frac{i_i}{A} = \cos\left(\frac{2\pi h}{h_\lambda} \right) \tag{79}$$

Solving equation (4) for h and substituting yields

$$\frac{i_i}{A} = \cos\left(\frac{2\pi k}{t} \right) \tag{80}$$

where

$$k = \frac{\mu(x - x_0)}{\tau t} \tag{81}$$

The constant k cannot be found by simply solving equation (80) for k and evaluating the expression for all $\frac{i_i}{A}$ since $\cos^{-1}\left(\frac{i_i}{A}\right)$ oscillates between -1 and 1 while t increases continually. Multiple values of k yield the same value of $\frac{i_i}{A}$ in equation (80) since cosine is a multiple-valued inverse function. Thus, it is necessary to add 2π to the value of k for each successive period. In addition, unless the oil is allowed to thin to less than one fringe in height, the multiple of 2π to be added is unknown. After careful inspection of this phenomenon, the following equation was derived which can be iteratively solved for k

$$k = \frac{t}{2\pi} S\left[\cos^{-1}\left(\frac{i_i}{A}\right) + 2\pi SP\right] \tag{82}$$

where

$$S = \begin{cases} +1 \text{ for } & m < \frac{k}{t} < m + \frac{1}{2} \\ -1 \text{ for } & m + \frac{1}{2} < \frac{k}{t} < m + 1 \end{cases} \tag{83}$$

and

$$P = \text{ integer portion of } \left(\frac{\frac{2k}{t} + 1}{2}\right) \tag{84}$$

The value of S may be represented analytically by

$$S = \frac{\sin\left(\frac{2\pi k}{t}\right)}{\left|\sin\left(\frac{2\pi k}{t}\right)\right|} \tag{85}$$

The iteration on equation (82) is a two variable iteration (on k and t_0 since the time t in equation (82) is referenced to the time origin t_0

However, the current method uses only the data elements at the zero crossings to determine the skin friction component from each data record. This results in using only 20 or 30 data elements of the 4000 recorded. Since the curve fitting procedure uses every data element recorded, it is likely to reduce the total number of data elements necessary and thereby reduce the amount of time necessary to record data.

7.0 DISCUSSION

The locations at which data were obtained fall into six basic groups plus a few miscellaneous points. Four of the groups, consisting of points 10-17, 20-27, 31-38, and 41-49, were arranged such that all the points within a group are located on a line extending away from the wing-body. The lowest numbered data point in each of these groups was furthest away from the wing body, and the rest count inward toward the wing-body. Points 1-9 and 61-66 were located in the nose region and are all located outside the line of low shear. Points 51 and 52 were located far from the wing-body along the side. Most of the remaining data points were located in the plane of symmetry of the wing-body.

Skin friction coefficient vectors measured at the various positions in the wing-body junction flow are plotted in Figures 30 and 31, and are presented in tabular form in Table 2. The first three columns of Table 2 contain data location information -- identification number, and the x', z' coordinates non-dimensionalized by the maximum wing thickness T. The next two columns,

labeled C_f and α, contain the magnitude and direction of the skin-friction coefficients obtained using the oil film interferometry method discussed in the previous chapter. The initial height of the oil films ($h = h_\lambda N_{0,2}$) used in this study were between $10\mu m$ and $20\mu m$.

The column labeled α_{vis} contains flow directions which were measured directly from TiO_2-Kerosene surface oil flow visualizations similar to that represented in Figure 2. To obtain these angles, a tangent was drawn to the oil streaks at the point of interest, and the angle of the tangent with respect to the tunnel centerline was measured. These angles could only be determined to within $\pm 3°$ in most locations with significantly higher uncertainties ($\pm 10°$) in the nose region (points 13-17). The angles measured from the surface oil flow visualization agree to within the experimental error of the angles measured using the Oil-Film Laser Interferometry technique in other areas away from the line of low shear. Near the line of low shear, the angles show the greatest disagreement. The heights of the oil films used in these flows were less than 20 μm. However, the oil used in the surface oil flow visualization was several times thicker, and varied in thickness inversely with the shear. Thus, these angles are more likely to be affected by pressure gradients.

The column labeled $C_{f_{log}}$ contains skin friction values at most of the locations examined in this thesis. These skin friction values were obtained by fitting the semi-logarithmic region of mean velocity profiles (measured using a laser anemometer) to the log law for equilibrium boundary layers (Devenport and Simpson, 1989) according to the equation

$$u+ = 2.5 \log_e y+ + 5.2 \tag{86}$$

where $y+ = \frac{yu_\tau}{\nu}$, $u_\tau = \sqrt{\frac{\tau_w}{\rho}}$, and $u+$ was taken to be $\frac{\sqrt{u^2 + w^2}}{u_\tau}$. However, since the log law is a two-dimensional formulation, this method was not expected to yield reliable values of C_f under the vortex legs, but provide a qualitative basis for comparison.

The skin friction coefficients obtained by fitting the semi-log region and those obtained by oil film interferometry are plotted as a function of ID number for comparison in Figure 32. In the region in front of the nose, both sets of skin friction coefficients exhibited the same trend, although the $C_{f\log}$ values exhibit much greater fluctuations. Near the maximum wing thickness, the trends are also alike, C_f increases as the wing is approached, with a drop in the magnitude near the line of low shear (located in the proximity of points 23 and 24). In this area, however, the values of $C_{f\log}$ are much higher than those measured using oil film interferometry. In the regions along the side and rear of the wing, the trends are again similar, and the discrepancy between the magnitudes decreases with distance downstream. Notice that these discrepancies between C_f and $C_{f\log}$ increase rapidly inside the line of separation. This trend is expected since the log law is not expected to hold under the vortex leg. Furthermore, it the differences between the two methods is smaller downstream, where the vortex strength has decreased, than upstream.

The close agreement away from the vortex, adds credence to both methods for such a flow. However, since the $C_{f\log}$ values can only be considered as a qualitative guide under the vortex, the similar trends exhibited by the C_f and the $C_{f\log}$ methods is encouraging. Sources of error due to three-dimensional effects will be discussed later in this chapter.

The column labeled $\alpha_{w/u}$ contains flow angles obtained by combining x' and z' velocity components which were measured by hot-wire anemometry (points 1-9) and laser Doppler velocimetry (points 10-27 and 61-66). The angles for points 10-27 were computed from the following equation

$$\alpha_{w/u} = \tan^{-1}\left(\frac{w}{u}\right) \tag{87}$$

The angles for points 61-66 were measured by Olcmen (1990) in a similar manner. Velocity component data were not available at other locations in the flow. The height at which the velocity components were measured at each location are presented in the final column, labeled $h_{w/u}$. The angles given at locations 1 and 2 are somewhere in the peak between the two legs of a Johnston (1960) hodograph plot. Therefore, the actual angles at these locations are at least as large as those given in Table 2, and probably slightly larger. The rest of the $\alpha_{w/u}$ data were located on the near-wall leg of the Hodograph plot and can therefore be considered accurate as near the wall as is known. Uncertainties were available only for points 61-66, and tend to be very large near the wall (characteristic of LDV angle measurements near the wall). At points 61-66, the LDV angles and the oil-film interferometry angles agreed to within the

experimental uncertainties given. The velocity-component angles and the laser interferometry angles follow the same general trend -- increasing as the flow approaches the wing, attaining a maximum near points 10-17, and decreasing around the side of the wing, as expected. However, the oil film interferometry angles exhibited much larger variations than the velocity component angles. However, as noted previously, as the wall is approached, the uncertainties in the LDV angles becomes very large -- even at 150 μm . No angles were available for comparison with the oil-film interferometry angles which were measured at the same height.

At several points in the flow (marked with a D in Table 1), data could not be obtained. A separation point exists along the centerline at $x'/T = -.47$. Points 29 and 30 are between this point and the model nose. In this region, the direction of flow is from the nose towards the separation point, and the flow direction changes rapidly away from the centerline (Figure 33). As a result, the oil does not flow over both of the laser beams. The situation could be remedied by significantly decreasing the beam separation. Points 39 and 40 are located behind the tail of the model. In this region, the oil was observed to diverge from the tunnel centerline (Figure 34). This divergence likewise prevented data from being obtained in this region since the oil did not flow over both of the laser beams.

At points marked with an A, B, or C in Table 1, data could not be obtained in one of the three directions of measurement. This occurred when the angle of measurement was nearly normal to the measurement direction, as

depicted in Figure 8. This data loss was not critical, but the uncertainties quoted are questionable since the largest source of uncertainty was normally the error of resulting from the least squares fit.

Three dimensional effects are illustrated in Figure 30. Note that downstream of the maximum wing thickness the flow speed and direction vary gradually. The exception to this is the data point furthest downstream and closest to the tunnel centerline (point 33). At this location, the flow diverges sharply from the centerline creating large shear gradients. At points upstream of and near the maximum wing thickness three-dimensional effects are larger due to the flow acceleration around the wing and are very significant close to the wing (points 13-17). effects. The flow angles change significantly over the distance between the laser beams, and the streamline radii of curvature are on the order of the distance between the laser beams. Since the laser beams were positioned such that the measurement location was located midway between the laser beams, the laser beams impinged on the test surface at different locations when aligned in each of the three measurement directions. The flow varied significantly over the distance between the laser beams. Therefore, skin friction measurements in the different directions (0°, −45°, and −60°) were measuring skin friction in significantly different flows. Attempts to combine these data produced absurd results. The angles predicted from the oil interferometer reduction method for points 13-17 were between 0° and 25° although the actual oil pattern was observed after the test runs to be approximately 50° to 60° .

Another possible source of error is the variation in thickness of the initial oil line. In all of the previous analyses, it was assumed that the initial oil line was of uniform thickness, and that as the oil thinned, lines parallel to the oil film leading edge were also of uniform thickness. If one end of the initial oil line is thicker than the other end (as shown in Figure 35) and the angle γ between the measurement direction and the flow angle is significant, the initial conditions along the oil film leading edge are not identical. Therefore, x_0 cannot be assumed identical for each of the laser beams and cannot be eliminated from the oil lubrication equations. However, during and after test runs in which the initial oil line was observed to have uneven thickness, fringes of constant thickness, visible in white light, were qualitatively observed to be very close to parallel to the oil film leading edge by the time the oil thinned enough to begin obtaining data. Thus, this non-uniform oil thickness was observed to be a transient effect which subsides quickly.

The pressure gradients encountered in this flow were found to have minimal effects on the oil-film interferometry method used. The largest pressure gradient effects occurred in the region near points 13-17. When the pressure gradient correction term was included for these points, the skin friction value produced from a given test run differed only in the fifth significant digit. Therefore, the pressure gradient effects were not included in the reduction of the remaining points.

The error induced by the unknown leading edge angle, β was on the order of 3% to 5% on the individual test runs. The least square error fitting procedure

tended to minimize this effect so that the uncertainty in β of $\pm 3°$ had little effect on the final results. The largest source of error was normally the disagreement between measurements in the three different directions when combined in the least square error fit.

8.0 CONCLUSIONS

In this study, improvements were made to the basic dual beam oil film laser interferometer system which increased the ease of applicability and decreased the uncertainty of the final results for a three-dimensional flow. This improved system was used to produce skin friction coefficients around a wing-body (hull-appendage) junction. In the course of this investigation, limitations of this system were encountered and methods for minimizing these limitations were discussed.

The laser assembly was secured in one of three pre-set directions atop a movable platform which in turn, was mounted on a perpendicular set of rails. This mounting decreased the time required to re-locate the laser assembly at new data point from 45 minutes to less than 5 minutes. In addition, an iterative procedure for accurately determining the time origin for each oil flow was developed.

The current interferometer system was not able to obtain data in the centerline of the wake or in front of the wing's leading edge due to the flow patterns. In addition, this method produced very poor results (angles off by more than 40° at some locations) in the presence of large three-dimensional effects.

It was not possible to make direct comparisons to vouch for the validity of these results. The intent of this study was not to confirm other results, but to produce needed skin friction values in a complex flow. It was possible to obtain flow angles from surface oil flow visualizations, hot wire data, and LDV data and compare these angles to the angles computed for the skin friction coefficients. The angles computed in this study agreed well with angles from the other methods in areas in which the flow was nearly two-dimensional. In areas where large three-dimensional effects were present, all of the angles generally disagreed with each other since all the angles were measured at different heights in the flow and the flow angle varies rapidly near the wall in these regions.

Skin friction data were available at some locations in the flow, was not quantitatively correct under the vortex, and the data inside the line of separation could only be considered qualitatively. Away from the line of separation, the values produced by the two methods agreed to within experimental uncertainty.

Significant improvements in the current system could be obtained by reducing the beam spacing $(x_2 - x_1)$ and the distance to the leading edge of the oil film $(x_1 - x_0)$. These distances, to a large extent, determine the applicability of the method to the flow. If the flow changes significantly over these distances, then the method will not work. Thus, reducing these distances will increase the

complexity of the flow that can be studied using oil-film laser interferometry. Furthermore, since this system measures the average shear stress over the area between the beams, reducing $(x_2 - x_1)$ will make the final result approach the actual point value more closely.

The author has several general suggestions for increasing the performance of the present system for application to very complex flows, such as the one in the present study. Some method or mechanical device to increase the accuracy of the angle of the initial oil line will reduce the error due to this effect. Although this effect was generally very small compared to the other errors involved, in order to obtain very low uncertainty data, this effect can be greatly reduced if considered beforehand. Also, since knowledge of the shear gradient is necessary, taking measurements on an orthogonal grid may prove useful. Furthermore, a method to make fine adjustments of the movable platform would be helpful, and a more solid support structure than the wooden frame used in this study should be constructed.

In further studies, closer investigation of the curve fitting method of data reduction should have high priority. The reduction in time necessary to obtain enough data for data reduction could potentially be as significant as the reduction in time which occurred in moving from a single beam method to a dual beam method. Also, especially important if the curve fitting method is used, the photodetectors should be operated in the photoconductive mode instead of the photovoltaic mode since the photovoltaic mode may distort the shape of the interference signal.

Bibliography

Agarwal, N. K., and Simpson, R. L. (1989): "A New Technique for Obtaining the Turbulent Pressure Spectrum from the Surface Pressure Spectrum," Journal of Sound and Vibration, vol. 135, pp. 346-350.

Ahn, S. (1986): "Some Unsteady Features of Turbulent-Boundary Layers," M.S. Thesis, Dept. of Aerospace Engineering, Virginia Polytechnic Institute and State University, Blacksburg, VA.

Cooke, I. O. (1988): "Skin Friction Measurements Around a Wing-Body Junction using Oil Film Laser Interferometry," M.S. Thesis, Department of Aerospace and Ocean Engineering, Virginia Polytechnic Institute and State University, Blacksburg, VA.

Devenport, W. J., Agarwal, N. K., Dewitz, M. B., Simpson, R. L., and Poddar, K., (1989): "An Experimental Study of Devices for Controlling the Flow Past a Wing-Body Junction," Report AERO-162, Department of Aerospace and Ocean Engineering, Virginia Polytechnic Institute and State University, Blacksburg, VA.

Devenport, W. J., and Simpson, R. L. (1990): "Time-dependent and Time-averaged Turbulence Structure near the nose of a Wing-Body Junction," Journal of Fluid Mechanics, vol. 210, pp. 23-55.

Devenport, W. J., and Simpson, R. L. (1988a): "Time Dependent Structure in Wing-Body Junction Flows," Turbulent Shear Flows, vol. 6, pp. 232-248.

Devenport, W. J., and Simpson, R. L. (1988b): "LDV Measurements in the Flow past a Wing-Body Junction," Fourth International Symposium on Applications of Laser Anemometry to Fluid Mechanics, Lisbon, Portugal.

Jenkins, F. A., and White, H. E. (1957): Fundamentals of Optics, third edition, McGraw-Hill Book Company, Inc., pp. 261-265.

Johnston, J. P. (1960): "On the Three-Dimensional Turbulent Boundary Layer Generated by Secondary Flow," Journal of Basic Engineering, vol. 82, pp. 233-248.

Kim, K. S., and Settles, G. S. (1988): "Skin Friction Measurements by Laser Interferometry in Swept Shock Wave/ Turbulent Boundary-Layer Interactions," AIAA 26th Aerospace Sciences Meeting, January 11-14.

Monson, J. D., Driver, D. M., and Szodruch, J. (1981): "Application of a Laser Interferometer Skin-Friction Meter in Complex Flows," ICIASF '81 Record, pp 232-243.

Monson, J. D., and Higuchi, H. (1981): "Skin Friction Measurements by a Dual-Laser-Beam Interferometer Technique, AIAA Journal, vol. 19, no. 6, pp. 739-744.

Murphy, J. D., and Westphal, R. V. (1985): "The Laser Interferometer Skin Friction Meter: A Numerical and Experimental Study," Proceeding, 3rd Symposium on Numerical and Physical Aspects of Aerodynamic Flows, Long Beach, VA. Olcmen, S. (1990): "Experimental Study of Three-Dimensional *Turbulent, Pressure Driven Boundary Layers,"* PhD. Dissertation, Department of Aerospace and Ocean Engineering, Virginia Polytechnic Institute and State University, Blacksburg, VA, Figure 62.

Squire, L. C. (1962): "In Flow Visualization in Wind Tunnels using Indicators," AGARDograph, vol. 70, pp 7-55.

Tanner, L. H., and Blows, L. G. (1976): "A Study of the Motion of Oil Films on Surfaces in Air Flow, with Application to the Measurement of Skin Friction," Journal of Physics, E.: Scientific Instruments, vol. 9, no. 3, pp. 194-202.

Westphal, R. V., Bachalo, W. D., and Houser, M. H. (1986): "Improved Skin Friction Interferometer," NASA TM-88216, NASA Ames Research Center, Moffet Field, CA

Table 1. Sample data reduction output

Part (a): First reduction iteration

N_1/N_2			C_f	$e(x_1)$	$e(x_2)$	dt
20/20	0	=	.00176	.00246	.00293	.01155
20/20	M	=	.00176	.00247	.00298	.01124
20/20	P	=	.00175	.00249	.00302	.00954
20/20	0NEG	=	.00185	.00247	.00331	.03068
20/20	MNEG	=	.00185	.00199	.00323	.02974
20/20	PNEG	=	.00187	.00202	.00328	.03404

Part (b): Second reduction iteration

N_1/N_2			C_f	$e(x_1)$	$e(x_2)$	dt
10/20	0	=	.00169	.00259	.00293	.01135
10/20	M	=	.00169	.00272	.00298	.01168
10/20	P	=	.00169	.00252	.00302	.01139
10/20	0NEG	=	.00180	.00186	.00331	.00848
10/20	MNEG	=	.00178	.00197	.00323	.00523
10/20	PNEG	=	.00183	.00180	.00328	.01417

Part (c): Final reduction iteration (dt = 0)

N_1/N_2			C_f	$e(x_1)$	$e(x_2)$	dt
10/20	0	=	.00176	.00256	.00317	.00000
10/20	M	=	.00176	.00268	.00321	.00000
10/20	P	=	.00176	.00251	.00329	.00000
10/20	0NEG	=	.00176	.00197	.00327	.00000
10/20	MNEG	=	.00176	.00201	.00320	.00000
10/20	PNEG	=	.00176	.00203	.00323	.00000

Table 2. Skin friction coefficients and comparisons

ID #	X/T	Z/T	C_f	α	$\alpha_{s/s}$	$C_{f_{log}}$	$\alpha_{w/a}$	$h_{w/a}$, μm
1	-1.03000	-0.25000	0.00141 ± 9.1%	-16.2 ° ± 2.5 °	-18°	.0016	-9.3°	255
2	-1.03000	-0.50000	0.00167 ± 5.7%	-19.8 ° ± 2.0 °	-23°	.0017	-14.2°	255
3	-0.66670	-0.50000	0.00191 ± 5.2%	-55.4 ° ± 2.7 °	-36°	.00155	-29.6°	280
4	-0.66670	-0.75000	0.00222 ± 7.9%	-39.1 ° ± 4.4 °	-34°	.00195	-26.2°	230
5	-0.32900	-1.01100	0.00287 ± 2.7%	-26.9 ° ± 1.4 °	-31°	.0036	-27.3°	255
6	0.00900	-0.87900	0.00388 ± 3.1%	-16.1 ° ± 1.3 °	-32°	.0042	-31.8°	205
7	0.02800	-1.13200	0.00357 ± 3.7%	-13.3 ° ± 1.5 °	-23°	.0039	-24.1°	255
8	0.36100	-0.98700	0.00444 ± 4.7%	-0.8 ° ± 1.5 °	-7°	.0051	-22.6°	230
9	0.36500	-1.24400	0.00371 ± 2.0%	-4.7 ° ± 1.6 °	-10°	.0050	-17.8°	255
10	-0.45781	-0.88723	0.00259 ± 4.4%	-33.2 ° ± 2.2 °	-34°	.0024	-36.3°	100
11	-0.30802	-0.75470	0.00283 ± 6.0%	-49.1 ° ± 3.4 °	-44°	.00265	-50.7°	100
12	-0.19568	-0.65531	0.00339 ± 4.6%	-56.8 ° ± 2.6 °	-46°	.0028	-52.2°	255
13A	-0.12078	-0.58905	0.00547 ± 9.3%	-10.8 ° ± 4.4 °		.0021	-59.3°	330
14A	-0.08333	-0.55592	0.00605 ±13.2%	-16.8 ° ± 6.7 °		.0025	-57.5°	255
15A	-0.04588	-0.52279				.0042	-63.0°	560
16A	-0.00843	-0.48965	0.00814 ±16.6%	0.5 ° ± 7.2 °		.0058	-69.0°	430
17A	0.02900	-0.45652	0.01046 ± 7.0%	-25.8 ° ± 3.5 °		.0078	-72.6°	90
18A	0.06646	-0.42339						
19	OMITTED							
20	0.75000	-1.32500	0.00382 ± 8.3%	-3.2 ° ± 0.7 °	-2°	.0045	-3.9°	180
21	0.75000	1.17500	0.00401 ± 5.4%	-2.0 ° ± 5.4 °	-1°	.0048	-6.9°	255
22	0.75000	-1.07500	0.00437 ± 5.4%	2.3 ° ± 1.9 °	-2°	.0055	-6.5°	255
23	0.75000	-1.00000	0.00468 ± 4.4%	-0.4 ° ± 1.5 °	-7°	.0050	-11.3°	380
24B	0.75000	-0.92500	0.00390 ± 2.5%	-8.3 ° ± 1.6 °	-10°	.0060	-15.0°	255
25	0.75000	-0.85000	0.00532 ± 9.4%	5.5 ° ± 2.1 °	-21°	.0078	-21.9°	330
26	0.75000	-0.77500	0.00702 ± 6.2%	-14.9 ° ± 2.1 °	-16°	.0098	-19.9°	330
27	0.75000	-0.70000	0.00740 ± 6.6%	-24.9 ° ± 2.6 °	-10°	.0100	-16.7°	255
28D	-0.86000	0.00000						
29D	-0.30000	0.00000						
30D	-0.20000	0.00000						
31	4.46100	-1.20000	0.00181 ± 6.9%	4.9 ° ± 1.8 °	-2°	.0018		
32	4.46100	-1.00000	0.00160 ± 6.1%	5.3 ° ± 2.0 °	-4°	.0017		
33	4.46100	-0.80000	0.00250 ± 2.8%	0.4 ° ± 1.7 °	-6°	.0026		
34	4.46100	-0.60000	0.00286 ± 3.3%	-5.6 ° ± 1.6 °	-7°	.0028		
35	4.46100	-0.50000	0.00292 ± 4.5%	-3.8 ° ± 1.6 °	-7°	.0028		

A - No data in 0 ° direction
B - No data in 60 ° direction
C - No data in 45 ° direction
D - No data available (See Discussion Section)

Table 2. Skin friction coefficients and comparisons

ID #	X/T	Z/T	C_f	α	$\alpha_{v/s}$	$C_{f_{log}}$	$\alpha_{w/u}$	$h_{w/u}$, μm
36	4.46100	-0.40000	0.00324 ± 7.1%	1.2 ° ± 1.9 °	-9°	.0032		
37	4.46100	-0.30000	0.00309 ± 5.3%	-11.9 ° ± 1.8 °	-9°	.0033		
38B	4.46100	-0.20000	0.00342 ± 3.0%	-35.4 ° ± 1.8 °	-11°	.0028		
39D	4.46100	-0.10000						
40D	4.46100	0.00000						
41B	3.18700	-1.48010	0.00249 ± 2.4%	14.0 ° ± 2.8 °	7°	.0025		
42	3.18700	-1.28010	0.00216 ±10.6%	2.9 ° ± 3.6 °	6°	.0023		
43A	3.18700	-1.08010						
44B	3.18700	-0.98015	0.00249 ± 3.8%	19.2 ° ± 2.6 °	5°	.0027		
45B	3.18700	-0.88015	0.00321 ± 1.8%	11.9 ° ± 3.9 °	5°	.0034		
46B	3.18700	-0.78015	0.00361 ± 3.5%	-1.7 ° ± 1.8 °	-2°	.0038		
47B	3.18700	-0.68015	0.00353 ± 4.3%	-4.5 ° ± 1.7 °	1°	.0040		
48B	3.18700	-0.58015	0.00382 ± 2.2%	7.9 ° ± 3.6 °	3°	.0042		
49B	3.18700	-0.48015	0.00417 ± 1.6%	4.3 ° ± 3.5 °	6°	.0047		
50B	2.71950	-1.56030	0.00280 ± 1.8%	10.4 ° ± 2.7 °	8°			
51B	1.78470	-1.48750	0.00333 ± 3.7%	6.6 ° ± 3.9 °	6°			
61C	0.76700	-1.24950	0.00393 ± 1.7%	-4.4 ° ± 2.2 °	-2°		-4 ° ± 1 °	150
62	0.42260	-1.16730	0.00392 ± 5.6%	-8.6 ° ± 1.9 °	-10°		-9 ° ± 3 °	150
63	0.09140	-1.04120	0.00374 ± 3.3%	-19.0 ° ± 1.5 °	-20°		-22 ° ± 10 °	150
64	-0.16720	-0.91330	0.00326 ± 3.3%	-38.9 ° ± 1.8 °	-38°		-32 ° ± 17 °	150
65	-0.47040	-0.72090	0.00252 ± 3.6%	-44.1 ° ± 2.1 °	-41°		-33 ° ± 14 °	150
66	-0.81020	-0.62070	0.00254 ±14.7%	-24.5 ° ± 6.6 °	-30°		-22 ° ± 12 °	150

A - No data in 0 ° direction
B - No data in 60 ° direction
C - No data in 45 ° direction
D - No data available (See Discussion Section)

Illustrations

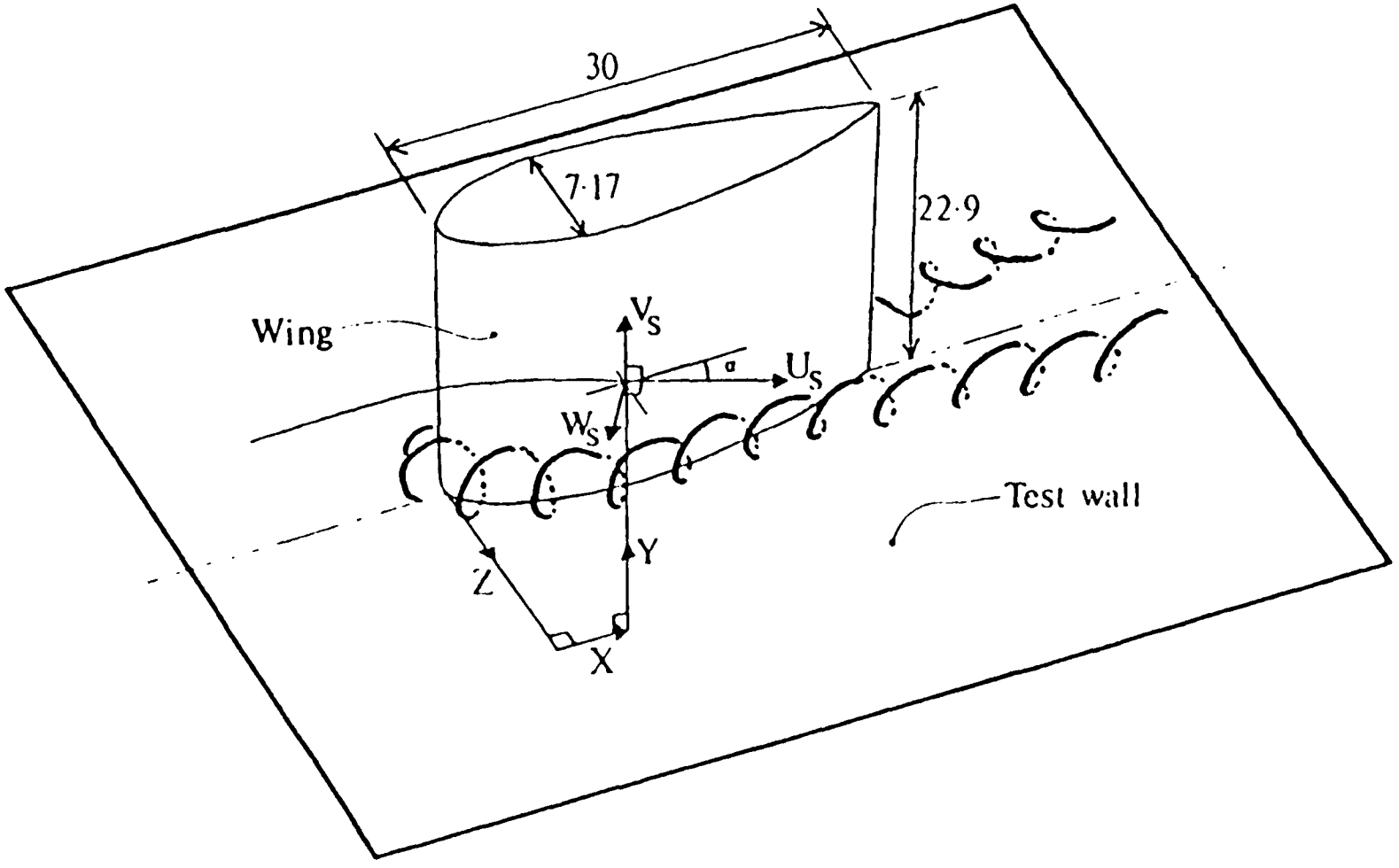

Figure 1. Perspective View of the wing-body junction.

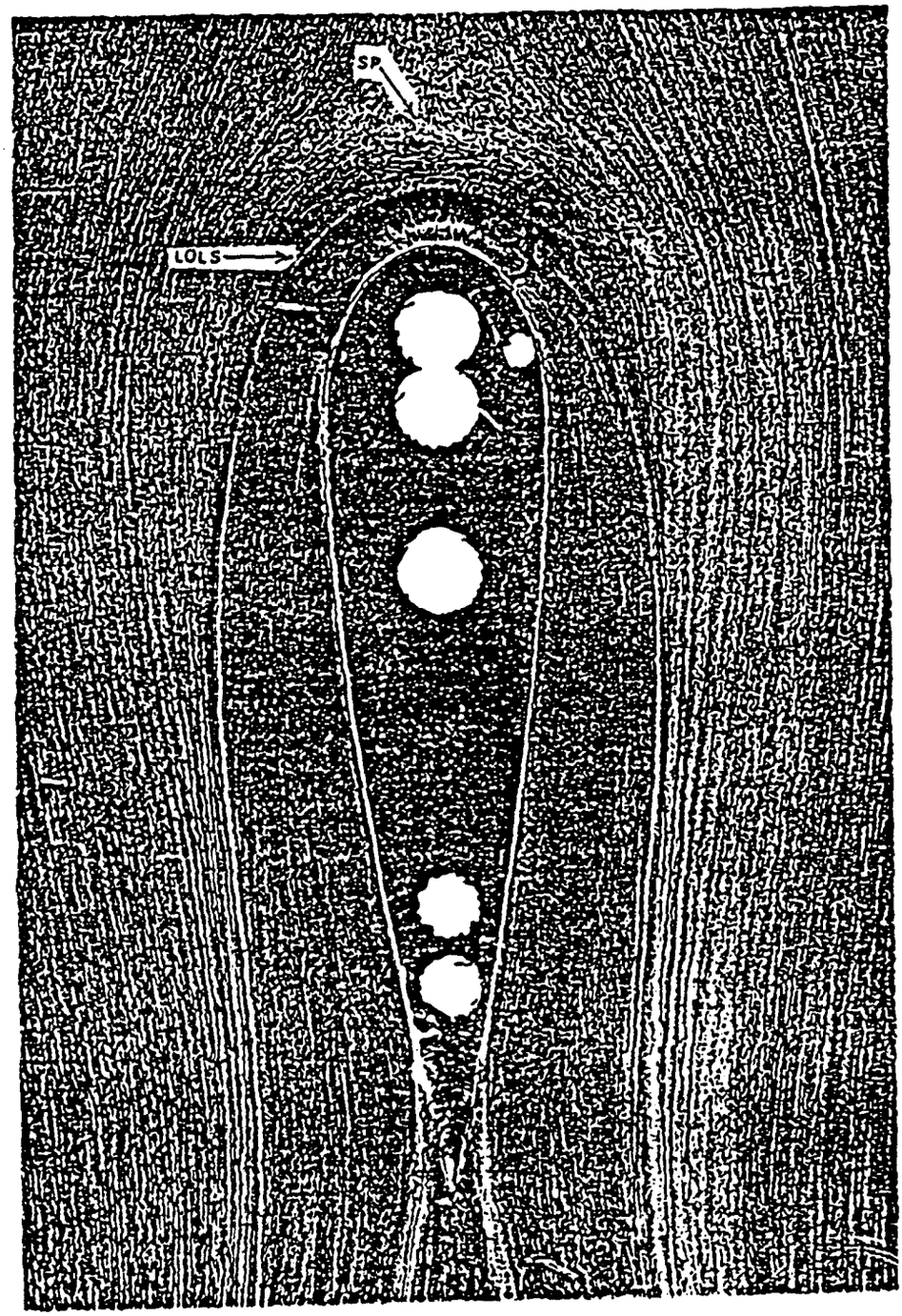

Figure 2. TiO_2-Kerosene Oil Flow Visualization: $Re_\theta = 6700$

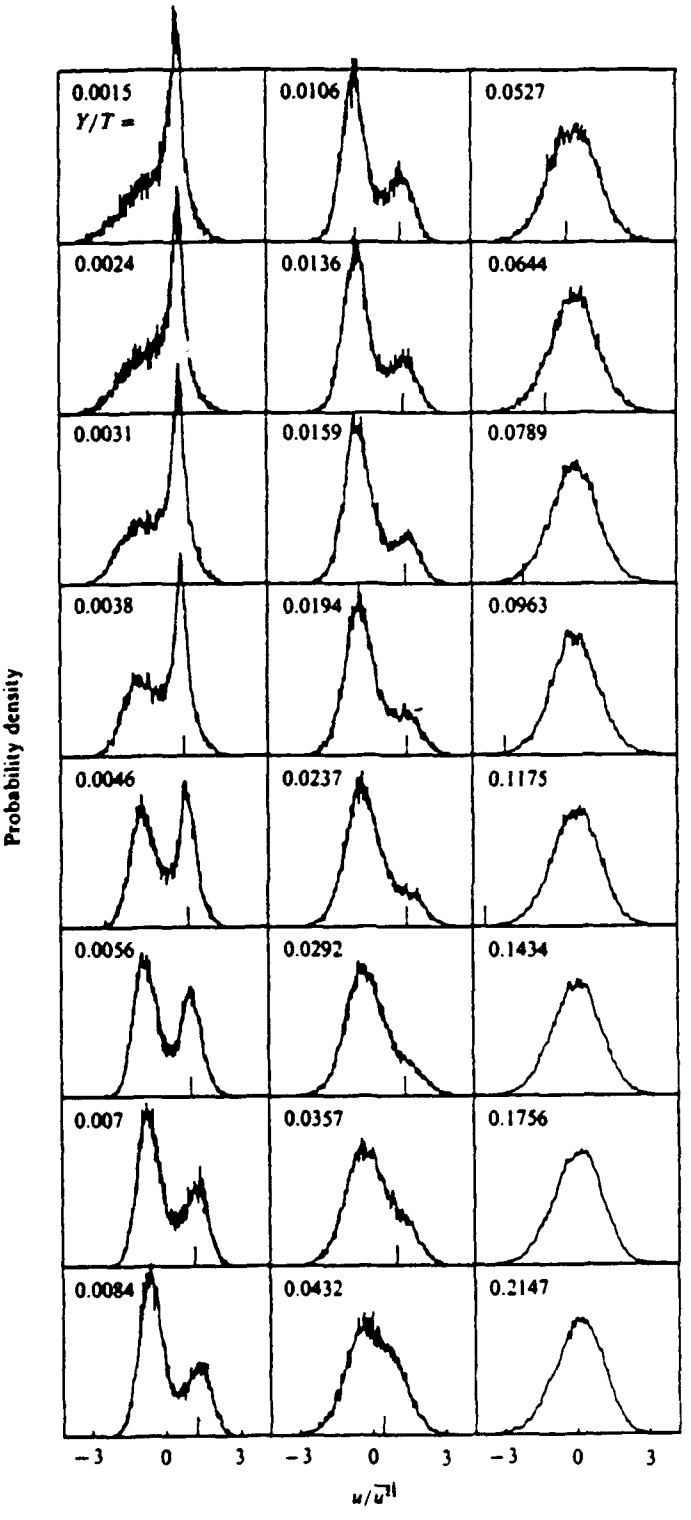

Figure 3. Probability density functions at X/T = -.20

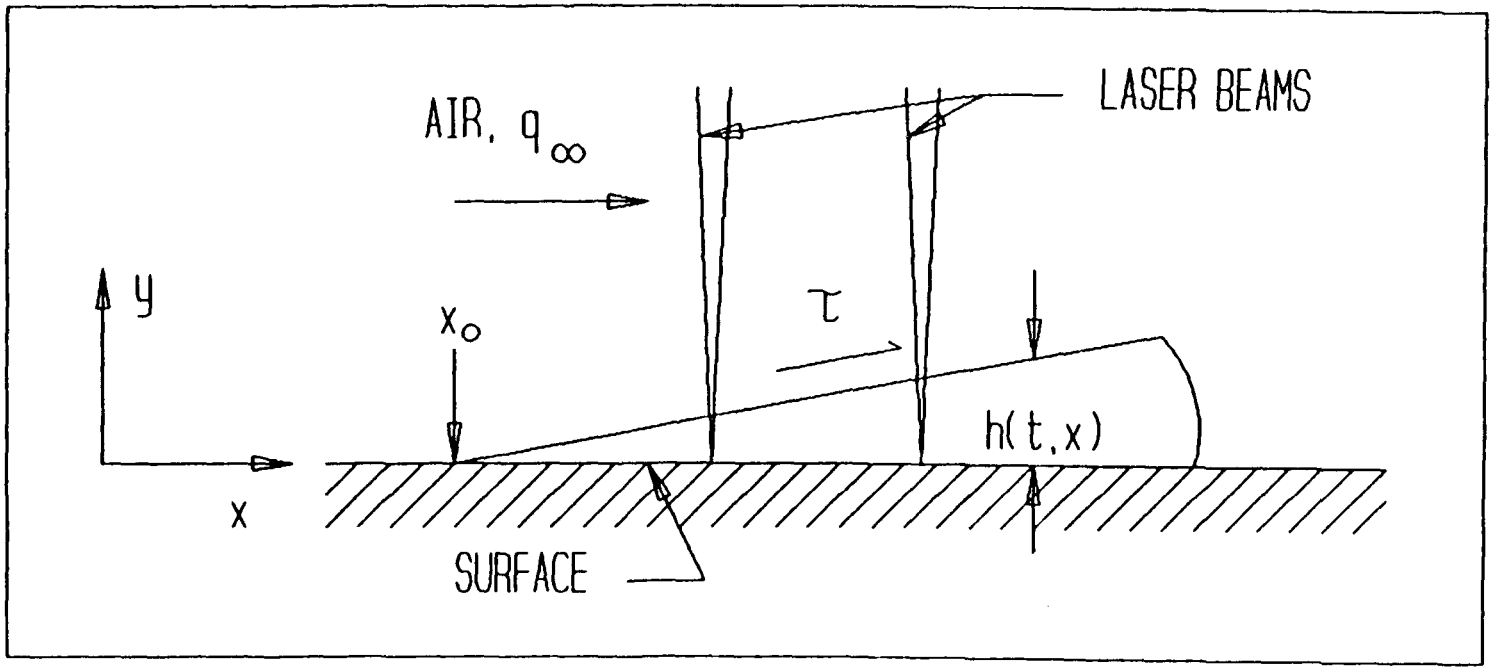

Figure 4. Two-dimensional oil flow nomenclature

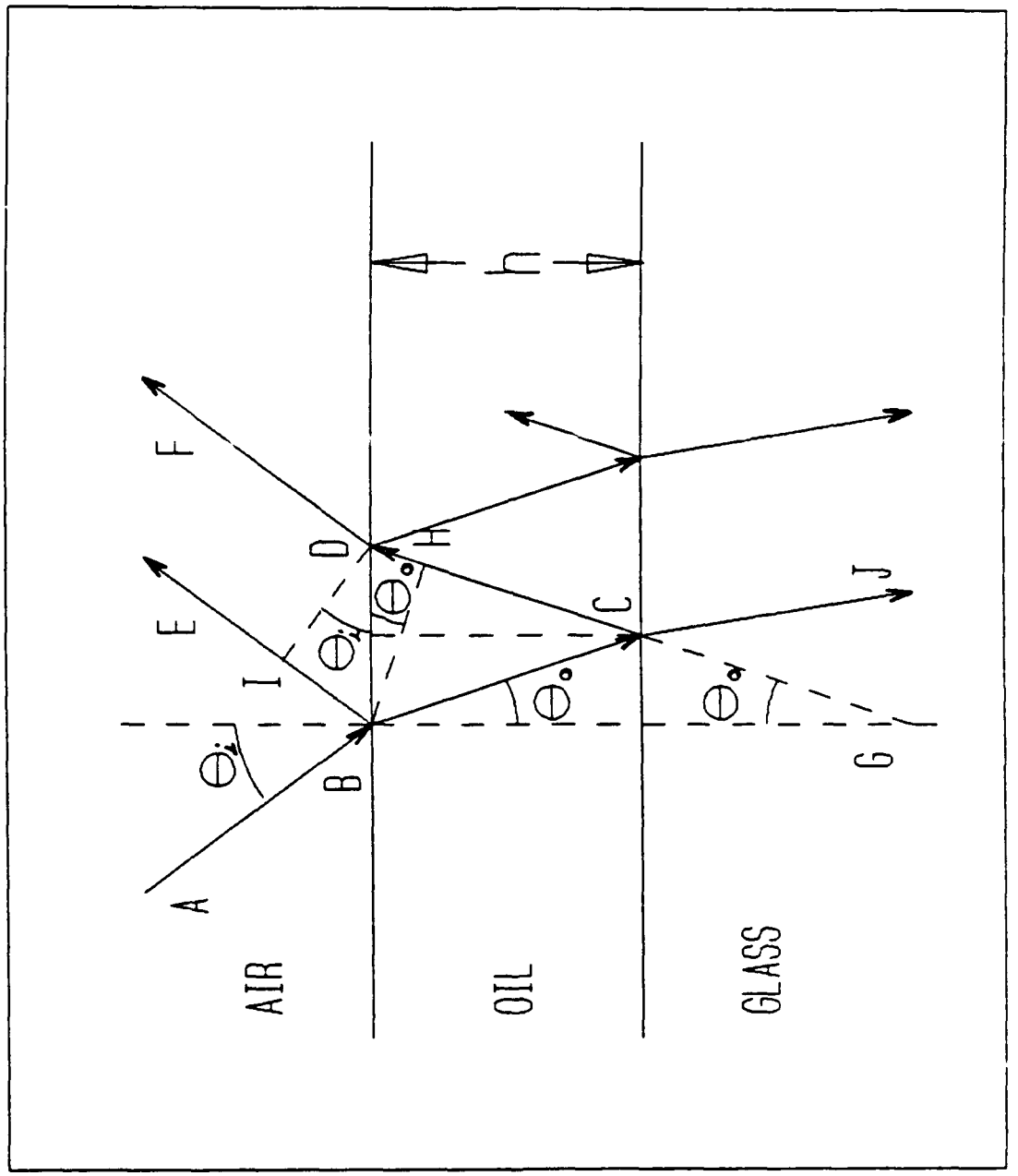

Figure 5. Geometry for optical pathlength difference

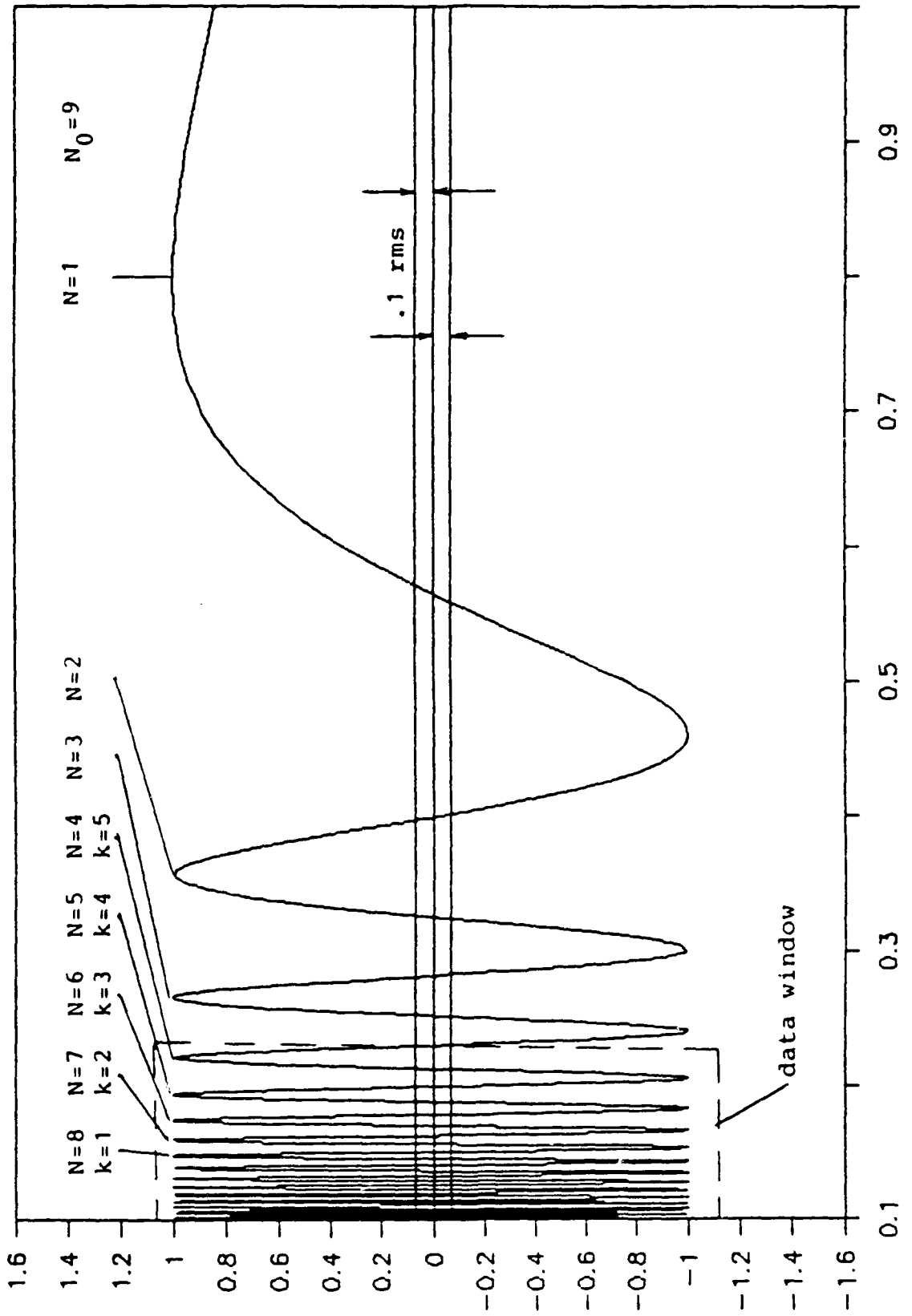

Figure 6. Fringe numbering nomenclature: Idealized sample output

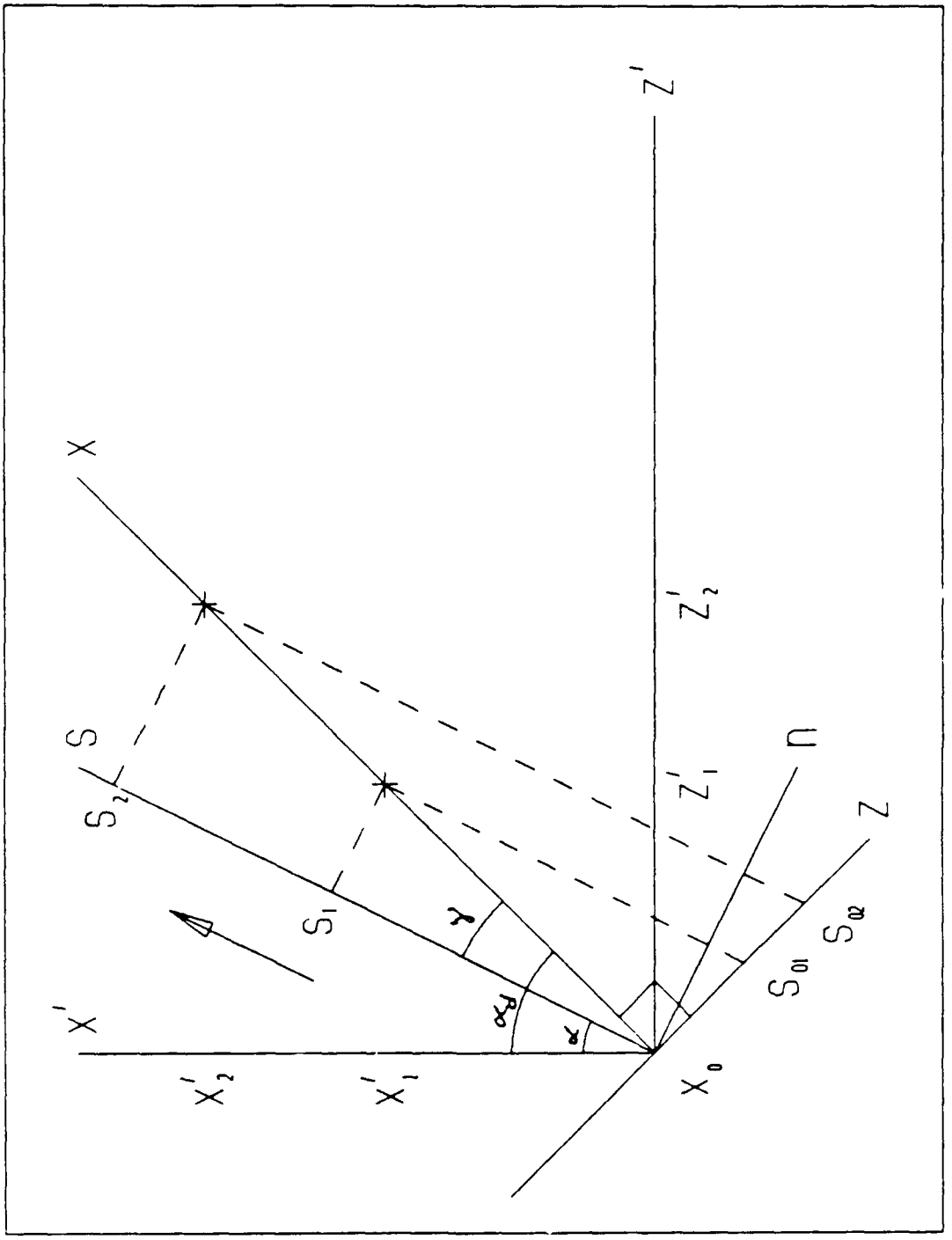

Figure 7. Geometry and notation for unknown oil flow direction

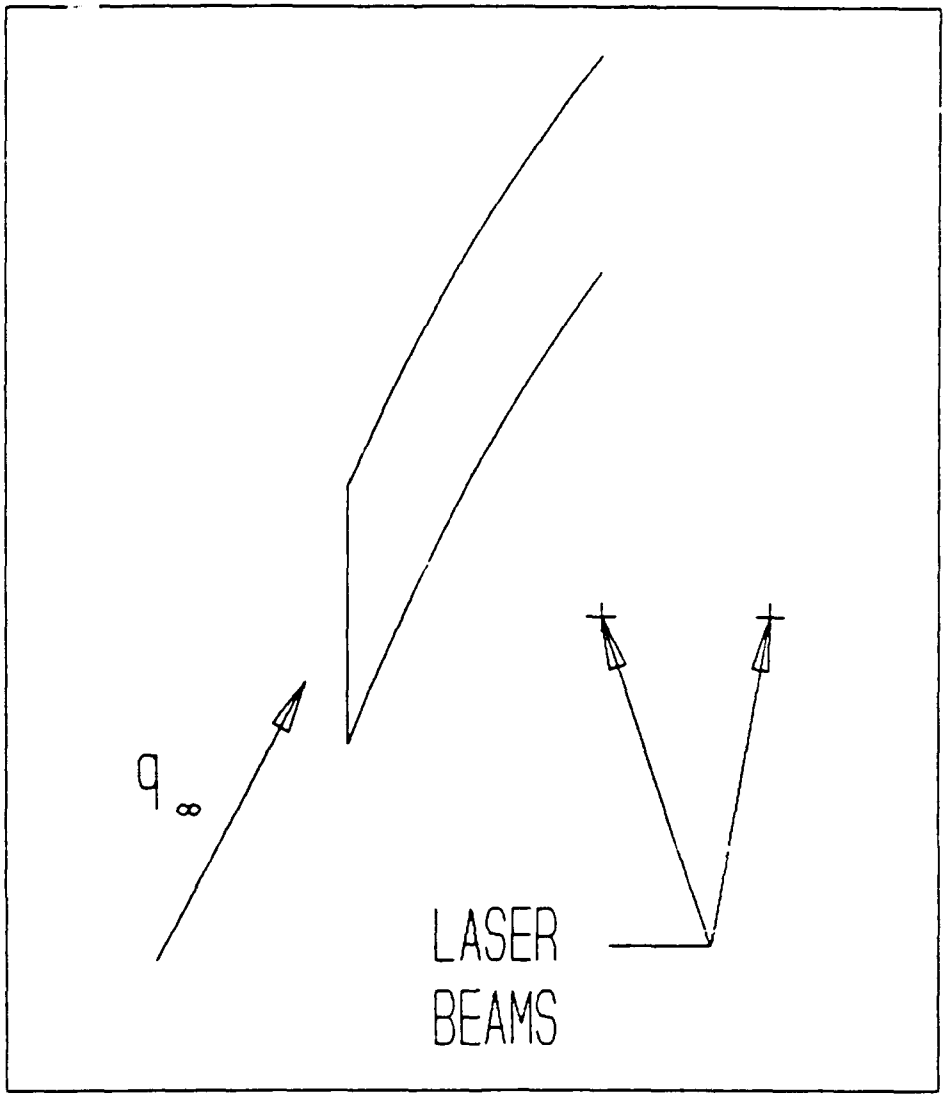

Figure 8. Problem area: flow direction near normal to measurement direction

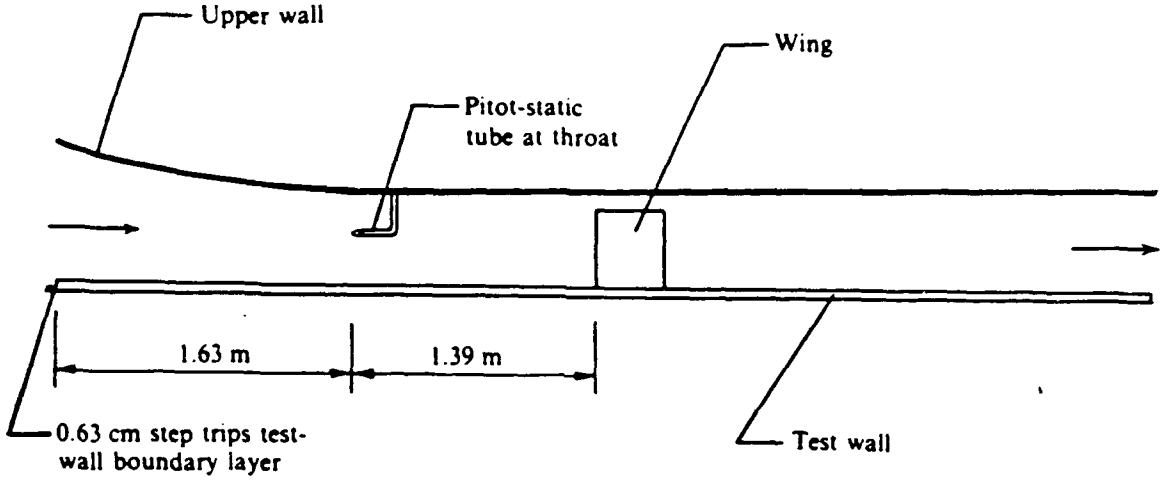

Figure 9. VPI&SU Low Speed Boundary Layer Wind Tunnel

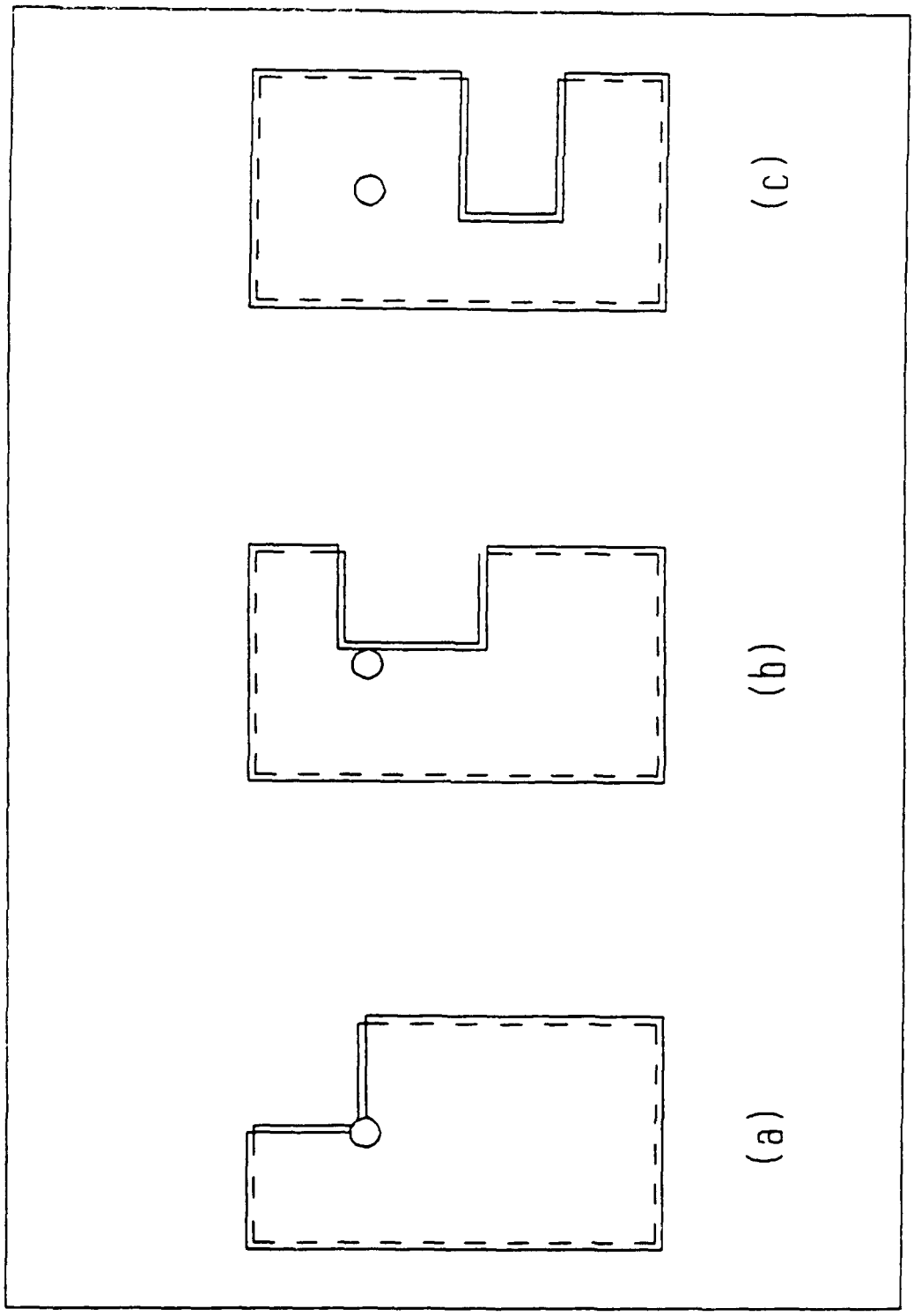

Figure 10. Plywood tunnel floor inserts

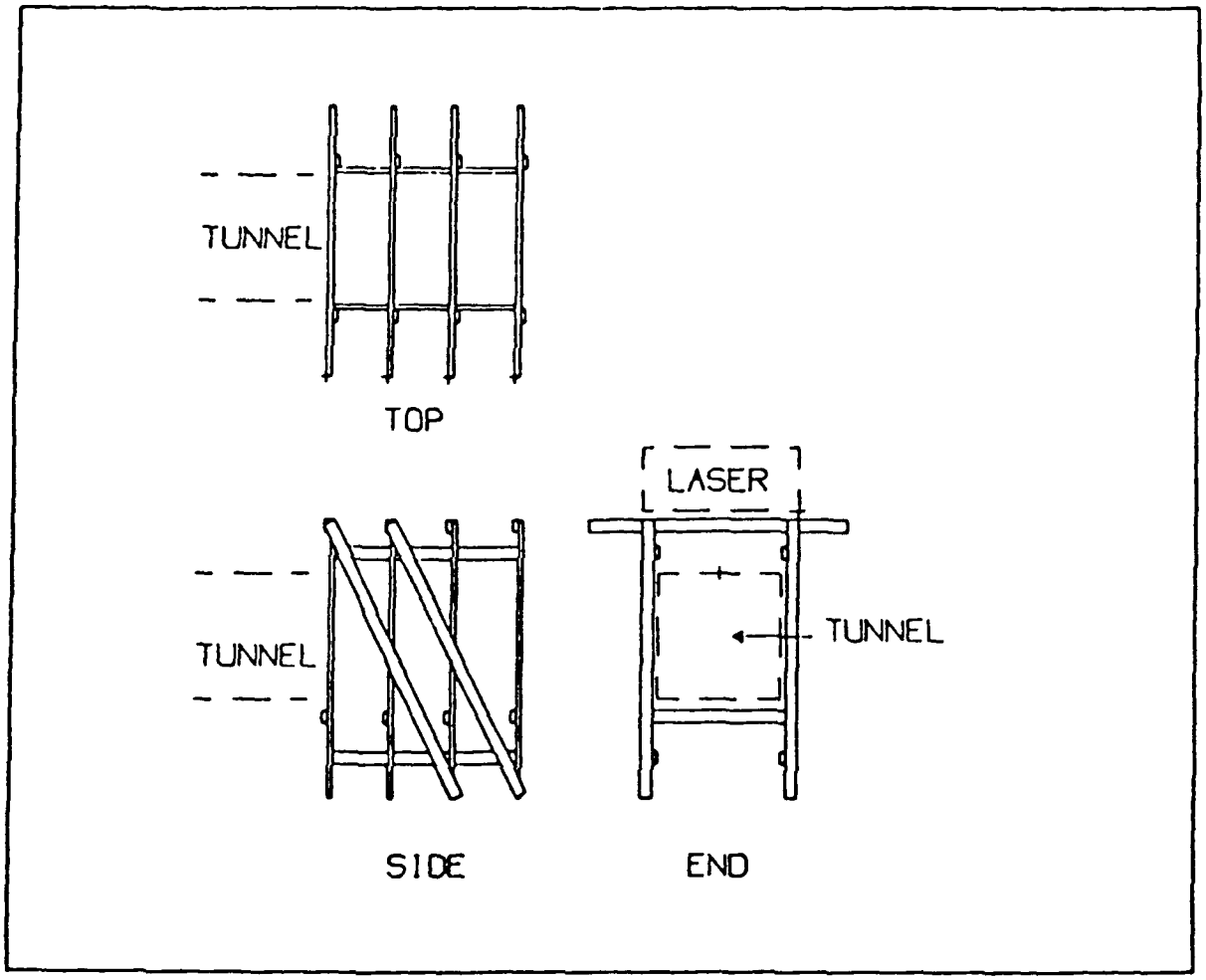

Figure 11. Wooden frame surrounding the wind tunnel

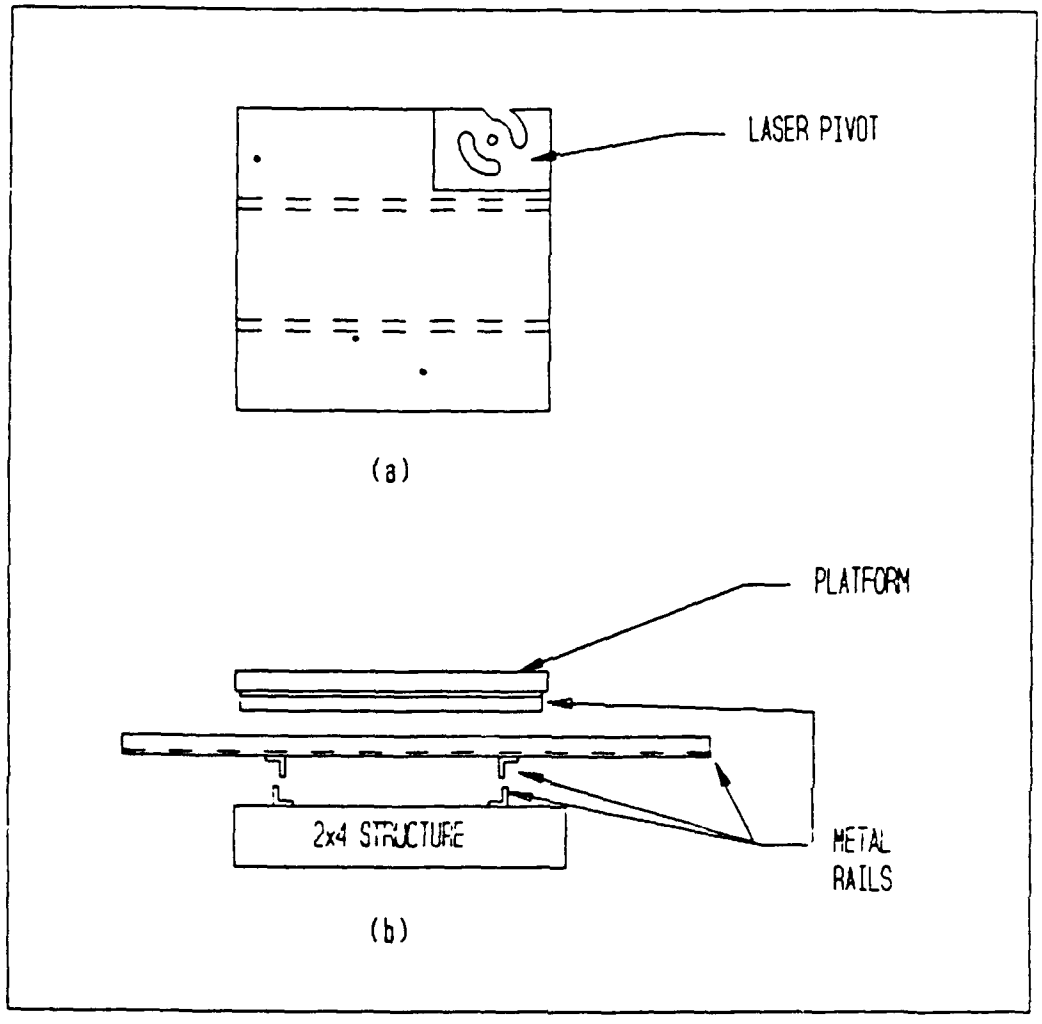

Figure 12. Movable platform and traversing rails

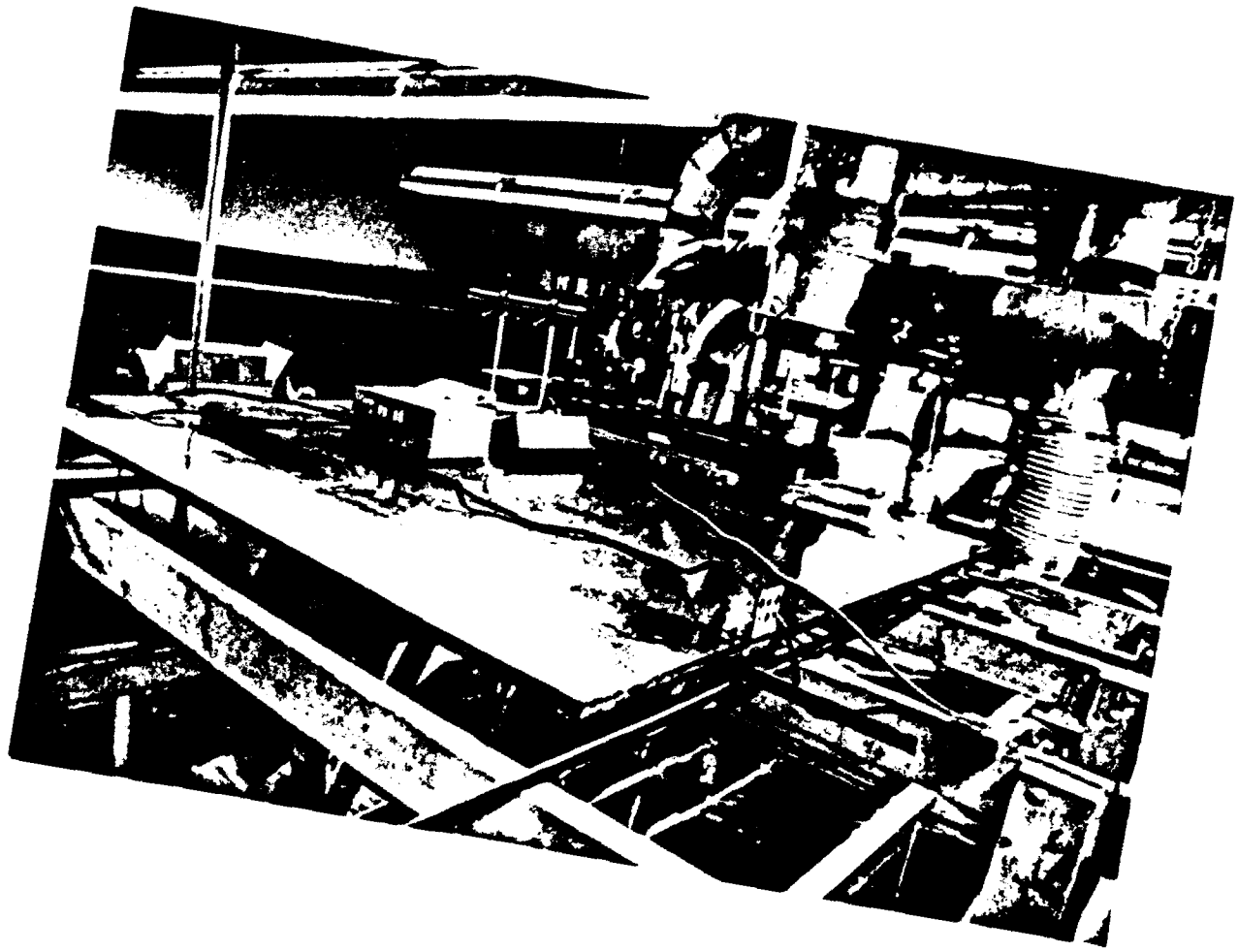

Figure 13. Photograph of movable platform mounted on wooden frame

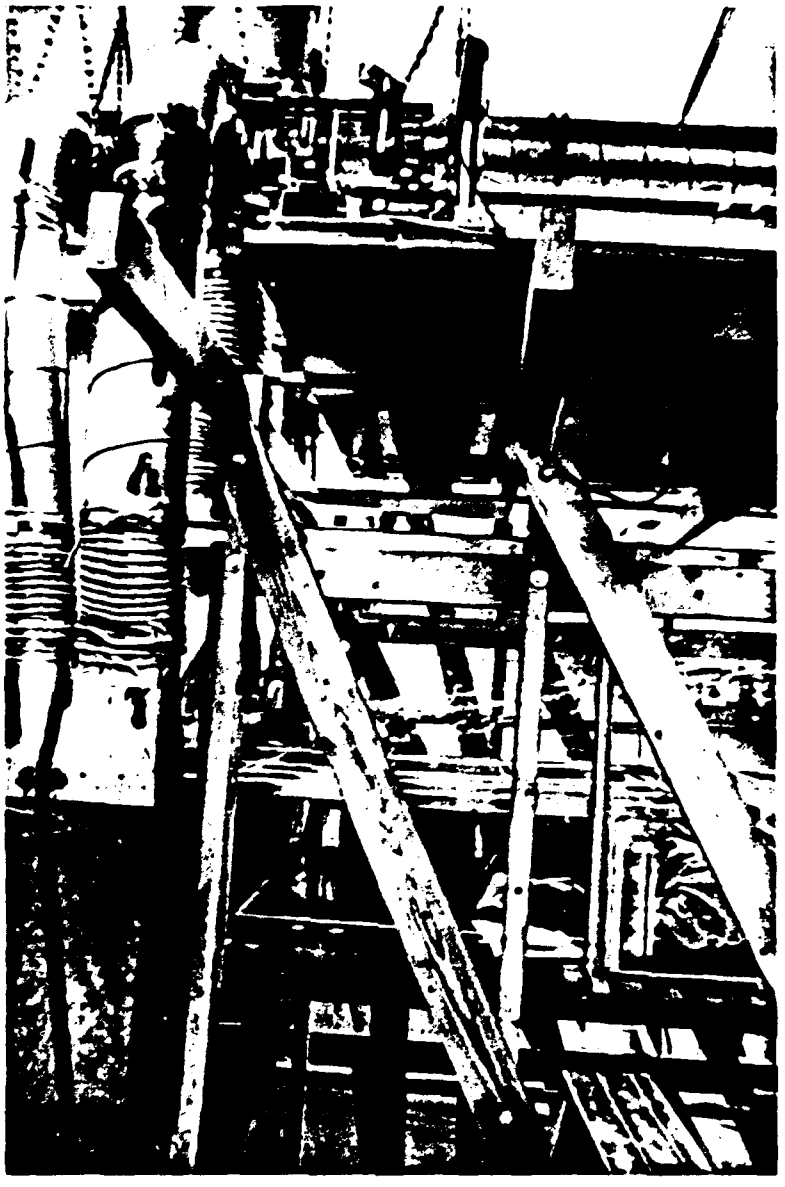

Figure 14. Photograph of entire apparatus

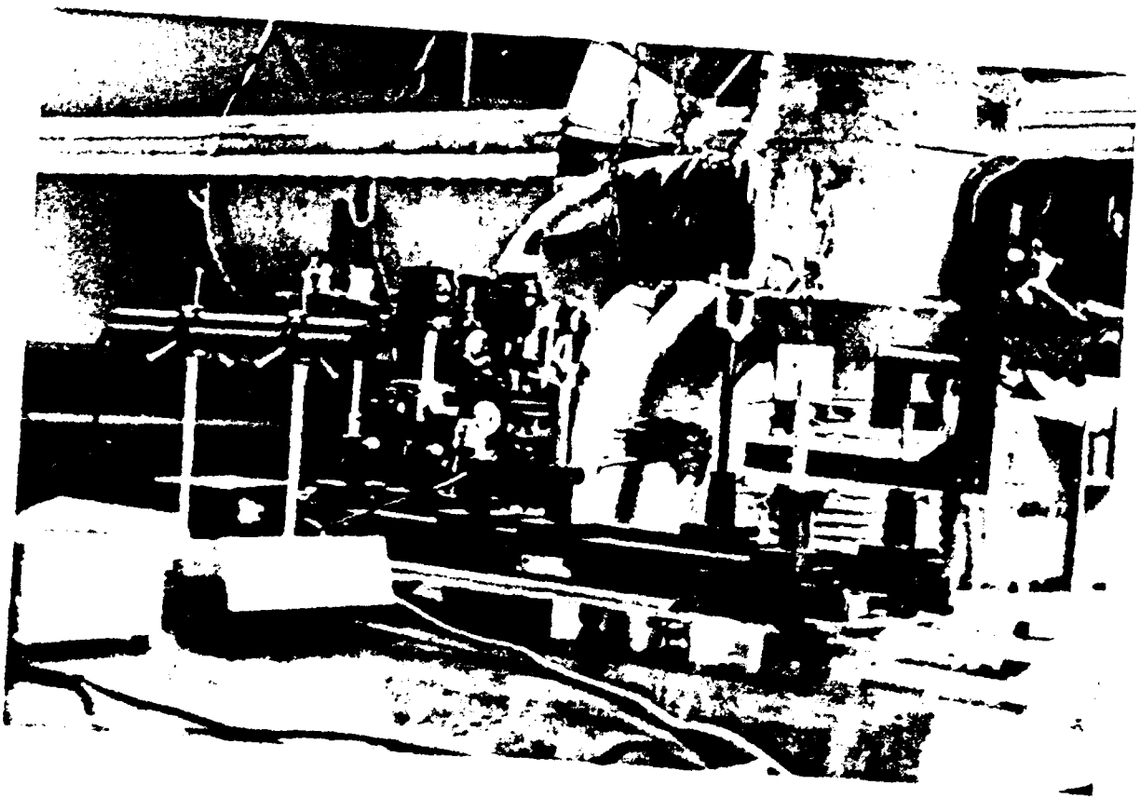

Figure 15. Side view of laser assembly

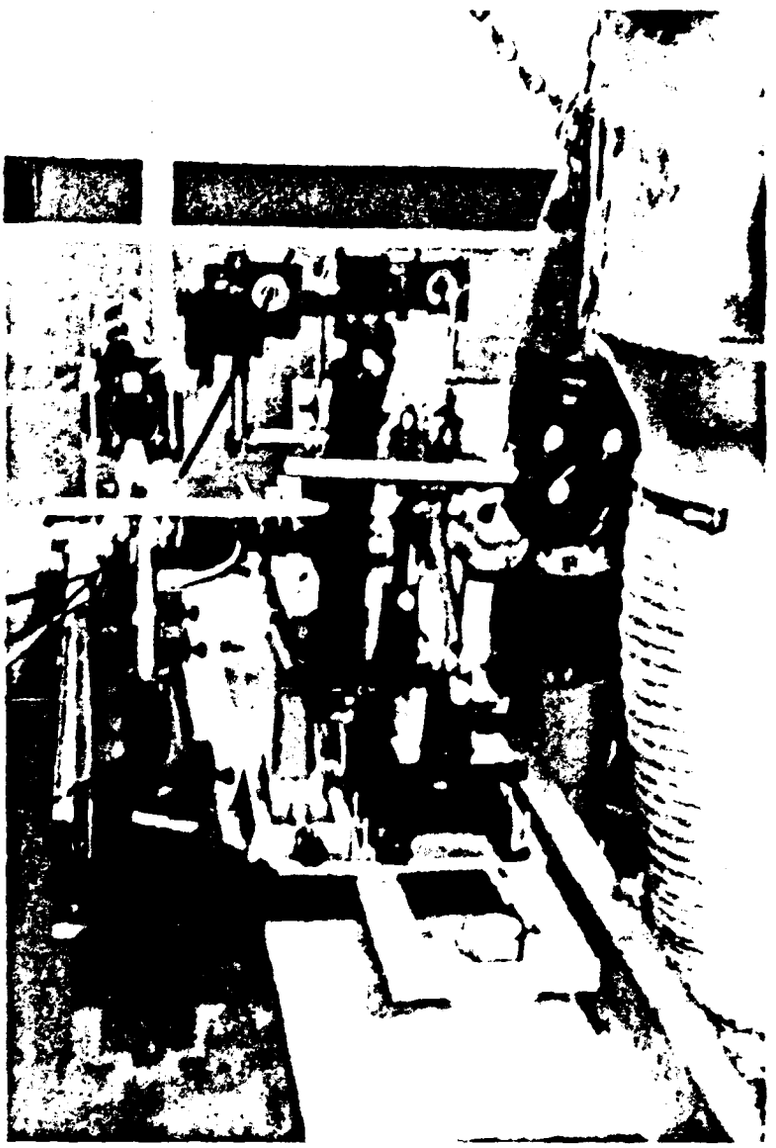

Figure 16. Laser assembly viewed from optical rail axis

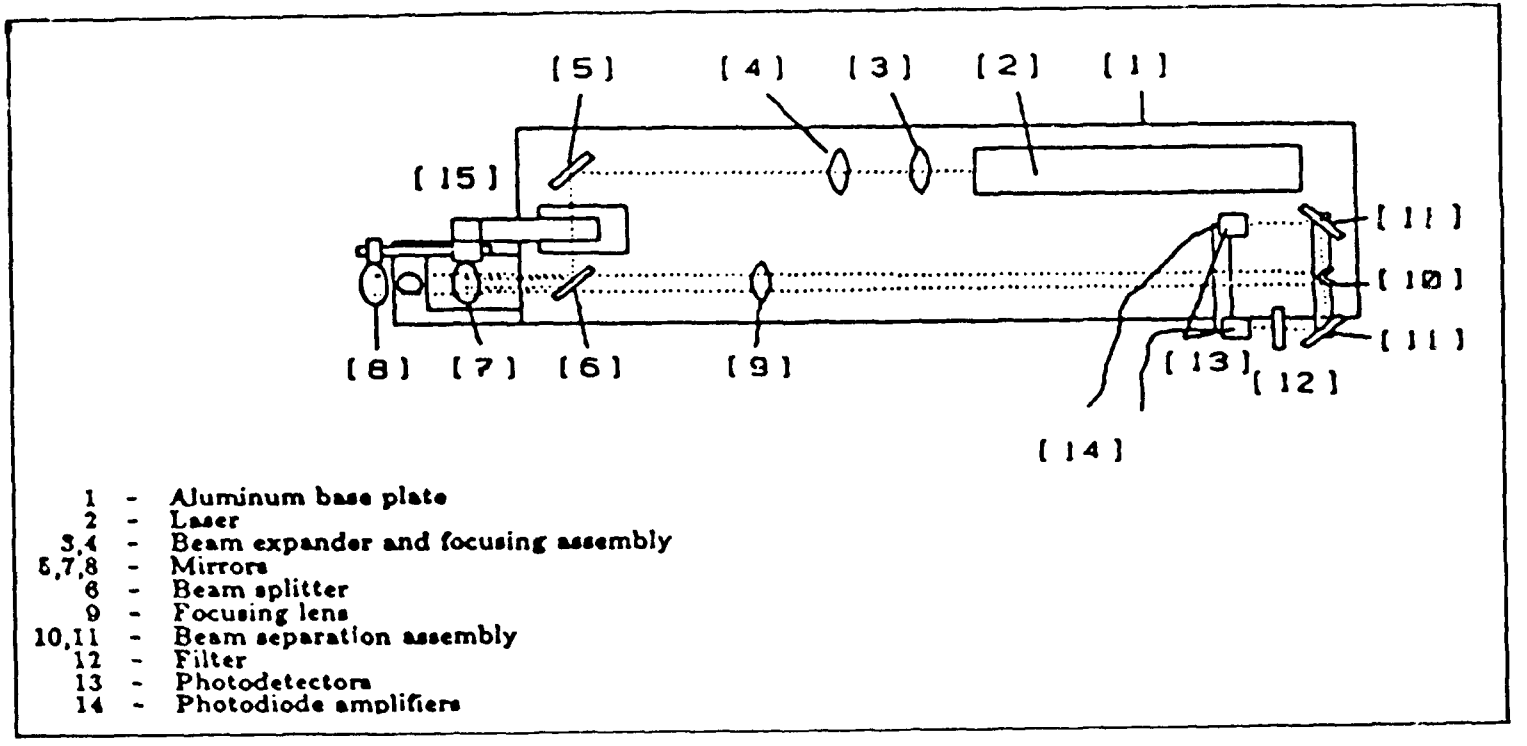

Figure 17. Laser assembly geometry diagram

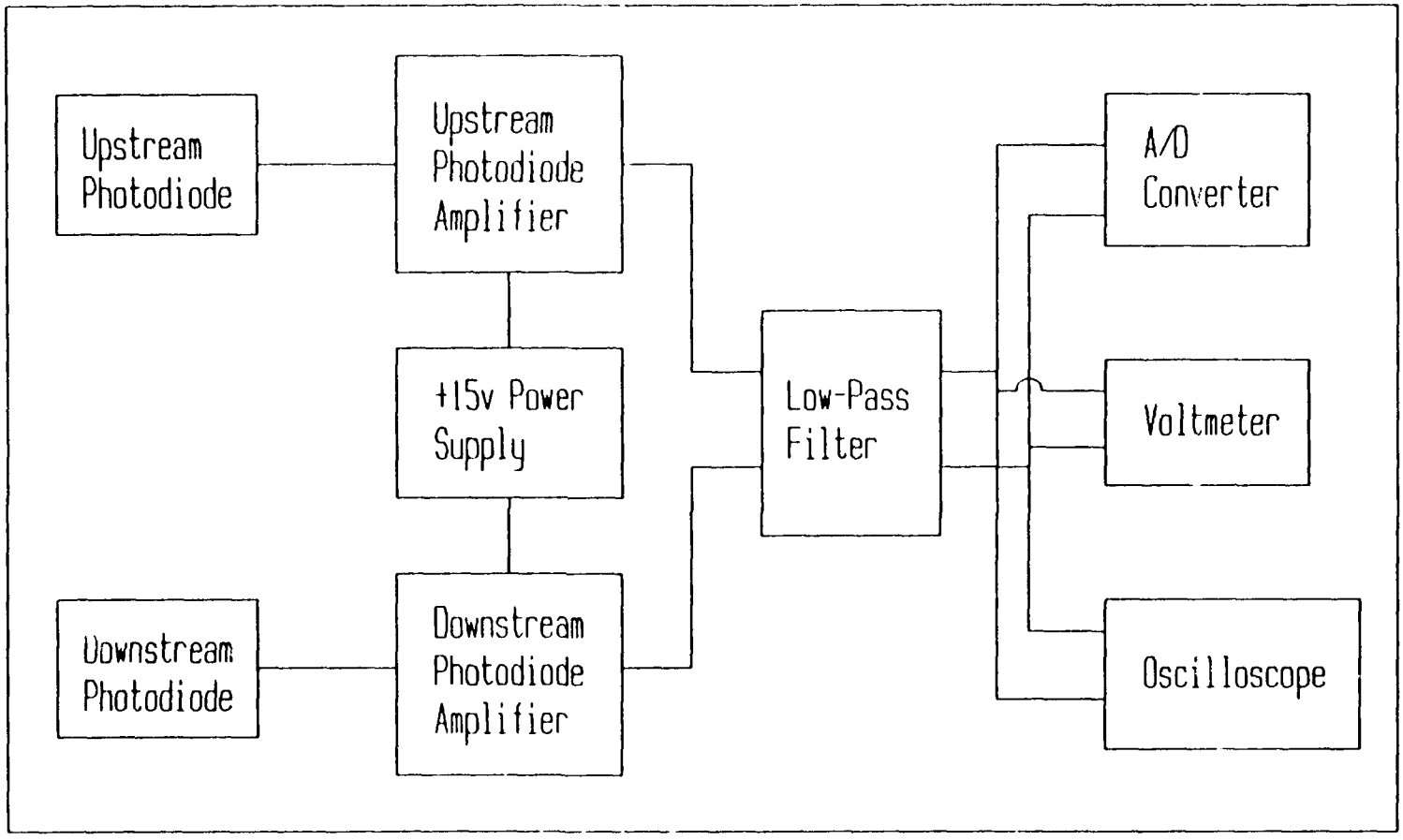

Figure 18. Box diagram of hardware components

Figure 19. Photograph of test surface with data location transparency attached

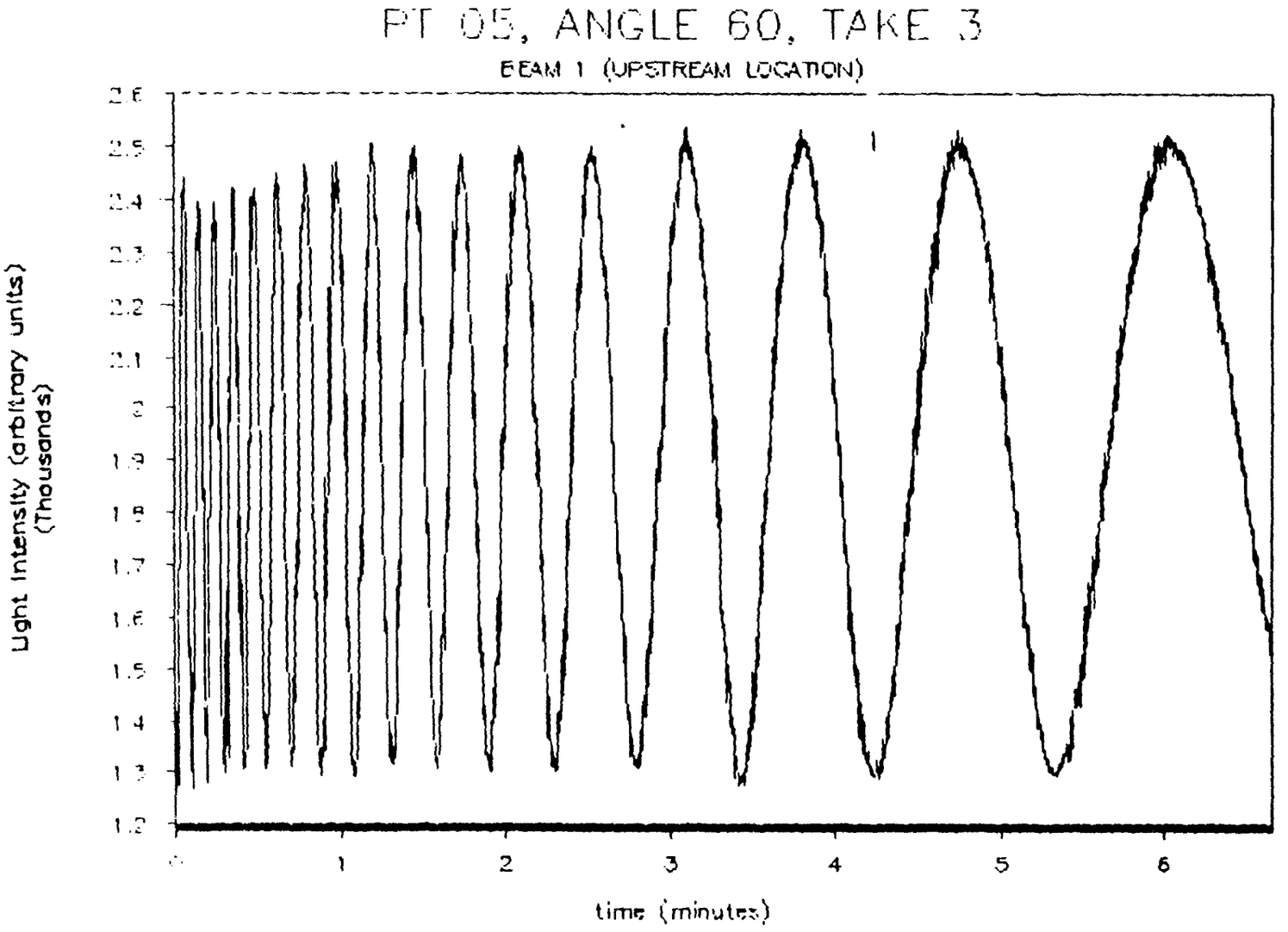

Figure 20. Sample photodetector output: Point 05, Angle 60, Take 3, upstream beam

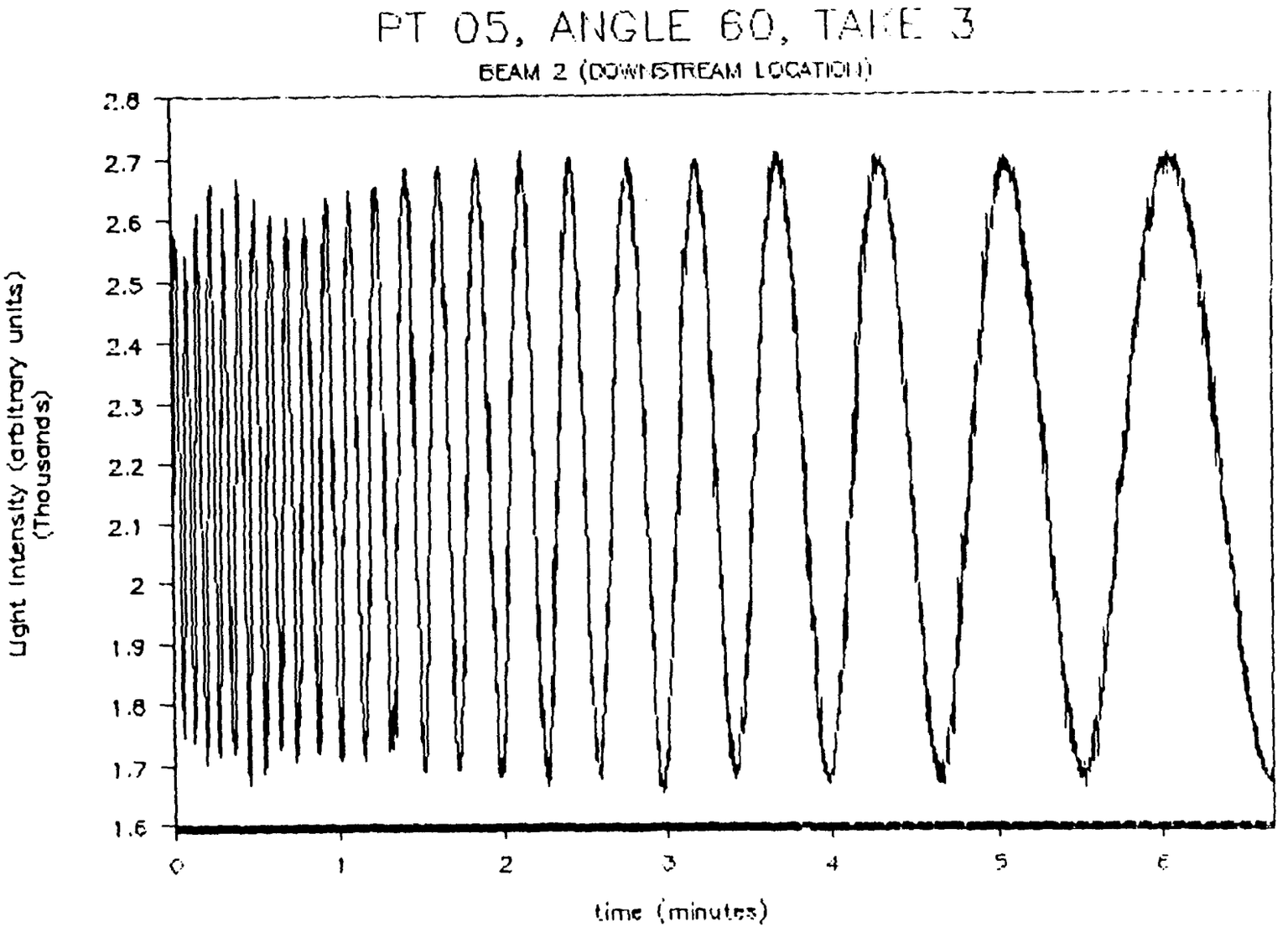

Figure 21. Sample photodetector output: Point 05, Angle 60, Take 3, downstream beam

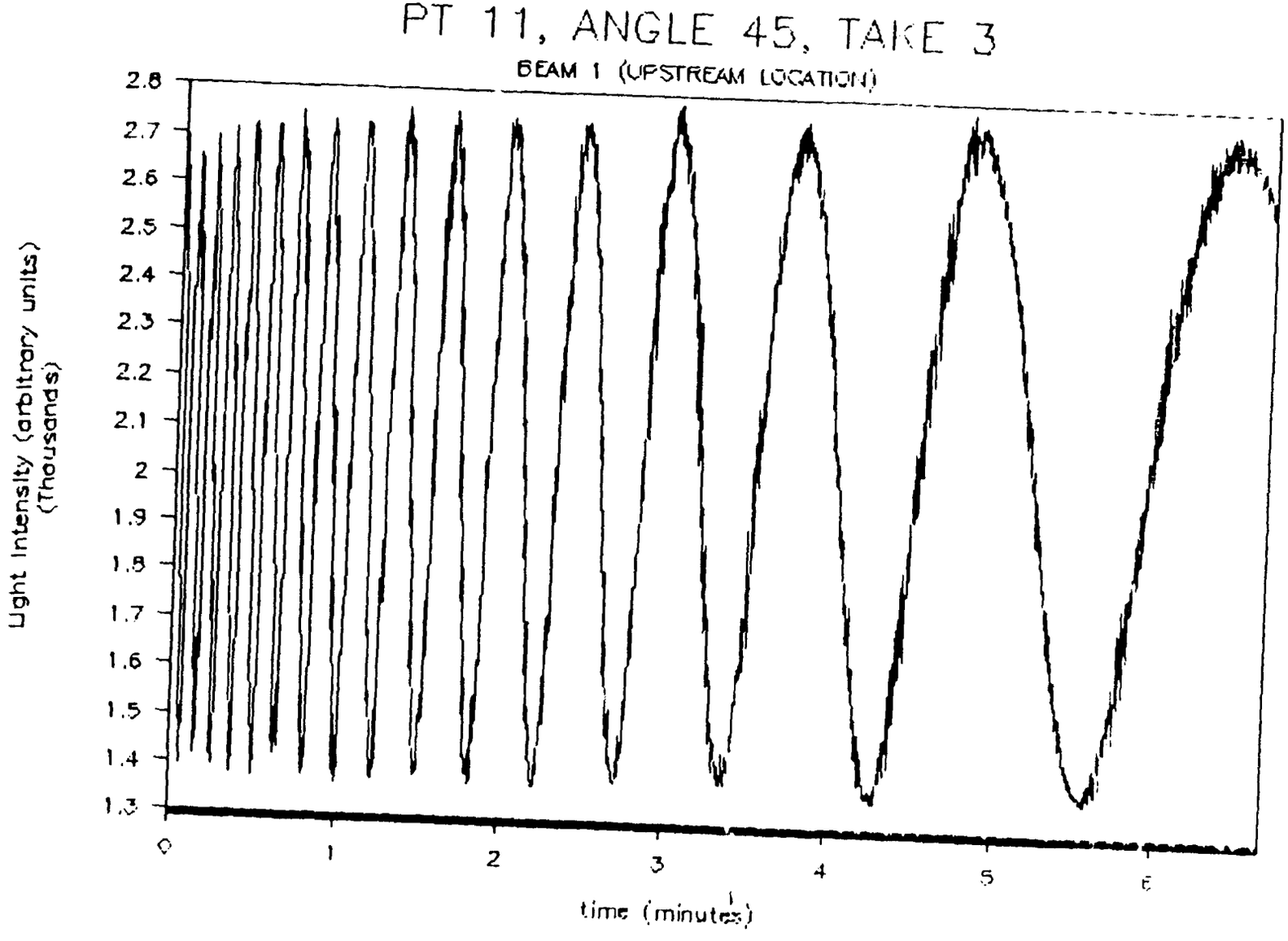

Figure 22. Sample photodetector output: Point 11, Angle 45, Take 3, upstream beam

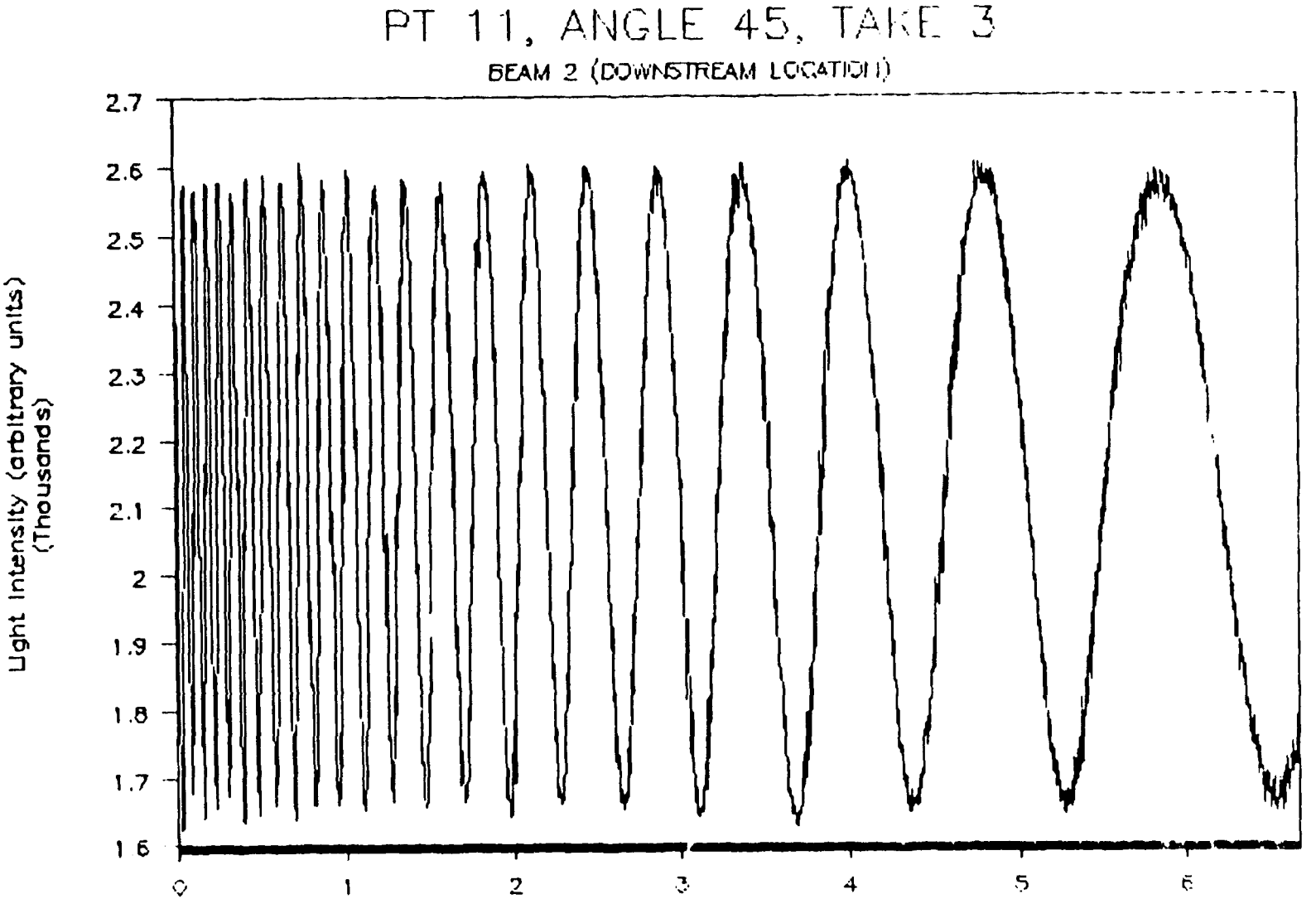

Figure 23. Sample photodetector output: Point 11, Angle 45, Take 3, downstream beam

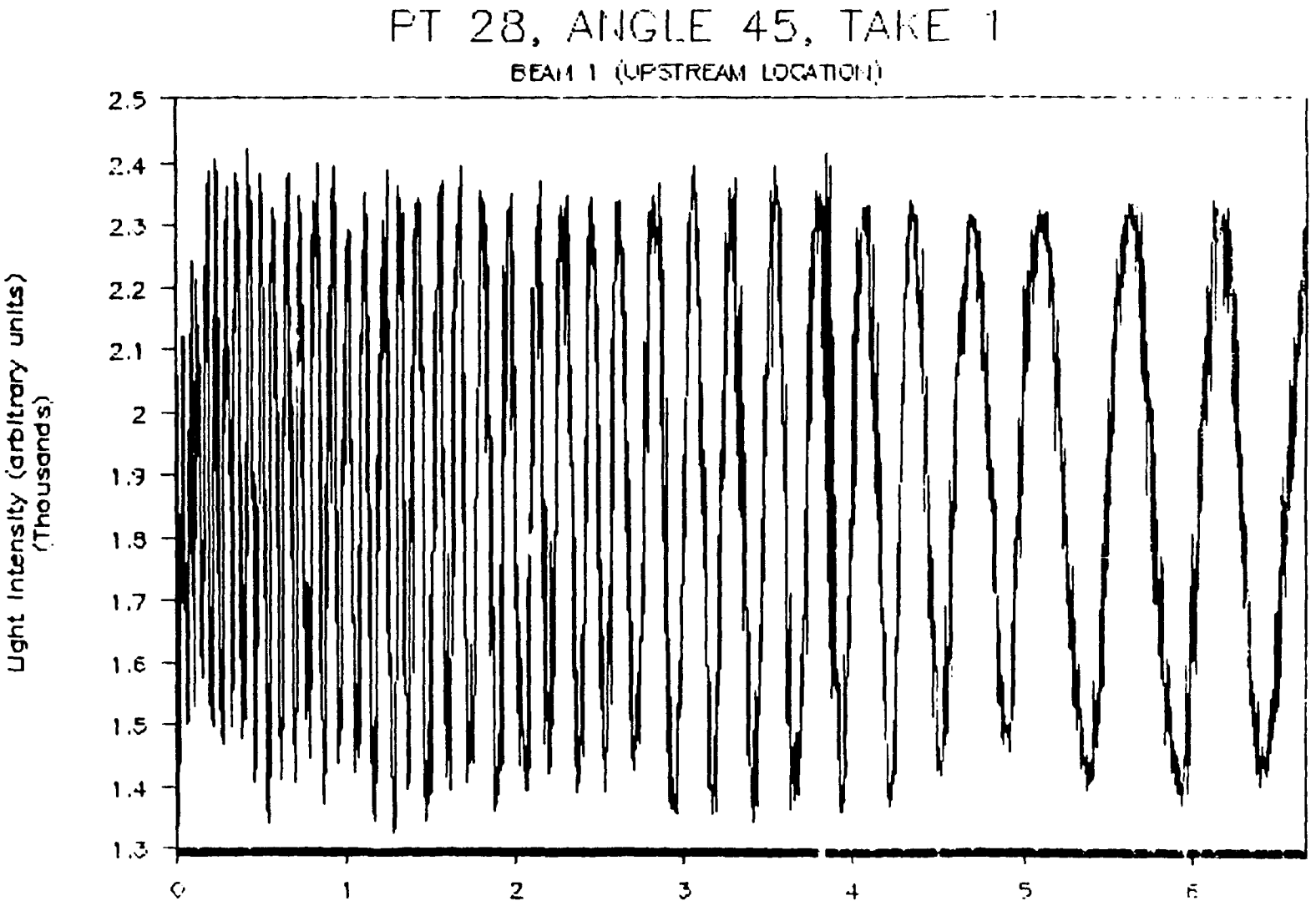

Figure 24. Sample "bad" photodetector output: Point 28, Angle 45, Take 1, upstream beam

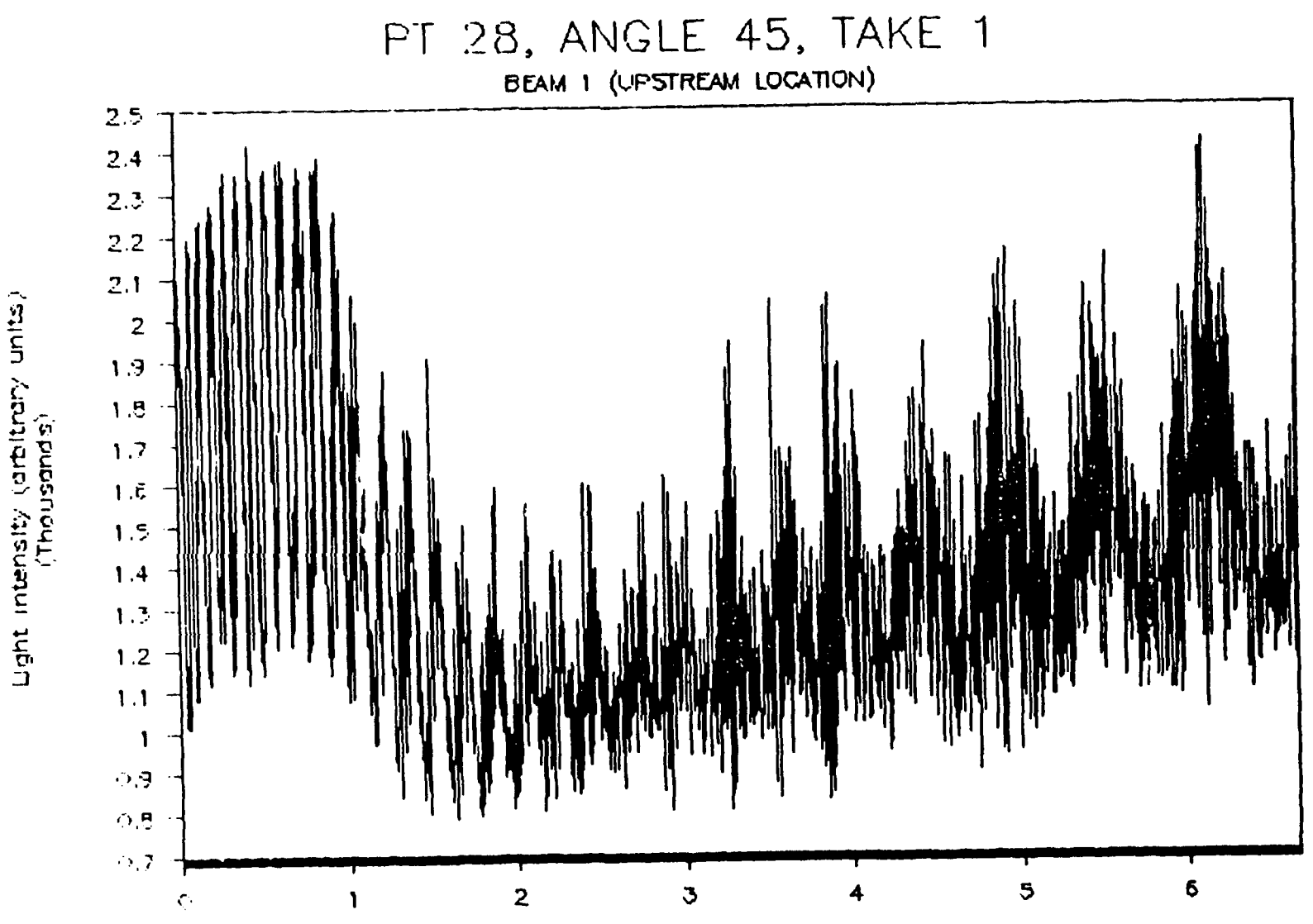

Figure 25. Sample "bad" photodetector output: Point 28, Angle 45, Take 1, downstream beam

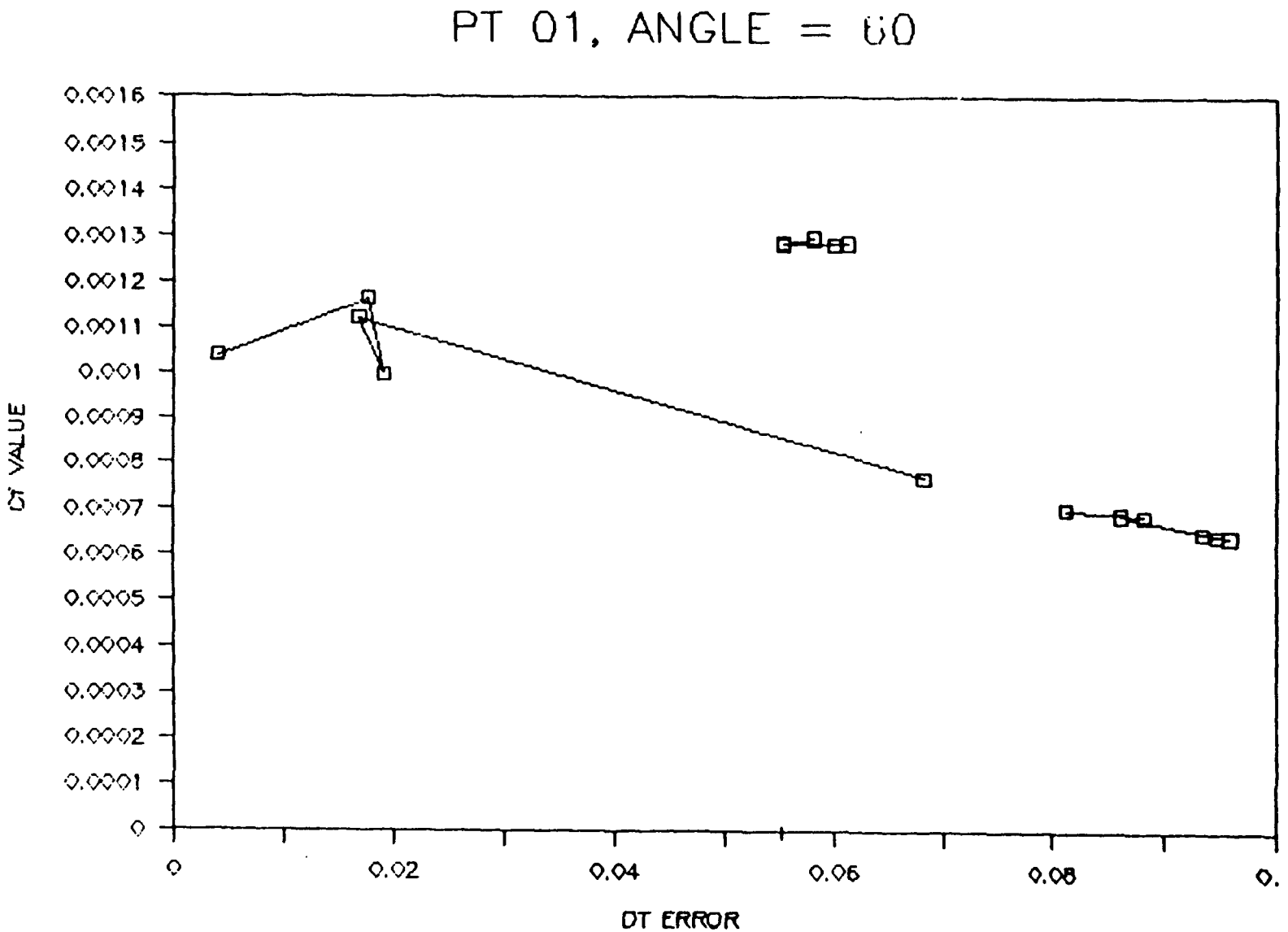

Figure 26. Skin friction coefficient magnitude vs. time origin error: Point 01, angle 60

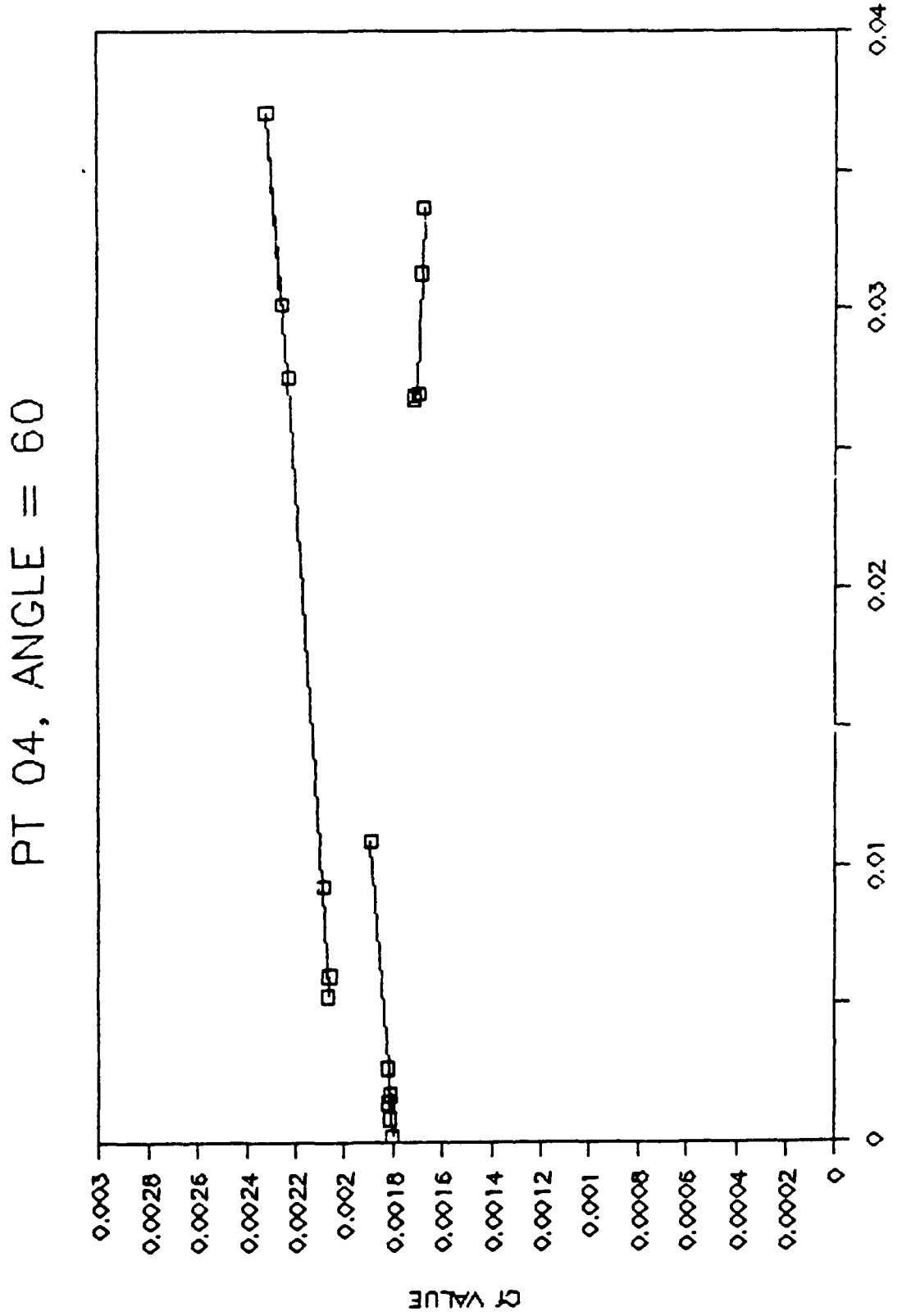

Figure 27. Skin friction coefficient magnitude vs. time origin error: Point 04, angle 60

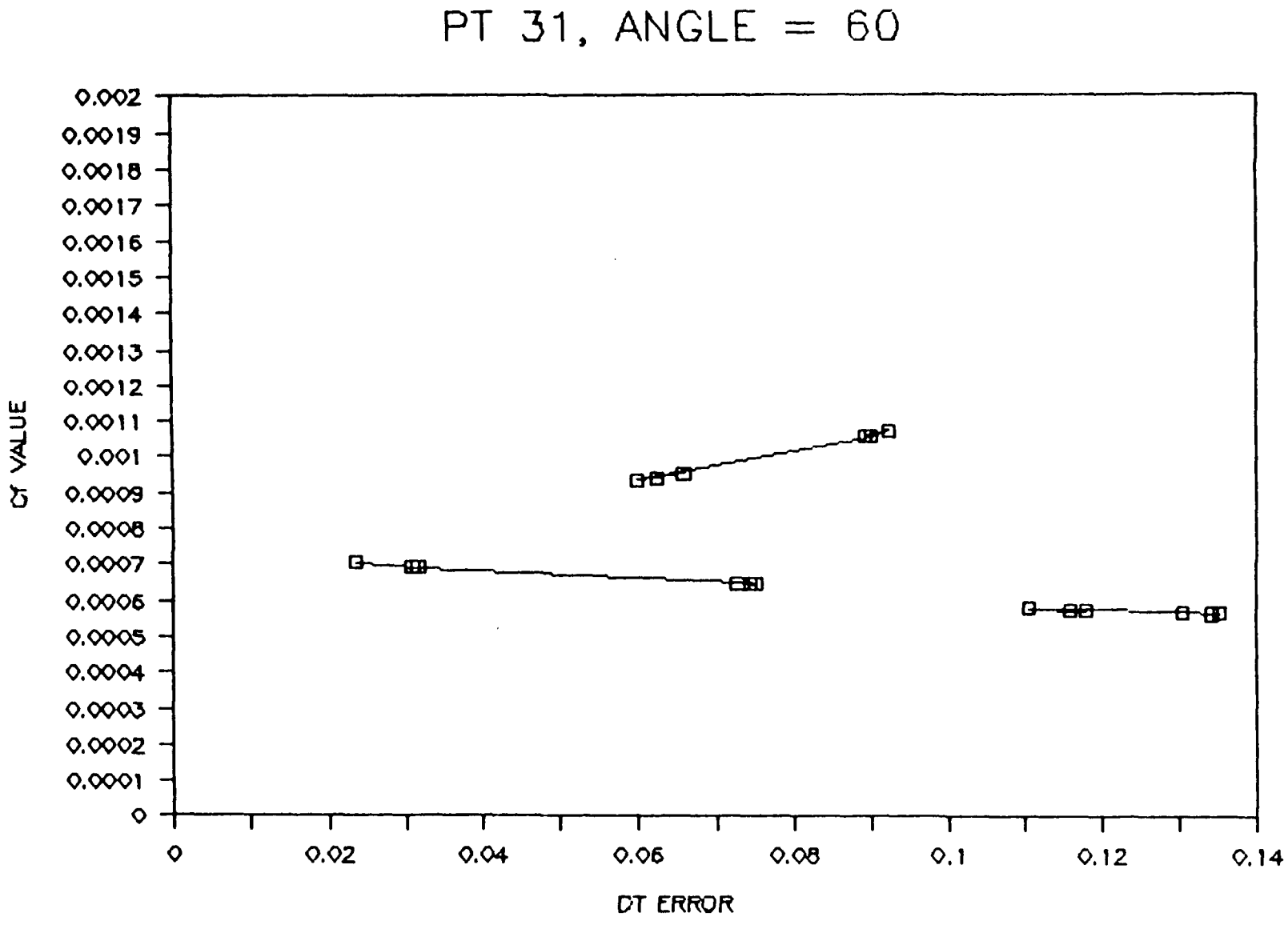

Figure 28. Skin friction coefficient magnitude vs. time origin error: Point 31, angle 60

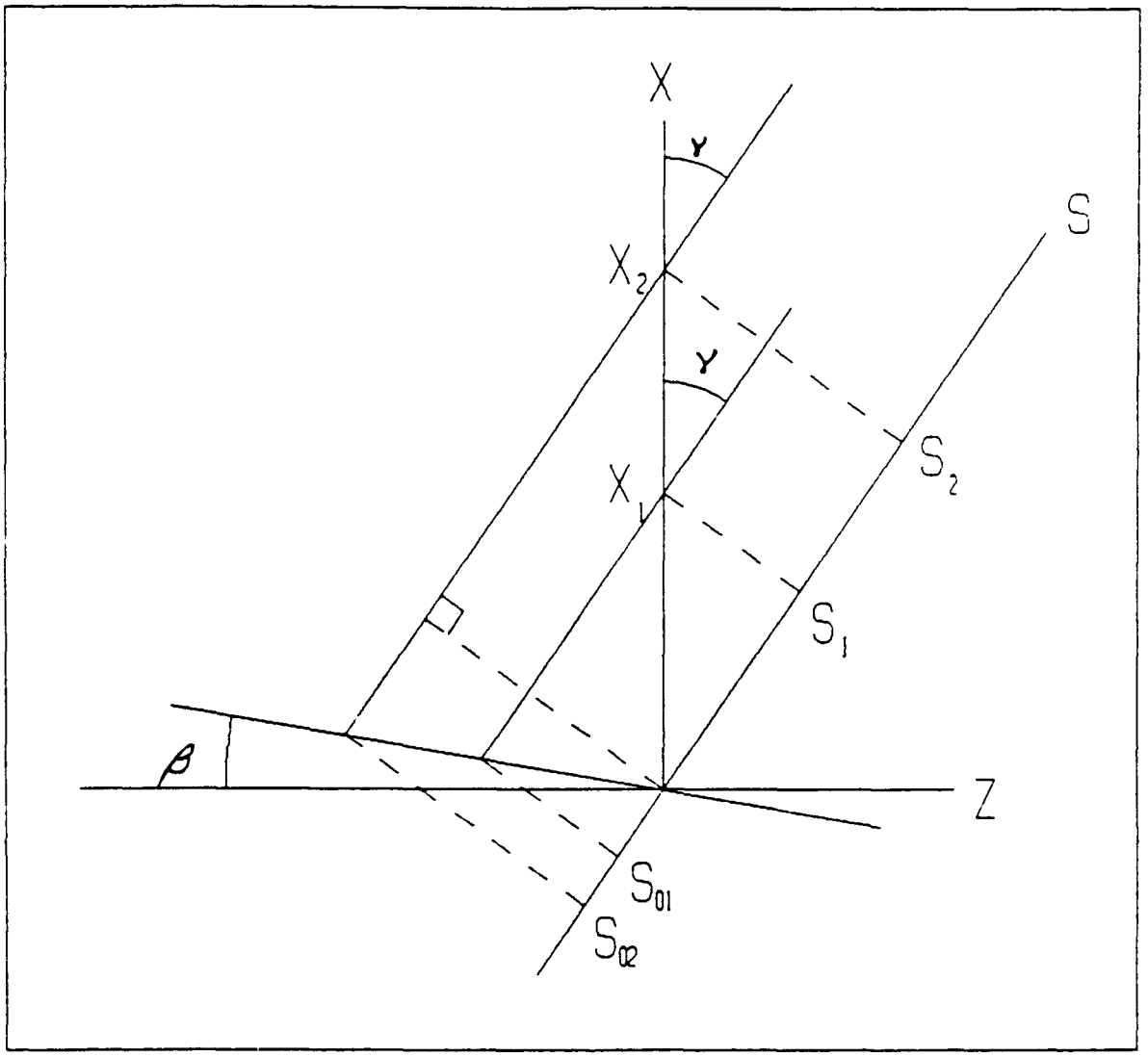

Figure 29. Non-perpendicularity Geometry and Notation: Error in angular position of oil film leading edge

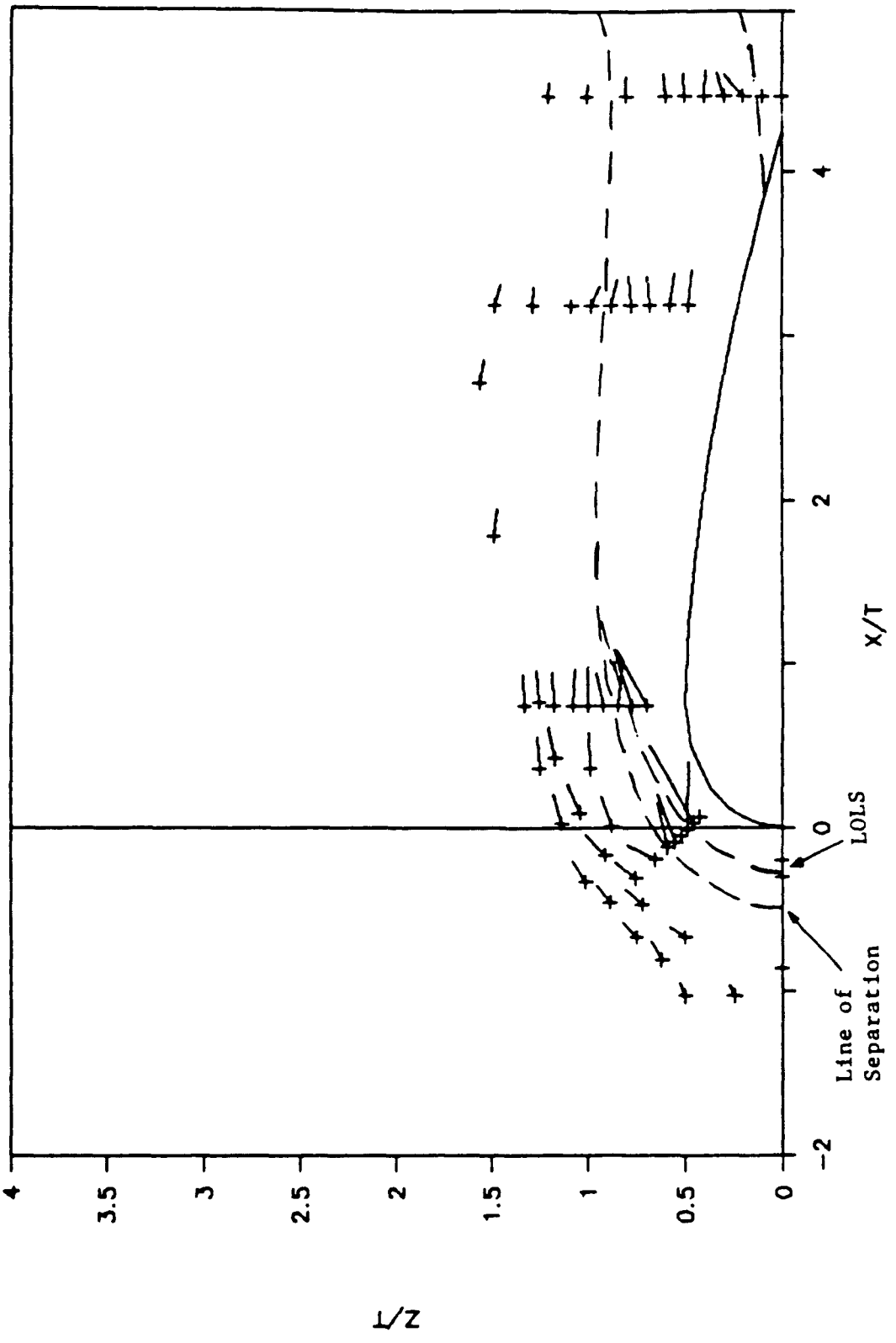

Figure 30. Skin friction coefficient vectors plotted: entire flowfield

Figure 31. Skin friction coefficient vectors plotted: front quadrant

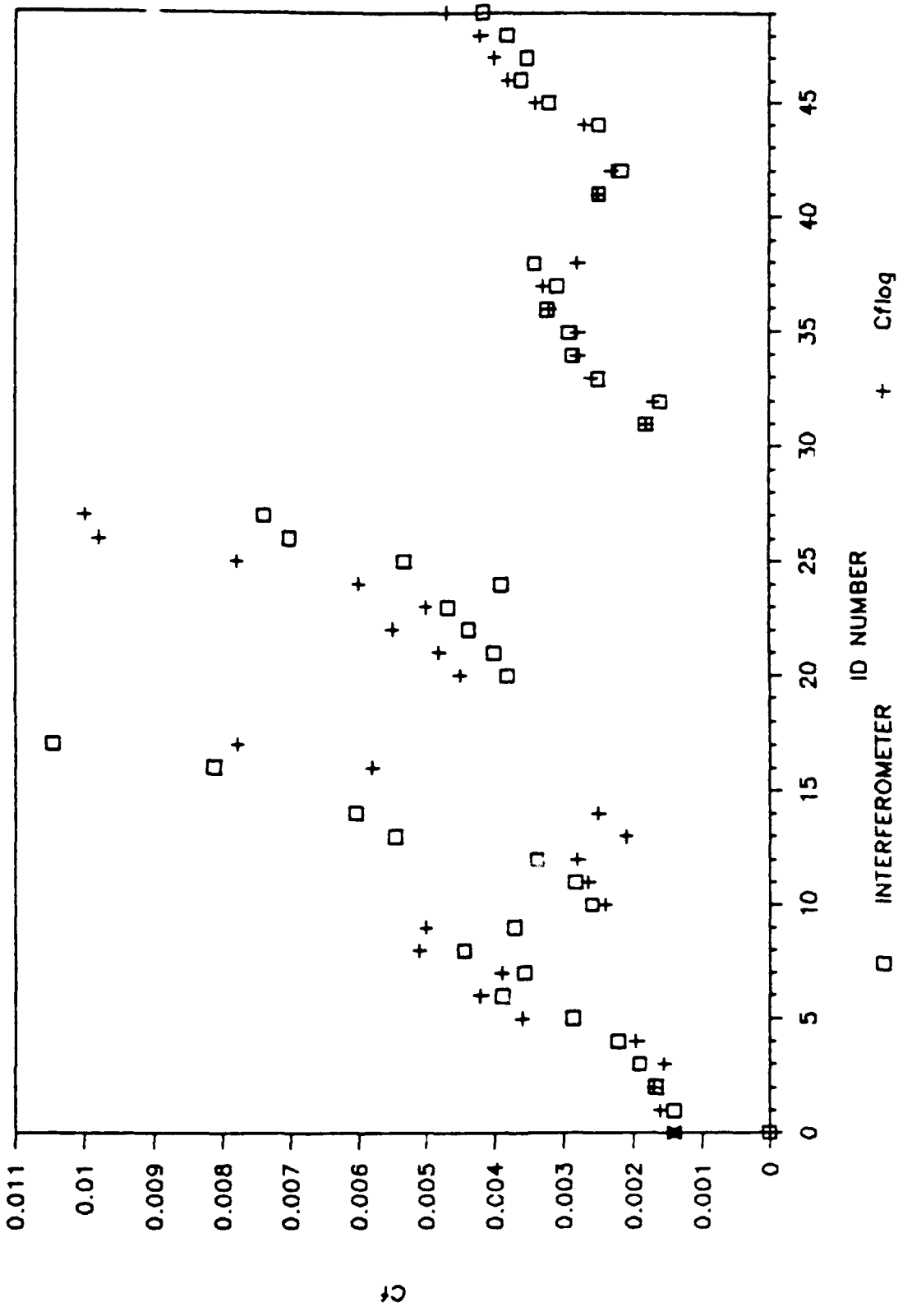

Figure 32. C_f vs. ID number

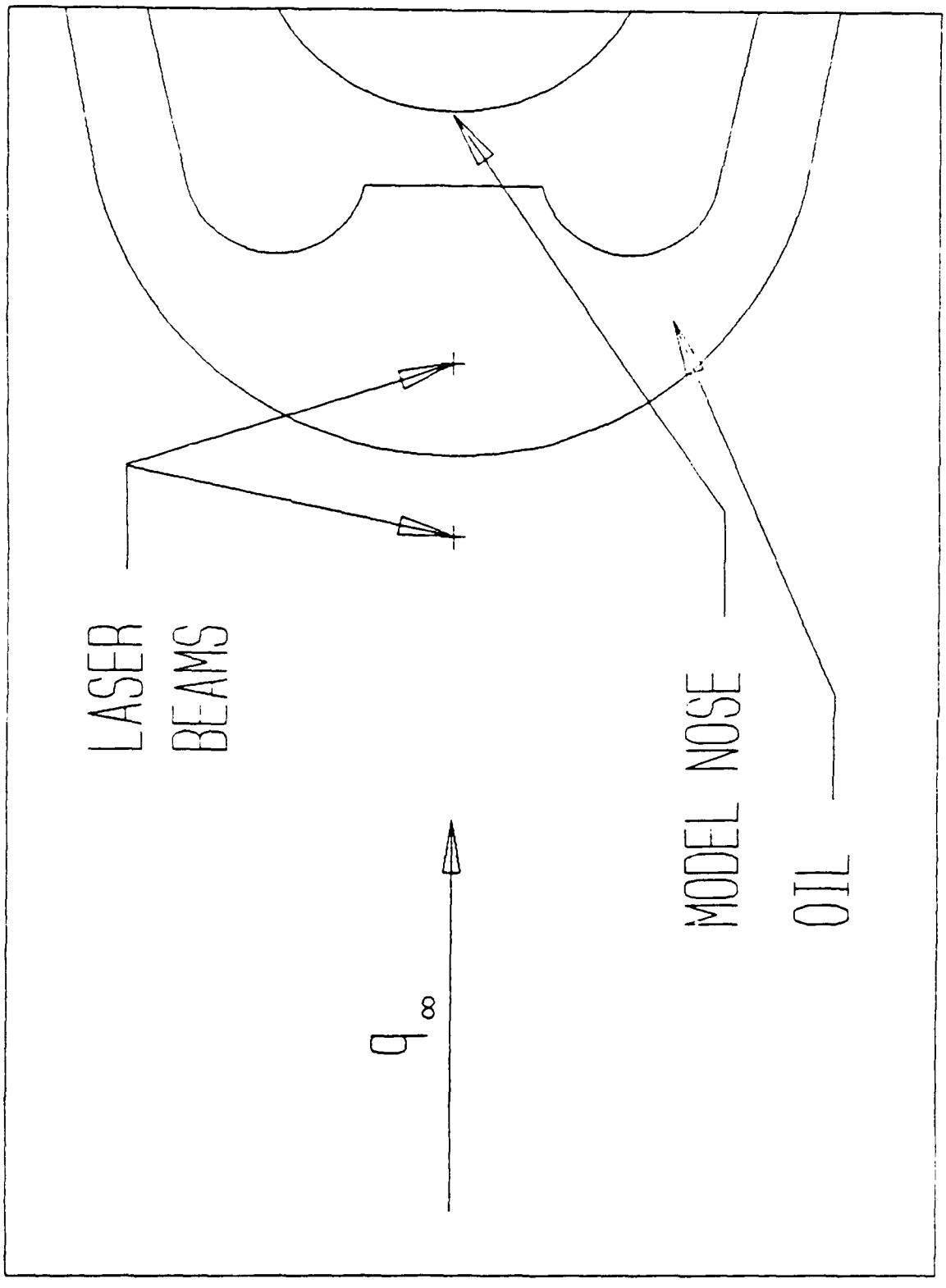

Figure 33. Problem area: oil flow pattern in front of wing leading edge

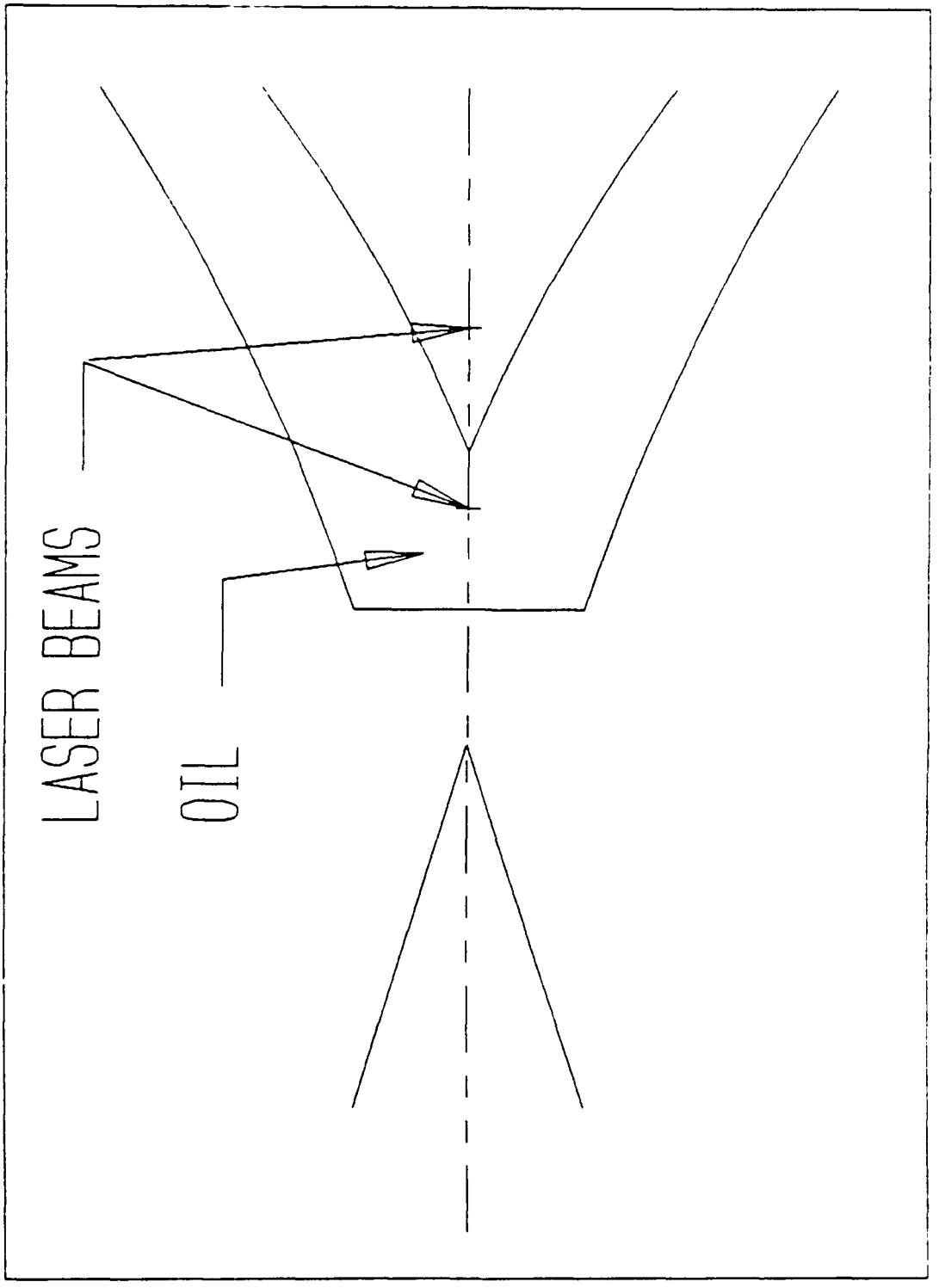

Figure 34. Problem area: oil flow pattern in tail region

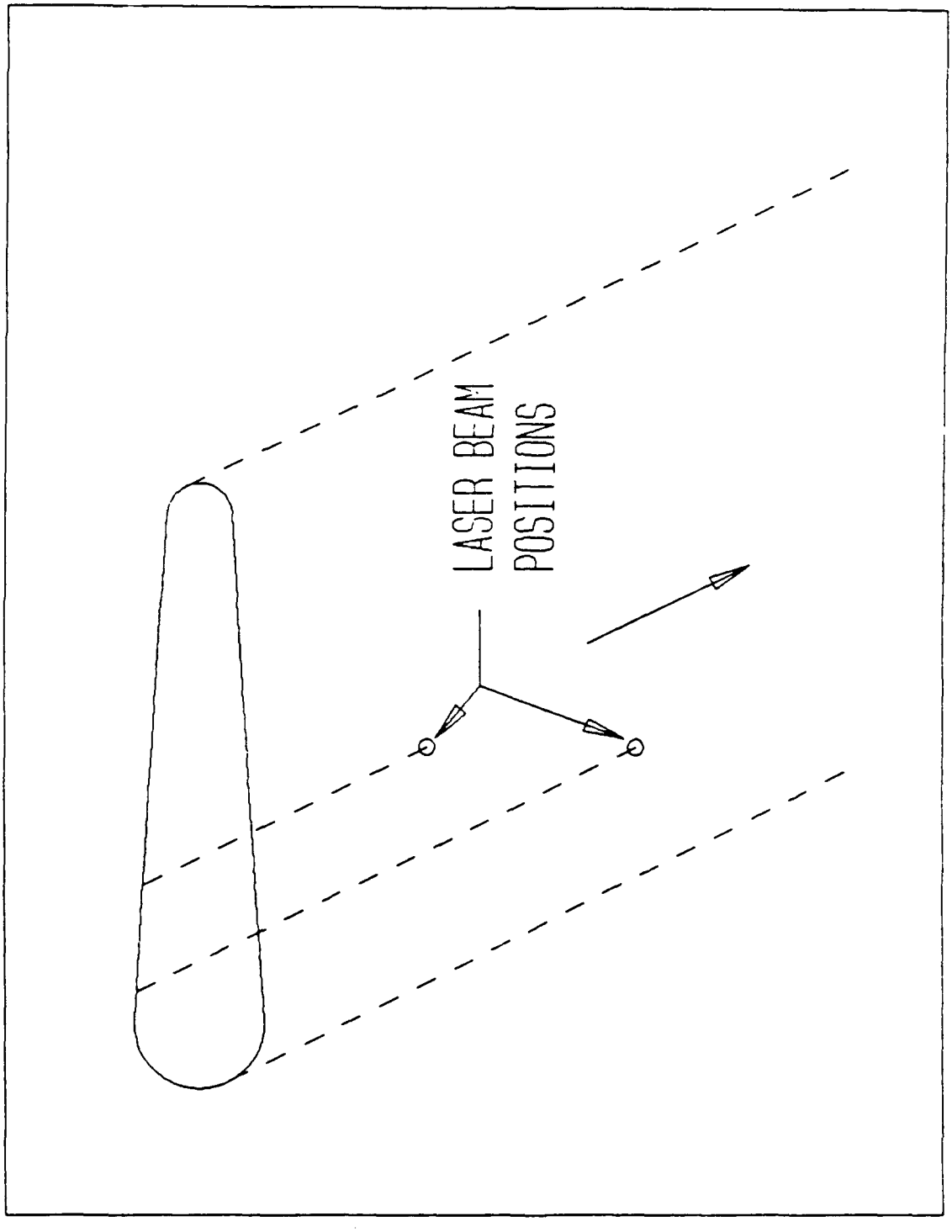

Figure 35. Non-uniform initial oil line thickness

Appendix A. PROGRAM OILAD32.BAS

```
1000 '
1005 DEFINT A-Z
1010 'OIL-FILM INTERFEROMETER A/D PROGRAM, VERSION 3.2 082587
1020 '
1030 'A/D PROGRAM FOR TWO BEAMS & INPUT CHNLS, W/O SCANNER & EXT TRIG
1040 GOSUB 20000
1050 'INPUT PARAMETERS FOR DATA FILE AND A/D CONVERSION
1080 CLS:PRINT:PRINT" OIL A/D PROGRAM & DATA FILE PARAMTERS":PRINT
1120 PRINT" A/D PROGRAM FOR DUAL BEAM LASER INTERFEROMETER ":PRINT
1130 PRINT" FOR USE W/O SCANNER OR EXT TRIGGER (VER. 3.1) ":PRINT
1140 PRINT:INPUT"        X-LOCATION OF MEASUREMENTS          ";X!
1145 PRINT:INPUT"    Z-LOCATION OF MEASUREMENTS  ";Z!
1150 PRINT:INPUT"    REF PRESSURE-Q  (IN. WATER)    ";UREF!
1155 PRINT:INPUT"    NUMBER OF DATA SAMPLES  ";NUM.CONV
1156 PRINT:INPUT"    DATA SAMPLING RATE IN HERTZ   ";HERTZ#
1160 PRINT:INPUT"        DISC FILE FOR RESULTS              ";D$
1180 PRINT:PRINT"    Ensure < CAPS LOCK > is on before continuing"
1190 PRINT:PRINT:PRINT:PRINT"Press any key to continue"
1200 A$ = INKEY$ A$ = "" THEN 1200
1300 CLOSE 1:OPEN D$ FOR OUTPUT AS #1
1310 PRINT#1,"X =  ";X!
1320 PRINT#1,"Z =  ";Z!
1330 PRINT#1,"Q =  ";UREF!
1400 PERIOD# = (1#/(2#*HERTZ#))*1000000#
1450 TICKS# = CINT(PERIOD#/1.25#-32768#) + 32768#
1460 PERIOD# = TICKS#*1.25#
1500 START.CHANNEL = 1:END.CHANNEL = 2
1600 NUM.CONV = ((END.CHANNEL-START.CHANNEL + 1)*NUM.CONV)*2
2000 GOSUB 21000
3060 PARM = (NUM.CONV-4)
4000 FOR ADDRESS = 0 TO PARM STEP 4:TPRINT = PEEK(ADDRESS) + PEEK(ADDRESS + 1)*256!
4005 TPRINTB = PEEK(ADDRESS + 2) + PEEK(ADDRESS + 3)*256!
4010 PRINT#1,TPRINT,TPRINTB
4020 NEXT
4030 END
20000 '
20010 ' Initialise A/D converter
20020 '
20030 BASE.ADDRESS = &H2EC
20040 COMMAND.REGISTER = BASE.ADDRESS + 1
20050 STATUS.REGISTER = BASE.ADDRESS + 1
20060 DATA.REGISTER = BASE.ADDRESS
20070 COMMAND.WAIT = &H4
20080 WRITE.WAIT = &H2
```

```
20090 READ.WAIT = &H5
20100 CSTOP = &HF
20110 CCLEAR = &H1
20120 CERROR = &H2
20130 CCLOCK = &H3
20140 CSAD = &HD
20150 CRAD = &HE
20160 EXT.CLOCK = &H40
20170 EXT.TRIGGER = &H80
20180 CDMA = &H10
20190 DUMMY = 5
20200 DMACHANNEL = 1
20210 DMAMODE = &H45
20220 BASEREG = 2
20230 COUNTREG = 3
20240 PAGEREG = &H83
20250 STARTPAGE = &H3000
20260 DEF SEG = STARTPAGE
20270 DMABASEL = &H0
20280 DMABASEH = &H0
20290 DMAPAGE = STARTPAGE/&H1000
20300 '
20310 'Stop and clear the DT2801.
20320 OUT  COMMAND.REGISTER, CSTOP
20330 TEMP = INP(DATA.REGISTER)
20340 WAIT STATUS.REGISTER,  COMMAND.WAIT
20350 OUT  COMMAND.REGISTER, CCLEAR
20360 '
20370 CLS:PRINT:PRINT"          SETTING UP INTERFACE"
20410 '
20420 'Get A/D gain.
20430 PRINT:INPUT " Gain of A/D (1,2,4 or 8) (2 for +/-5v)";GAIN.CODE
20440 GAIN.CODE = LOG(GAIN.CODE)/LOG(2)
20450 '
20460 'Get A/D channel.
20470 PRINT:INPUT" Signal A (Front Beam)-USE A/D CH #1";S.CHANNEL:PRINT
20480 E.CHANNEL = S.CHANNEL + 1
20490 PRINT"SIGNAL B (REAR BEAM) ON CH#2"
20500 PRINT:PRINT:PRINT"Press any key to continue"
20510 A$ = INKEY$ A$ = "" THEN 20510
20520 RETURN
21000 '
21010 ' Instruct the A/D to take data
21020 '
21030 WAIT STATUS.REGISTER,COMMAND.WAIT
21040 OUT COMMAND.REGISTER,CSAD
21050 WAIT STATUS.REGISTER,WRITE.WAIT,WRITE.WAIT
21060 OUT DATA.REGISTER,GAIN.CODE
21070 WAIT STATUS.REGISTER,WRITE.WAIT,WRITE.WAIT
21080 OUT DATA.REGISTER,START.CHANNEL
21090 WAIT STATUS.REGISTER,WRITE.WAIT,WRITE.WAIT
21100 OUT DATA.REGISTER,END.CHANNEL
21110 WAIT STATUS.REGISTER,WRITE.WAIT,WRITE.WAIT
21120 OUT DATA.REGISTER,DUMMY
21130 WAIT STATUS.REGISTER,WRITE.WAIT,WRITE.WAIT
21140 OUT DATA.REGISTER,DUMMY
21150 WAIT STATUS.REGISTER,COMMAND.WAIT
21160 OUT COMMAND.REGISTER,CCLOCK
21170 PH# = INT(TICKS#/256)
21175 PL# = TICKS#-PH#*256
21180 PERIODH = PH#
21185 PERIODL = PL#
21190 WAIT STATUS.REGISTER,WRITE.WAIT,WRITE.WAIT
21200 OUT DATA.REGISTER,PERIODL
21210 WAIT STATUS.REGISTER,WRITE.WAIT,WRITE.WAIT
21220 OUT DATA.REGISTER,PERIODH
21230 DMACOUNT = (NUM.CONV*2)-1
21240 DMACOUNTH = INT(DMACOUNT/256)
21250 DMACOUNTL = DMACOUNT-DMACOUNTH*256
21260 OUT 11,DMAMODE            ' set DMA mode
21270 OUT 12,0                  ' clear byte flip-flop
21280 OUT BASEREG,DMABASEL      ' set DMA memory base address
```

```
21290 OUT BASEREG,DMABASEH      '
21300 OUT COUNTREG,DMACOUNTL    ' set DMA byte count
21310 OUT COUNTREG,DMACOUNTH    '
21320 OUT PAGEREG,DMAPAGE       ' set DMA memory page
21330 OUT 10,DMACHANNEL         ' enable DMA channel mask
21340 WAIT STATUS.REGISTER,COMMAND.WAIT
21350 STATUS = INP(STATUS.REGISTER)
21360 IF (STATUS AND &H80) THEN GOTO 22000
21370 WAIT STATUS.REGISTER,COMMAND.WAIT
21380 OUT COMMAND.REGISTER,CRAD + CDMA + COMMAND
21390 WAIT STATUS.REGISTER,COMMAND.WAIT
21400 STATUS = INP(STATUS.REGISTER)
21410 IF (STATUS AND &H80) THEN GOTO 22000
21420 RETURN
22000 '
22010 'Error handling for A/D
22020 '
22030 PRINT"FATAL BOARD ERROR"
22040 PRINT"STATUS REGISTER VALUE IS ";HEX$(STATUS);" HEXIDECIMAL"
22050 PRINT:GOSUB 22100
22060 PRINT"ERROR REGISTER VALUES ARE:"
22070 PRINT"     BYTE 1 -  ";HEX$(ERROR1);"  HEXIDECIMAL"
22080 PRINT"     BYTE 2 -  ";HEX$(ERROR2);"  HEXIDECIMAL"
22090 PRINT:GOTO 22240
22100 '
22110 'Read the error register
22120 OUT COMMAND.REGISTER,CSTOP:TEMP = INP(DATA.REGISTER)
22130 WAIT STATUS.REGISTER,COMMAND.WAIT
22140 OUT COMMAND.REGISTER,CERROR
22150 WAIT STATUS.REGISTER,READ.WAIT
22160 ERROR1 = INP(DATA.REGISTER)
22170 WAIT STATUS.REGISTER,READ.WAIT
22180 ERROR2 = INP(DATA.REGISTER)
22190 STOP
22200 '
22210 'Illegal Status Register.
22220 PRINT"FATAL ERROR - ILLEGAL STATUS REGISTER VALUE"
22230 PRINT"STATUS REGISTER VALUE IS ";HEX$(STATUS);" HEXIDECIMAL"
22240 STOP
```

Appendix B. PROGRAM OILCF.FOR

```
CCC --------PROGRAM OILCF----------
C
C
C  VERSION 6 INPUTS NZEROB AND NZEROA MAXIMUMS
C          AND PRINTS T0 FOR EACH BEAM
C          NOTE: PRINTER IS REQUIRED
C
C
CCC REDUCES DIGITAL OUTPUT OF PHOTODIODE TO A COEFFICIENT OF
CCC     SKIN FRICTION BY USE OF OIL LUBRICTION THEORY.
CCC
CCC USES THE FOLLOWING SUBROUTINES :
CCC
CCC     SMTHPD--SMOOTHES RAW DIGITAL OUTPUT OF PHOTODIODE
CCC     SOILFM-IDENTIFIES FRINGES OF PHOTODIODE OUTPUT
CCC     SLUBFT-APPLES LUBRICATION THEORY TO DATA
CCC     CLFCLC--CALCULATES THE WALL SHEAR FOR THE OIL FILM
CCC
CCC     THIS PROGRAM IS BASED ON SUBROUTINE USED BY DR. WESTPHAL
CCC          AT NASA-AMES AND GIVEN IN NASA TM-88216 "IMPROVED
CCC          SKIN FRICTION INTERFEROMETER"
CCC
CCC
CCC
CCC      THIS PROGRAM READS THE INPUT DATA FILE AS A SEQUENTIAL
CCC        ACCESS FILE (FILE #1), PARAMETERS ARE READ IN
CCC         FROM THE SCREEN. OUTPUT FILES WRITTEN ARE:
CCC           #12-SMOOTHED INPUT DATA (INTEGER COUNTS)
CCC           #13 & #14-BEAM A&B ZEROES AND TIME LOCATIONS
CCC SET DIMENSION, REALS, INTEGERS, COMMONS, AND DATA
CCC
      IMPLICIT DOUBLE PRECISION (A-H)
      IMPLICIT DOUBLE PRECISION (O-Z)
      INTEGER IRAWA(5000),IRAWB(5000),NZA(6),NZB(6),ICHK(6),FORM
      CHARACTER*18 SOURCE,OUTFIL
      COMMON/FITCOM/CFNFIT,ASLFIT,TSTFIT,ZERO(200),NZERO,RMSERR
      EXTERNAL FITERR
      DOUBLE PRECISION MUNOM,NOIL,MINUS,ERRA(6),ERRB(6),DT(6),CFM(6),ERO
     !OT(6),T0A(6),T0B(6)
      DO 203, K = 1,6
      ERRA(K) = 0.D0
  203 ERRb(K) = 0.D0
      NUL = 0
      WRITE(*,*)' INPUT NUMBER OF ZEROES TO USE FOR BEAM A'
      READ(*,*)NA
      WRITE(*,*)' INPUT NUMBER OF ZEROES TO USE FOR BEAM B'
      READ(*,*)NB
CCC
CCC
CCC OPEN INPUT AND OUTPUT FILES
CCC
CCC
CCC     INPUT FILE #1--RAW DIGITAL PHOTODIODE OUTPUT
```

```
      WRITE(*,11)
11    FORMAT(5X,'ENTER FILE #1,DATA')
      OPEN(1,FILE=' ',STATUS='OLD')
      INQUIRE(1,NAME=SOURCE)
      OPEN(9,FILE='LPT1',STATUS='OLD')
      WRITE(9,*)SOURCE
CCC
CCC     OUTPUT FILE #12---SMOOTHED INPUT DATA (INTEGER)
      WRITE(*,13)
13    FORMAT(5X,'ENTER FILE #12,OUTPUT')
      OPEN(12,FILE=' ',STATUS='NEW')
CCC     OUTPUT FILE #13-BEAM A ZEROES AND THEIR LOCATIONS
      WRITE(*,14)
14    FORMAT(5X,'ENTER FILE #13,OUTPUT')
      OPEN(13,FILE=' ',STATUS='NEW')
CCC     OUTPUT FILE #14---BEAM B ZEROES AND THEIR LOCATIONS
      WRITE(*,15)
15    FORMAT(5X,'ENTER FILE #14,OUTPUT')
      OPEN(14,FILE=' ',STATUS='NEW')
CCC
CCC     READ IN FREQUENCY OF DATA TO COMPUTE THE DELTA-TIME
CCC       BETWEEN DATA POINTS   (FREQ IN HERTZ)
      WRITE(*,1)
1     FORMAT(2X,'ENTER FREQUENCY (IN HERTZ) OF DATA TO COMPUTE DELTA-T')
      READ(*,*)FREQ
       DELT=1D0/FREQ
CCC READ IN PARAMETER VALUES FOR THE FOLLOWING:
CCC
CCC       PARAMETERS FOR THE SMTHPD SUBROUTINE
CCC  NRAWMX-NUMBER DATA PTS, LENGTH OF IRAWA & IRAWB ARRAYS
CCC  FACTOR-SMOOTHING FACTOR, BTWN 1 & 0  1-FLAT CURVE  0-NO SMOOTH
CCC  MODEP-TYPE OF SMOOTHING,BTWN 0 & 10,0-CAUSAL,1-3 PT (ALSO #
CCC    OF TIMES 3 PT SMOOTHING IS USED IF 1-10)
      WRITE(*,50)
50    FORMAT(5X,'ENTER FACTOR,MODEP')
      READ(*,*)FACTOR,MODEP
CCC
CCC
CCC     PARAMETERS FOR THE SOILFM SUBROUTINE
CCC MINFA&B-MIN ARGUMENT FOR DATA REDUCTION (MIN DIMENSION OF RAW DATA)
CCC MAXFA&B-MAX "                    " (MAX DIMENSION)
CCC NINTA&B-MIN # OF PTS IN ONE INTERVAL USED TO FIND ZERO CROSSING
CC        LINE, GREATER THAN 1
CCC RMSFA&B-FRACTION OF RMS TO USE FOR TESTING IF PT IS IN REGION
CCC       NEAR ZERO
CCC NZMAXA&B-AMT OF STORAGE FOR ZERO( ) IN CALLING PROGRAM
      WRITE(*,51)
51    FORMAT(5X,'ENTER MINFA,MAXFA,NINTA,RMSFA,NZMAXA & -B VALUES')
      READ(*,*)MINFA,MAXFA,NINTA,RMSFA,NZMAXA,MINFB,MAXFB,NINTB,
     &RMSFB,NZMAXB
CCC
CCC
CCC     PARAMETERS FOR THE SLUBFT SUBROUTINE
CCC MODEA&B-SPECIFIES IF INITIAL TIME BASE TO BE FIT OR AN INPUT,
CCC         MODE_=1 TSTFP IS INPUT    MODE_=2 TSTFP FOUND FROM FIT
CCC         TSTFPA & -B ARE THE TIME BASE FOR FIT
      WRITE(*,52)
52    FORMAT(5X,'ENTER MODEA,MODEB,TSTFPA,TSTFPB')
      READ(*,*)MODEA,MODEB,TSTFPA,TSTFPB
CCC
CCC
CCC     PARAMETERS FOR THE FRICTION CALCULATION
CCC TCOIL-OIL TEMP IN DEG CELSIUS
CCC TCNOM-NOMINAL OIL TEMP FOR USE IN DOW CORNING EQN IN DEG CEL
CCC MUNOM-NOMINAL OIL VISCOSITY FOR USE IN DOW CORNING EQN
CCC NOIL-OIL INDEX OF REFRACTION
CCC WLLSER-LASER WAVELENGTH IN METERS, 0.6328X10-6 FOR HE-NE
CCC ANGIN-LASER BEAM INCIDENCE ANGLE IN DEG
CCC DXBEAM-BEAM SEPARATION IN METERS FROM FRONT TO REAR BEAM
      WLLSER=.6328D-06
      WRITE(*,*)' ENTER BEAM SPACING IN mm'
      READ(*,*)DXBEAM
```

```
      DXBEAM = DXBEAM/1000.D0
      MUNOM = .0479538D0
      NOIL = 1.40125D0
      WRITE(*,*)' ENTER ANGLE OF INCIDENCE IN DEGREES'
      READ(*,*)ANGIN
      TCNOM = 25.D0
CCC
CCC
CCC     FLOW PARAMETERS
CCC QE-DYNAMIC PRESSURE OF FLOW, IN. WATER
CCC READ QE FROM SCREEN
      WRITE(*,3)
3     FORMAT(5X,'ENTER QE(DYNAMIC PRESS) IN in. water')
      READ(*,*)QE
C     CONVERT QE FROM IN. WATER TO N/M
      QE = QE*248.9460171D0
CCC READ OI TEMP FROM SCREEN
      WRITE(*,35)
35    FORMAT(5X,'ENTER TCOIL (OIL TEMP IN DEG C) AND PRESSURE
     &GRADIENT (IN N/M
      READ(*,*)TCOIL,DPDX
CCC   NUMBER OF DATA POINTS TO PROCESS
      WRITE(*,4)
4     FORMAT(5X,'ENTER NUMBER OF DATA POINTS TO PROCESS')
      READ(*,*)NRAWMX
      ITYP = 1
      READ(1,30)X,XVAL
      READ(1,30)Y,YVAL
      READ(1,30)Q,QVAL
30    FORMAT(A2,F5.2)
CCC
CCC
CCC READ IN DIGITAL INPUT DATA SIGNAL FROM A/D CONVERTER
CCC     FOR THE PHOTODIODE OUTPUT
      DO 40 I = 1,NRAWMX
      READ(1,*,END = 4000)IRAWA(I),IRAWB(I)
40    CONTINUE
CCC
CCC DO CALCULATIONS
CCC
CCC       CALL SUBROUTINES TO:
CCC          1)SMOOTH OUTPUT OF PHOTODIODE
CCC          2)I.D. FRINGES
CCC          3)FIT LUBRICATION THEORY TO DATA
CCC          4)CALCULATE CF BASED ON TYPE OF OIL
CCC
CCC
CCC          DO THE FOLLOWING SUBROUTINES FOR EACH BEAM
CCC
CCC
CCC     DO SMOOTHING FOR BOTH BEAM A&B AND WRITE THE SMOOTHED
CCC        OUTPUT TO FILE #12
CCC
4000  CONTINUE
      CLOSE(1)
      WRITE(*,100)
100   FORMAT(5X,'ENTRY')
      CALL SMTHPD(IRAWA,NRAWMX,FACTOR,MODEP)
      CALL SMTHPD(IRAWB,NRAWMX,FACTOR,MODEP)
      WRITE(*,55)
55    FORMAT(5X,'SMTHPD CHECK FOR BEAMS A&B-NOW WRITE DATA TO #12')
      DO 600 I = 1,NRAWMX
      WRITE(12,*)IRAWA(I),IRAWB(I)
600   CONTINUE
      CLOSE (12)
      OPEN(2,FILE = 'SOURCE.DAT',STATUS = 'NEW')
      WRITE(2,6674)SOURCE,'OUT'
      REWIND 2
      READ(2,6675)OUTFIL
      CLOSE(2)
      OPEN(3,FILE = OUTFIL,STATUS = 'NEW')
CCC
```

```
CCC    CONTINUE CALCULATIONS FOR ONE BEAM AT A TIME,
CCC     FIRST FOR BEAM A:
CCC
54    CALL SOILFM(IRAWA,NRAWMX,MINFA,MAXFA,NINTA,AVGA,RMSA,RMSFA,
     &ZERO,NZMAXA,NZERO,ITYP)
      THICKA = WLLSER*REAL(NZEROA)
C
C  MAX NZEROA = NA
C
      IF(NZERO.GT.NA) THEN
      L = 0
      DO 700 K = NZERO-NA+1,NZERO
      L = L + 1
  700 ZERO(L) = ZERO(K)
      NZERO = NA
      ENDIF
      WRITE(*,56)
56    FORMAT(5X,'SOILFM A CHECK-AVG,RMS,NZERO')
      WRITE(*,*)AVGA,RMSA,NZERO
      IF(NZERO.EQ.0) THEN
      WRITE(*,*)' NZEROA = 0 FOR THIS CASE'
      WRITE(*,*)' ITYP =',ITYP
      NZEROA = 0
      NZEROB = 0
      AERR = 0.D0
      BERR = 0.D0
      GO TO 6665
      ENDIF
      NZEROA = NZERO
      DO 500 I = 1,NZERO
      ZERO(I) = ZERO(I)*DELT
      WRITE(13,*)I,ZERO(I)
500   CONTINUE
      AZERO1 = ZERO(1)
      CALL SLUBFT(ZERO,NZERO,MODEA,CFNFPA,ASLFPA,TSTFPA,ERROR)
      aerr = error
      WRITE(*,57)CFNFPA,ASLFPA,TSTFPA
57    FORMAT(5X,'SLUBFT CHK, END OF BEAM A CHK-CFNFP,ASLFPA,TSTFPA',
     &,,F12.4,1X,F12.4,1X,F12.4)
CCC   SECOND FOR BEAM B- REAR BEAM
      CALL SOILFM(IRAWB,NRAWMX,MINFB,MAXFB,NINTB,AVGB,RMSB,RMSFB,
     &ZERO,NZMAXB,NZERO,ITYP)
      THICKB = WLLSER*NZEROB
C
C  MAX NZEROB = NB
C
      IF(NZERO.GT.NB) THEN
      L = 0
      DO 710 K = NZERO-NB+1,NZERO
      L = L + 1
  710 ZERO(L) = ZERO(K)
      NZERO = NB
      ENDIF
      WRITE(*,59)
59    FORMAT(5X,'SOILFM B CHECK-AVG,RMS,NZERO')
      WRITE(*,*)AVGB,RMSB,NZERO
      IF(NZERO.EQ.0) THEN
      WRITE(*,*)' NZEROB = 0 FOR THIS CASE'
      WRITE(*,*)' ITYP =',ITYP
      NZEROA = 0
      NZEROB = 0
      BERR = 0.D0
      GO TO 6665
      ENDIF
      NZEROB = NZERO
      DO 7010 I = 1,NZERO
      ZERO(I) = (ZERO(I)*DELT) + .05D0
      WRITE(14,*)I,ZERO(I)
7010  CONTINUE
      BZERO1 = ZERO(1)
      CALL SLUBFT(ZERO,NZERO,MODEB,CFNFPB,ASLFPB,TSTFPB,ERROR)
      BERR = ERROR
```

```
      WRITE(*,60)
60    FORMAT(5X,'SLUBFT B')
      WRITE(*,701)CFNFPB,ASLFPB,TSTFPB
701   FORMAT(5X,'SLUBFT CHK, END OF BEAM B CHK-CFNFP,ASLFPB,TSTFPB',
     &/,F12.4,1X,F12.4,1X,F12.4)
      II=0
      AVGTFB=((TSTFPB+ZERO(NZEROB))-(TSTFPB+ZERO(1)))/2D0
3000  II=II+1
      TFCHKB=TSTFPB+ZERO(II)
      IF(TFCHKB.EQ.AVGTFB) GOTO 3200
      IF(TFCHKB.LT.AVGTFB) GOTO 3000
      TFBPCT=(AVGTFB-(TSTFPB+ZERO(II)))/AVGTFB
      ENBAVG=(CFNFPB-FLOAT(II))-TFBPCT
      GOTO 3500
3200  ENBAVG=CFNFPB-FLOAT(II)
3500  WRITE(*,3550)AVGTFB,TFCHKB,TFBPCT,ENBAVG
3550  FORMAT(2X,'AVG EFFECTIVE TIME,CHECK FOR AVG EFF TIME',/,
     &'PCT DIFFERENCE FOR AVG EFF TIME, AVG EFF FRINGE NUMBER',/,
     &F12.5,2X,F12.5,2X,F8.4,2X,F8.4)
CCC   CALCULATE C(X2)-C(X1) FOR THE SHEAR CALCULATION
      DELNT=1D0*(ASLFPB-ASLFPA)
      WRITE(*,1080)DELNT,aerr,berr
1080  FORMAT(2X,'DELTA CX CHK-DELNT,aerr,berr'/3(2X,F12.4))
CCC   DO ROUTINE TO CALCULATE THE SHEAR
CCC   THEN USE SHEAR TO FIND FRICTION COEFFICIENT
      CALL CFCLC(TCOIL,TCNOM,MUNOM,NOIL,WLLSER,ANGIN,DXBEAM,
     CDPDX,ENBAVG,DELNT,TAU,TAUBAR,EPSI,IER)
      CF=TAUBAR/QE
CCC
CCC
CCC WRITE OUTPUT DATA TO SCREEN
CCC OUTPUT DATA IS TAUBAR,CF,QE,AVG,RMS,NZERO,CFNFP,TSTFP,ASLFP
CCC
4010  FORMAT(5X,'TAUBAR= ',F16.8,/,5X,'CF= ',F16.8,/,5X,'QE= ',
     &F16.8)
      WRITE(*,4010)TAUBAR,CF,QE
      WRITE(*,4020)AVGA,RMSA,NZEROA,CFNFPA,TSTFPA,ASLFPA
      WRITE(*,4030)AVGB,RMSB,NZEROB,CFNFPB,TSTFPB,ASLFPB
      WRITE(*,*)' HEIGHT OF OIL FILM =',CFNFPA*WLLSER*1E6,' microns'
6665  CONTINUE
      DENOM = (TSTFPA+AZERO1 + TSTFPB+BZERO1)*.5d0
      IF(ITYP.LT.6) THEN
      CFM(ITYP) = CF
      ERRA(ITYP) = AERR
      ERRB(ITYP) = BERR
      T0A(ITYP) = TSTFPA
      T0B(ITYP) = TSTFPB
      NZA(ITYP) = NZEROA
      NZB(ITYP) = NZEROB
      DT(ITYP) = ABS(TSTFPA-TSTFPB)/DENOM
      ENDIF
      IF(ITYP.EQ.6) THEN
        ERRA(6) = AERR
        ERRB(6) = BERR
        T0A(6) = TSTFPA
        T0B(6) = TSTFPB
        NZA(6) = NZEROA
        NZB(6) = NZEROB
        DT(6) = ABS(TSTFPA-TSTFPB)/DENOM
        CFM(6) = CF
        CFAVG = (CFM(2)+CFM(3)+CFM(1)+CFM(4)+CFM(5)+CFM(6))/6.D0
        PLUS = DMAX1(CFM(2),CFM(3),CFM(1),CFM(4),CFM(5),CFM(6)) - CFAVG
        MINUS = CFAVG - DMIN1(CFM(2),CFM(3),CFM(1),CFM(4),CFM(5),CFM(6))
        DO 199 IJ = 1,6
 199    EROOT(IJ) = SQRT(ERRA(IJ)*ERRA(IJ) + ERRB(IJ)*ERRB(IJ) + DT(IJ)*
     1DT(IJ))
        WRITE(*,6666)
        DO 201 IJ = 1,6
        IF(IJ.EQ.1)ASSIGN 6667 TO FORM
        IF(IJ.EQ.2)ASSIGN 6668 TO FORM
        IF(IJ.EQ.3)ASSIGN 6669 TO FORM
        IF(IJ.EQ.4)ASSIGN 6670 TO FORM
```

```
      IF(IJ.EQ.5)ASSIGN 6671 TO FORM
      IF(IJ.EQ.6)ASSIGN 6672 TO FORM
      WRITE(3,FORM)NZA(IJ),NZB(IJ),CFM(IJ),ERRA(IJ),ERRB(IJ),DT(IJ)
  201  WRITE(*,FORM)NZA(IJ),NZB(IJ),CFM(IJ),ERRA(IJ),ERRB(IJ),DT(IJ)
      WRITE(*,6673)CFAVG,PLUS,MINUS
      WRITE(9,6666)
      DO 202 IJ = 1,6
      IF(IJ.EQ.1)ASSIGN 6667 TO FORM
      IF(IJ.EQ.2)ASSIGN 6668 TO FORM
      IF(IJ.EQ.3)ASSIGN 6669 TO FORM
      IF(IJ.EQ.4)ASSIGN 6670 TO FORM
      IF(IJ.EQ.5)ASSIGN 6671 TO FORM
      IF(IJ.EQ.6)ASSIGN 6672 TO FORM
  202  WRITE(9,FORM)NZA(IJ),NZB(IJ),CFM(IJ),ERRA(IJ),ERRB(IJ),DT(IJ),T0
     1A(IJ),T0B(IJ)
      WRITE(9,*)' '
C      WRITE(9,*)' HEIGHT OF OIL FILM = ',CFNFPA*WLLSER*1E6,' microns'
C
C *** check for bad cf values ***
C
      DO 204 IJ = 1,6
  204  ICHK(IJ) = 0
      DO 205 IJ = 1,6
      IF(NZB(IJ).EQ.0) ICHK(IJ) = 1
      IF(dt(IJ).GT..02) ICHK(IJ) = 1
      IF(ERRA(IJ).GT..004) ICHK(IJ) = 1
      IF(ERRB(IJ).GT..004) ICHK(IJ) = 1
      IF(NZA(IJ).LT.10) ICHK(IJ) = 1
      IF(NZB(IJ).LT.10) ICHK(IJ) = 1
  205  IF(ICHK(IJ).EQ.1) NUL = NUL + 1
      GO TO 5000
     ENDIF
     ITYP = ITYP + 1
     GO TO 54
CC
CC    ***** WRITE TO OUT FILE *****
CC
5000  CLOSE (3)
     CLOSE (13)
     CLOSE (14)
6666  FORMAT(24X,'CF',10X,'ERRA',7X,'ERRB',8X,'DT')
6667  FORMAT(1X,I2,'/',I2,5X,'0    = ',F12.8,3F11.5,2F16.5)
6668  FORMAT(1X,I2,'/',I2,5X,'M    = ',F12.8,3F11.5,2F16.5)
6669  FORMAT(1X,I2,'/',I2,5X,'P    = ',F12.8,3F11.5,2F16.5)
6670  FORMAT(1X,I2,'/',I2,5X,'0NEG = ',F12.8,3F11.5,2F16.5)
6671  FORMAT(1X,I2,'/',I2,5X,'MNEG = ',F12.8,3F11.5,2F16.5)
6672  FORMAT(1X,I2,'/',I2,5X,'PNEG = ',F12.8,3F11.5,2F16.5)
6673  FORMAT(20x,'CF-AVG = ',F12.8/20X,'MAX-PLUS  = + ',F9.5/20X,'MAX-MINU
    &S = -',F9.5)
6999  FORMAT(F12.8,4F11.5)
6674  FORMAT(A18,t13,a3)
6675  FORMAT(8X,A10)
4030  FORMAT(2X,'AVGB = ',F16.8,/,2X,'RMSB = ',F16.8,/,2X,'NZEROB = ',
    &I4,/,2X,'CFNFPB = ',F16.8,/,2X,'TSTFPB = ',F16.8,/,2X,
    &'ASLFPB = ',F16.8)
4020  FORMAT(2X,'AVGA = ',F16.8,/,2X,'RMSA = ',F16.8,/,2X,'NZEROA = ',
    &I4,/,2X,'CFNFPA = ',F16.8,/,2X,'TSTFPA = ',F16.8,/,2X,
    &'ASLFPA = ',F16.8)
     STOP
     END
CCC
CCC
CCC
CCC ********SUBROUTINES**************
CCC
CCC
     SUBROUTINE SMTHPD(IRAWDT,NRAWMX,FACTOR,MODEP)
CCC
CCC SUBROUTINE SMTHPD--SMOOTH OUTPUT OF PHOTODIODE
CCC
     IMPLICIT DOUBLE PRECISION (A-H)
     IMPLICIT DOUBLE PRECISION (O-Z)
```

```
      INTEGER IRAWDT(NRAWMX)
      IF(MODEP.GT.0) GOTO 250
      IF(FACTOR.LE.0.) GOTO 999
      IF(FACTOR.GT.1.) GOTO 999
      FACT1M = 1.-FACTOR
      SMOOTH = DBLE(IRAWDT(1))
      DO 200 I = 1,NRAWMX
      SMOOTH = SMOOTH*FACTOR + DBLE(IRAWDT(I))*FACT1M
      IRAWDT(I) = INT(SMOOTH + .5)
200   CONTINUE
      GOTO 999
250   CONTINUE
      IMAX = NRAWMX-1
      DO 400 J = 1,MODEP
      OLD = DBLE(IRAWDT(1))
      DO 300 I = 1,IMAX
      SMOOTH = (OLD + DBLE(2*IRAWDT(I) + IRAWDT(I + 1)))/4.0
      OLD = DBLE(IRAWDT(I))
      IRAWDT(I) = INT(SMOOTH + .5)
300   CONTINUE
      SMOOTH = (OLD + 3.0*DBLE(NRAWMX))/4.0
      IRAWDT(NRAWMX) = INT(SMOOTH + .5)
400   CONTINUE
999   RETURN
      END
CCC
CCC
CCC
CCC
CCC
      SUBROUTINE SOILFM(IRAWDT,NRAWMX,MINFIT,MAXFIT,NINTMN,AVG,RMS,
     &RMSFCT,ZERO,NZEMAX,NZERO,ITYP)
CCC SUBROUTINE SOILFM1---FRINGE I.D. ALGORITHM, FINDS ZERO CROSSINGS
CCC                      OF EACH FRINGE
      IMPLICIT DOUBLE PRECISION (A-H)
      IMPLICIT DOUBLE PRECISION (O-Z)
      DOUBLE PRECISION AVG,RMS,ZERO(NZEMAX)
      INTEGER IRAWDT(NRAWMX)
      IF(MINFIT.LT.1) MINFIT = 1
      IF(MAXFIT.GT.NRAWMX) MAXFIT = NRAWMX
      IF((RMSFCT.LT..1D0).OR.(RMSFCT.GT.2.D0)) GOTO 990
      IF((NINTMN.LT.1).OR.(NINTMN.GT.10)) GOTO 990
      AVG = 0.0D0
      RMS = 0.0D0
      DO 300 I = MINFIT,MAXFIT
      IIND = I-MINFIT + 1
      AVG = AVG + (DBLE(IRAWDT(I))-AVG)/DBLE(IIND)
300   CONTINUE
      DO 305 I = MINFIT,MAXFIT
      IIND = I-MINFIT + 1
      DEVIAT = DBLE(IRAWDT(I))-AVG
      RMS = RMS + (DEVIAT*DEVIAT-RMS)/DBLE(IIND)
305   CONTINUE
      RMS = DSQRT(RMS)
      IF(ITYP.EQ.2.OR.ITYP.EQ.5) AVG = AVG - .1*RMS
      IF(ITYP.EQ.3.OR.ITYP.EQ.6) AVG = AVG + .1*RMS
      NZERO = 0
      IENFL = 0
      NIN = 0
      DO 500 I = MINFIT,MAXFIT
      IF(DABS(DBLE(IRAWDT(I))-AVG).LT.(RMS*RMSFCT)) GOTO 410
402   CONTINUE
      IF((IENFL.EQ.1).AND.(NIN.GE.NINTMN)) GOTO 420
405   CONTINUE
      IENFL = 0
      NIN = 0
      GOTO 490
410   CONTINUE
      IF(IENFL.EQ.0) IMIN = I
      IMAX = I
      NIN = IMAX-IMIN + 1
      IENFL = 1
```

```
      IF (I.EQ.MAXFIT) GOTO 402
      GOTO 490
420   CONTINUE
      IF (ITYP.LE.3) THEN
      IF (DBLE(IRAWDT(IMIN)).GE.AVG) GOTO 405
      IF (DBLE(IRAWDT(IMAX)).LE.AVG) GOTO 405
      ELSE
      IF (DBLE(IRAWDT(IMIN)).LE.AVG) GOTO 405
      IF (DBLE(IRAWDT(IMAX)).GE.AVG) GOTO 405
      ENDIF
      SX = 0.0D0
      SY = 0.0D0
      SXX = 0.0D0
      SYY = 0.0D0
      DO 450 JJ = IMIN,IMAX
      RJJ = DBLE(JJ-IMIN)
      SX = SX + RJJ
      SXX = SXX + RJJ*RJJ
      SY = SY + DBLE(IRAWDT(JJ))-AVG
      SXY = SXY + (DBLE(IRAWDT(JJ))-AVG)*RJJ
450    CONTINUE
      D = DBLE(NIN)*SXX-SX*SX
      A = (SXX*SY-SX*SXY) D
      B = (DBLE(NIN)*SXY-SX*SY) D
      ZDUM = -A B + DBLE(IMIN)
      WRITE(*,3000) B,IMIN,IMAX,ZDUM
3000  FORMAT(' B = ',E15.7,' IMIN = ',I5,' IMAX = ',I5,' ZERO = ',E15.7)
      IF(B.LE.0.) GOTO 405
      IF((ZDUM.LT.DBLE(IMIN)).OR.(ZDUM.GT.DBLE(IMAX))) GOTO 405
      NZERO = NZERO + 1
      IF(NZERO.GT.NZEMAX) STOP 'SCZERO: LACK OF STORAGE'
      ZERO(NZERO) = -A/B + DBLE(IMIN)
      GOTO 405
499    CONTINUE
500    CONTINUE
      GOTO 999
990    STOP 'SCZERO : BAD ARGUMENT VALUE'
999    RETURN
      END
CCC
CCC
CCC
CCC
CCC SUBROUTINE SLUBFT TO FIT DATA TO LINEAR LUBRICATION THEORY
CCC
SUBROUTINE SLUBFT(ZEROP,NZEROP,MODELF,CFNFP,ASLFP,TSTFP,ERROR)
      IMPLICIT DOUBLE PRECISION (A-H)
      IMPLICIT DOUBLE PRECISION (O-Z)
      DOUBLE PRECISION PARAM(2),DELTA(2),ZEROP(200)
      COMMON/FITCOM/ CFNFIT,ASLFIT,TSTFIT,ZERO(200),NZERO,RMSERR
      EXTERNAL FITERR
      ABSERR = 0.0025D0
      TOL = 0.00002D0
      ERRMAX = 0.05D0
      ITMAX = 100
      NZERO = NZEROP
      DO 5 I = 1,NZERO
5     ZERO(I) = ZEROP(I)
      CFNFIT = DBLE(NZERO)
      IF(MODELF.EQ.1) TSTFIT = TSTFP
      IF(MODELF.EQ.2) TSTFIT = 0.0D0
      DELTA(1) = 1.0D0
      DELTA(2) = ZERO(2)-ZERO(1)
      PARAM(1) = CFNFIT
      PARAM(2) = TSTFIT
      OLDERR = FITERR(MODELF,PARAM)
      ITNO = 0
15    ITNO = ITNO + 1
      CALL GRIDLS(MODELF,PARAM,DELTA,DUM,FITERR)
      WRITE(*,2000)ITNO,DUM
2000  FORMAT('ITERATION NO. = ',I5,'ERROR = ',F12.5)
      CFNFIT = PARAM(1)
```

```
      TSTFIT = PARAM(2)
      IF(DUM.LT.ABSERR.and.dabs(dum-olderr).lt.tol)GOTO 20
      IF(DABS(DUM-OLDERR).LT.TOL) GOTO 20
      IF((ITNO.GT.ITMAX).AND.(DUM.LT.ERRMAX)) GOTO 20
      IF(ITNO.GT.ITMAX)GOTO 990
      OLDERR = DUM
      GOTO 15
20    CFNFP = CFNFIT
      ASLFP = ASLFIT
      TSTFP = TSTFIT
      ERROR = DUM
      GOTO 999
990   CONTINUE
      STOP 'SCCFIT: NO CONVERGENCE'
999   RETURN
      END
      DOUBLE PRECISION FUNCTION FITERR(MODELF,PARAM)
      IMPLICIT DOUBLE PRECISION (A-H)
      IMPLICIT DOUBLE PRECISION (O-Z)
      DOUBLE PRECISION PARAM(2)
      COMMON FITCOM CFNFIT,ASLFIT,TSTFIT,ZERO(200),NZERO,RMSERR
      CFNFIT = PARAM(1)
      IF(MODELF.EQ.2) TSTFIT = PARAM(2)
      SC = 0.
      SCC = 0.
      DO 1 I = 1,NZERO
      CI = (CFNFIT-DBLE(I))*(ZERO(I)+TSTFIT)
      SC = SC + (CI-SC) DBLE(I)
      SCC = SCC + (CI*CI-SCC) DBLE(I)
1     CONTINUE
      RMSERR = DSQRT(SCC-SC*SC)
      ASLFIT = SC
      FITERR = RMSERR/ASLFIT
      RETURN
      END
CCC
CCC SUBROUTINE GRIDLS
CCC
      SUBROUTINE GRIDLS(NTERMS,A,DELTAA,CHISQR,FCHISQ)
      IMPLICIT DOUBLE PRECISION (A-H)
      IMPLICIT DOUBLE PRECISION (O-Z)
      DIMENSION A(NTERMS),DELTAA(NTERMS)
      CHISQR = 0.0D0
      DO 90 J = 1,NTERMS
      CHISQ1 = FCHISQ(NTERMS,A)
      FN = 0.0D0
      DELTA = DELTAA(J)
41    A(J) = A(J) + DELTA
      CHISQ2 = FCHISQ(NTERMS,A)
      IF(CHISQ1-CHISQ2) 51,41,61
51    DELTA = -DELTA
      A(J) = A(J) + DELTA
      SAVE = CHISQ1
      CHISQ1 = CHISQ2
      CHISQ2 = SAVE
61    FN = FN + 1.
      A(J) = A(J) + DELTA
      CHISQ3 = FCHISQ(NTERMS,A)
      IF(CHISQ3-CHISQ2) 71,81,81
71    CHISQ1 = CHISQ2
      CHISQ2 = CHISQ3
      GOTO 61
81    DELTA = DELTA*(1.D0/(1.D0 + (CHISQ1-CHISQ2)/(CHISQ3-CHISQ2)) + 0.5D0)
      A(J) = A(J)-DELTA
84    DELTAA(J) = DELTAA(J)*FN/3.D0
90    CONTINUE
      CHISQR = FCHISQ(NTERMS,A)
      RETURN
      END
CCC
CCC SUBROUTINE CFCLC-TO CALCULATE THE FRICTION COEFF
```

```
CC
CCC
      SUBROUTINE CFCLC(TCOIL,TCNOM,MUNOM,NOIL,WLLSER,ANGIN,DXBEAM,
     &DPDX,ENBAVG,DELNT,TAU,TAUBAR,EPSI,IER)
      IMPLICIT DOUBLE PRECISION (A-H)
      IMPLICIT DOUBLE PRECISION (O-Z)
      DOUBLE PRECISION PI,MUOIL,OPOIL,MUNOM,NOIL
      PARAMETER (PI = 3.1415926D0)
      INTEGER IER
      IER = 1
      IF((TCOIL.LT.0.D0).OR.(TCOIL.GT.100.D0)) GOTO 990
      IF((TCNOM.LT.-200.D0).OR.(TCNOM.GT.200.D0)) GOTO 990
      IF((MUNOM.LT.0.D0).OR.(MUNOM.GT.1.D6)) GOTO 990
      IF((WLLSER.LT.0.D0).OR.(WLLSER.GT.10.D-6)) GOTO 990
      IF((NOIL.LT.0.D0).OR.(NOIL.GT.5.D0)) GOTO 990
      IF((ANGIN.LT.0.D0).OR.(ANGIN.GT.90.D0)) GOTO 990
      IF((DXBEAM.LT.0.D0).OR.(DXBEAM.GT.1.D0)) GOTO 990
      IF((DELNT.LT.-1.D-6).OR.(DELNT.GT.1.D6)) GOTO 990
      MUOIL = MUNOM/(DEXP(0.0146D0*(TCOIL-TCNOM)))
      ANGOIL = DASIN(DSIN(PI*ANGIN/180.D0)/NOIL)
      OPOIL = WLLSER/(2.D0*NOIL*DCOS(ANGOIL))
      TAU = MUOIL*DXBEAM*DELNT/OPOIL
      EPSI = (OPOIL*DPDX*ENBAVG)/TAU
      TAUBAR = TAU/(1D0-EPSI)
      GOTO 999
990   IER = 0
999   RETURN
      END
```

Appendix C. PROGRAM PMCF.FOR

```
      IMPLICIT DOUBLE PRECISION (A-H,O-Z)
      CHARACTER*2 PT,ANG,T,END*4,OUTFIL(9)*17,REDFIL(9)*17,END2*4,PRE*7,
     1PRE2*7
      DIMENSION CF00(6),CF45(6),CF60(6),C0(3),C45(3),C60(3),DC0(3),DC45(
     13),DC60(3),DCX0(3),DCX45(3),DCX60(3),DCZ0(3),DCZ45(3),DCZ60(3),HT0
     2(3),HT45(3),HT60(3),AXWT(9),AZWT(9),CM(9),COSA(9),COSG(9),SINA(9),
     3Q(9),PX(9),PZ(9),QX(9),QZ(9),TX(9),TZ(9),AMAT(9,10),DUM(9,10)
      OPEN(1,FILE='DATFIL.DAT',STATUS='NEW')
 1000 FORMAT(A2)
 1010 FORMAT(1X,A7,3A2,A4)
 1020 FORMAT(A18)
 1030 FORMAT(1X,'POINT NUMBER',A3,':'/11X,'N0 =',I3,5X,'N45 =',I3,5X,'N6
     10 =',I3/11X,'MAGNITUDE =',F11.7,10X,'ANGLE =',F7.1,' degrees'/19X,'
     2+/-',F7.1,'%',17X,'+/-',F7.1,' degrees'/)
 1035 FORMAT(10X,'CXBAR =',F11.7,20X,'CZBAR =',F11.7/9X,'DCXBAR =',F1
     11.7,'%'19X,'DCZBAR =',F11.7,'%'/13X,'SIGCX =',F11.7,'%',20X,'SIG
     2CZ =',F11.7,'%')
 1036 FORMAT(10X,'DCX0(',I1,') =',F11.7,'%',17X,'DCZ0(',I1,') =',F11
     1.7,'%')
 1037 FORMAT(10X,'DCX45(',I1,') =',F11.7,'%',17X,'DCZ45(',I1,') =',F11
     1.7,'%')
 1038 FORMAT(10X,'DCX60(',I1,') =',F11.7,'%',17X,'DCZ60(',I1,') =',F11
     1.7,'%')
 1039 FORMAT(')
 1040 FORMAT(18X,F11.7,3F11.5)
 1046 FORMAT(13X,'C0(',I1,') =',F11.7,17X,'DC0(',I1,') =',F11.7)
 1047 FORMAT(13X,'C45(',I1,') =',F11.7,17X,'DC45(',I1,') =',F11.7)
 1048 FORMAT(13X,'C60(',I1,') =',F11.7,17X,'DC60(',I1,') =',F11.7)
 1050 FORMAT(1X,'DIFF =',F11.8,'%')
 1111 FORMAT(5X,'1',7X,'2',7X,'3',7X,'4',7X,'5',7X,'6',7X,'7'
     1,7X,'8',7X,'9',7X,'10')
 1112 FORMAT(10D8.1)
C
C     ***** INITIALIZE VARIABLES *****
C
      R2D = 180./(4.*ATAN(1.))
      PI = 4.*ATAN(1.)
      N0 = 0
      N45 = 0
      N60 = 0
      SIGCX = 0
      SIGCZ = 0
      DELX0 = 0
      DELZ0 = 0
      DELX45 = 0
      DELZ45 = 0
      DELX60 = 0
      DELZ60 = 0
      DO 301 K = 1,3
      C0(K) = 0
      DC0(K) = 0
      C45(K) = 0
      DC45(K) = 0
```

```
      C60(K) = 0
  301 DC60(K) = 0
      COS45 = COS(PI*.25)
      SIN45 = COS45
      COS60 = COS(PI/3.)
      SIN60 = SIN(PI/3.)
      BETA = 3.*PI/180.
C
C     ***** GENERATE NINE FILENAMES *****
C
      WRITE(*,*)' ENTER POINT NUMBER'
      READ(*,1000) PT
      WRITE(*,*)' ENTER INITIAL GUESS FOR ALPHA'
      READ(*,*)ALPHA
      ALPHA = ALPHA/R2D
      END = '.OUT'
      END2 = '.RED'
      PRE = 'C:\OUT\'
      PRE2 = 'C:\RED\'
      K = 1
      ANG = '00'
    1 DO 10 I = 1,3
      IF(I.EQ.1)T = 'T1'
      IF(I.EQ.2)T = 'T2'
      IF(I.EQ.3)T = 'T3'
      WRITE(1,1010)PRE2,PT,ANG,T,END2
   10 WRITE(1,1010)PRE,PT,ANG,T,END
      IF(K.EQ.1)THEN
        ANG = '45'
      ELSE
        ANG = '60'
      ENDIF
      K = K + 1
      IF(K.LT.4) GO TO 1
      REWIND 1
      DO 20 I = 1,9
      READ(1,1020) REDFIL(I)
   20 READ(1,1020) OUTFIL(I)
      CLOSE (1)
C
C     ***** READ IN CF VALUES *****
C
      DO 40 I = 1,3
      I0 = 0
      OPEN(1,FILE = REDFIL(I),STATUS = 'OLD',IOSTAT = ION)
      IF(ION.NE.0) THEN
        WRITE(*,*)' REDFILE',I,' NOT FOUND'
      ELSE
      READ(1,*)HT0(I)
      ENDIF
      CLOSE(1)
      J = 1
      OPEN(1,FILE = OUTFIL(I),STATUS = 'OLD',IOSTAT = IONUM)
      IF(IONUM.NE.0) GO TO 39
   29 I0 = I0 + 1
   30 READ(1,1040)CF00(I0),ERRA,ERRB,DT
      J = J + 1
      IF(ERRA.GT..004.OR.ERRB.GT..004.OR.ERRA.LT..00001.OR.ERRB.LT..0000
     11.OR.DT.GT..00001) THEN
        IF(J.LT.7) THEN
          GOTO 30
        ENDIF
      ENDIF
      IF(J.LT.7) GOTO 29
      IF(I0.LT.2) GOTO 39
      N0 = N0 + 1
      HT0(N0) = HT0(I)
      DO 35 JJ = 1,I0
      CF00(JJ) = CF00(JJ)*(1. - COS(-ALPHA)*HT0(N0))
   35 C0(N0) = C0(N0) + CF00(JJ)
      C0(N0) = C0(N0)/I0
      FACTOR = (1.-HT0(N0)*COS(-ALPHA))
```

```
   DO 36 JJ = 1,I0
36 DC0(N0) = DC0(N0) + (CF00(JJ) - C0(N0))**2
   DC0(N0) = SQRT(DC0(N0)/(I0-1))
39 CLOSE(1)
40 CONTINUE
   DO 60 I = 4,6
   I45 = 0
   OPEN(1,FILE = REDFIL(I),STATUS = 'OLD',IOSTAT = ION)
   IF(ION.NE.0) THEN
    WRITE(*,*)' REDFILE',I,' NOT FOUND'
   ELSE
   READ(1,*)HT45(I-3)
   ENDIF
   CLOSE(1)
   J = 1
   OPEN(1,FILE = OUTFIL(I),STATUS = 'OLD',IOSTAT = IONUM)
   IF(IONUM.NE.0) GO TO 59
49 I45 = I45 + 1
50 READ(1,1040)CF45(I45),ERRA,ERRB,DT
   J = J + 1
   IF(ERRA.GT..004.OR.ERRB.GT..004.OR.ERRA.LT..00001.OR.ERRB.LT..0000
  11.OR.DT.GT..00001) THEN
    IF(J.LT.7) THEN
     GOTO 50
    ENDIF
   ENDIF
   IF(J.LT.7) GOTO 49
   IF(I45.LT.2) GOTO 59
   N45 = N45 + 1
   HT45(N45) = HT45(I-3)
   DO 55 JJ = 1,I45
   CF45(JJ) = CF45(JJ)*(1. - COS(PI*.25-ALPHA)*HT45(N45))
55 C45(N45) = C45(N45) + CF45(JJ)
   C45(N45) = C45(N45)/I45
   DO 56 JJ = 1,I45
56 DC45(N45) = DC45(N45) + (CF45(JJ) - C45(N45))**2
   DC45(N45) = SQRT(DC45(N45)/(I45-1))
59 CLOSE(1)
60 CONTINUE
   DO 80 I = 7,9
   I60 = 0
   OPEN(1,FILE = REDFIL(I),STATUS = 'OLD',IOSTAT = ION)
   IF(ION.NE.0) THEN
    WRITE(*,*)' REDFILE',I,' NOT FOUND'
   ELSE
   READ(1,*)HT60(I-6)
   ENDIF
   CLOSE(1)
   J = 1
   OPEN(1,FILE = OUTFIL(I),STATUS = 'OLD',IOSTAT = IONUM)
   IF(IONUM.NE.0) GO TO 79
69 I60 = I60 + 1
70 READ(1,1040)CF60(I60),ERRA,ERRB,DT
   J = J + 1
   IF(ERRA.GT..004.OR.ERRB.GT..004.OR.ERRA.LT..00001.OR.ERRB.LT..0000
  11.OR.DT.GT..00001) THEN
    IF(J.LT.7) THEN
     GOTO 70
    ENDIF
   ENDIF
   IF(J.LT.7) GOTO 69
   IF(I60.LT.2) THEN
    I60 = I60-1
    GOTO 79
   ENDIF
   N60 = N60 + 1
   HT60(N60) = HT60(I-6)
   DO 75 JJ = 1,I60
   CF60(JJ) = CF60(JJ)*(1. - COS(PI/3.-ALPHA)*HT60(N60))
75 C60(N60) = C60(N60) + CF60(JJ)
   C60(N60) = C60(N60)/REAL(I60)
   DO 76 JJ = 1,I60
```

```
   76 DC60(N60) = DC60(N60) + (CF60(JJ) - C60(N60))**2
      DC60(N60) = SQRT(DC60(N60)/(160-1))
   79 CLOSE(1)
   80 CONTINUE
C
C  COMPUTE MAGNITUDE AND DIRECTION
C
      OLDA = ALPHA
      NTOT = N0 + N45 + N60
  150 CONTINUE
      CALL LSQ(N0,N45,N60,C0,C45,C60,CX,CZ,AEL,BEL,DEL,DENOM)
      CXBAR = CX
      CZBAR = CZ
      ALPHA = ATAN(CZ/CX)
      WRITE(*,*)' ALPHA = ',ALPHA*R2D
      IF(ABS(ALPHA-OLDA).GT..05/R2D) THEN
      DO 147 JJ = 1,N0
      C0(JJ) = C0(JJ)*(1.-HT0(JJ)*COS(-ALPHA))/(1.-HT0(JJ)*COS(OLDA))
  147 FACTOR = (1.-HT0(JJ)*COS(-ALPHA))
C 147 WRITE(*,*)' C0(JJ),FACTOR',C0(JJ),FACTOR
      DO 148 JJ = 1,N45
      C45(JJ) = C45(JJ)*(1.-HT45(JJ)*COS(PI*.25-ALPHA))/(1.-HT45(JJ)*COS
     1(PI*.25-OLDA))
  148 FACTOR = 1.-HT45(JJ)*COS(PI*.25-ALPHA)
C 148 WRITE(*,*)' C45(JJ),FACTOR',C45(JJ),FACTOR
      DO 149 JJ = 1,N60
      C60(JJ) = C60(JJ)*(1.-HT60(JJ)*COS(PI/3.-ALPHA))/(1.-HT60(JJ)*COS(
     1PI/3.-OLDA))
  149 FACTOR = (1.-HT60(JJ)*COS(PI/3.-ALPHA))
C 149 WRITE(*,*)' C60(JJ),FACTOR',C60(JJ),FACTOR
      OLDA = ALPHA
      GO TO 150
      ENDIF
      DO 151 JJ = 1,N0
  151 DC0(JJ) = SQRT(DC0(JJ)*DC0(JJ) +((1.-1./(1.-TAN(-ALPHA)*TAN(BETA))
     1)*C0(JJ))**2)
      DO 160 JJ = 1,N0
      SIGCZ = SIGCZ + (C0(JJ)*TAN(ALPHA)-CZBAR)**2
  160 SIGCX = SIGCX + (C0(JJ) - CXBAR)**2
      DO 161 JJ = 1,N45
  161 DC45(JJ) = SQRT(DC45(JJ)*DC45(JJ) +((1.-1./(1.-TAN(PI*.25-ALPHA)*T
     1AN(BETA)))*C45(JJ))**2)
      DO 170 JJ = 1,N45
      SIGCX = SIGCX + (C45(JJ)*COS(ALPHA) COS(PI*.25-ALPHA) - CXBAR)**2
  170 SIGCZ = SIGCZ + (C45(JJ)*SIN(ALPHA)/COS(PI*.25-ALPHA) - CZBAR)**2
      DO 171 JJ = 1,N60
  171 DC60(JJ) = SQRT(DC60(JJ)*DC60(JJ) +((1.-1./(1.-TAN(PI/3.-ALPHA)*TA
     1N(BETA)))*C60(JJ))**2)
      DO 180 JJ = 1,N60
      SIGCX = SIGCX + (C60(JJ)*COS(ALPHA) COS(PI/3.-ALPHA) - CXBAR)**2
  180 SIGCZ = SIGCZ + (C60(JJ)*SIN(ALPHA)/COS(PI/3.-ALPHA) - CZBAR)**2
      SIGCX = SIGCX/NTOT
      SIGCZ = SIGCZ/NTOT
C
C     ***** ITERATE TO GET UNCERTAINTIES *****
C
      DO 190 K = 1,N0
      C0(K) = C0(K) + DC0(K)
      CALL LSQ(N0,N45,N60,C0,C45,C60,CX,CZ,AEL,BEL,DEL,DENOM)
      C0(K) = C0(K) - DC0(K)
      DCX0(K) = (CXBAR - CX)**2
  190 DCZ0(K) = (CZBAR - CZ)**2
      DO 200 K = 1,N45
      C45(K) = C45(K) + DC45(K)
      CALL LSQ(N0,N45,N60,C0,C45,C60,CX,CZ,AEL,BEL,DEL,DENOM)
      C45(K) = C45(K) - DC45(K)
      DCX45(K) = (CXBAR - CX)**2
C     WRITE(*,*)' CX,CXBAR = ',CX,CXBAR
  200 DCZ45(K) = (CZBAR - CZ)**2
      DO 210 K = 1,N60
      C60(K) = C60(K) + DC60(K)
      CALL LSQ(N0,N45,N60,C0,C45,C60,CX,CZ,AEL,BEL,DEL,DENOM)
```

```
      C60(K) = C60(K) - DC60(K)
      DCX60(K) = (CXBAR - CX)**2
  210 DCZ60(K) = (CZBAR - CZ)**2
C
C     ***** COMPUTE FINAL UNCERTAINTY ON CX AND CZ *****
C
      DO 220 K = 1,N0
      DELX0 = DELX0 + DCX0(K)
  220 DELZ0 = DELZ0 + DCZ0(K)
      DO 230 K = 1,N45
      DELX45 = DELX45 + DCX45(K)
  230 DELZ45 = DELZ45 + DCZ45(K)
      DO 240 K = 1,N60
      DELX60 = DELX60 + DCX60(K)
  240 DELZ60 = DELZ60 + DCZ60(K)
C
      DCXBAR = SQRT(SIGCX + DELX0 + DELX45 + DELX60)
      DCZBAR = SQRT(SIGCZ + DELZ0 + DELZ45 + DELZ60)
C
C     ***** COMPUTE MAGNITUDE AND DIRECTION AND PRINT OUTPUT *****
C
      CFMAG = SQRT(CXBAR*CXBAR + CZBAR*CZBAR)
      ANGLE = ATAN(CZBAR/CXBAR)*180./PI
      DADX = CZBAR/(CZBAR*CZBAR + CXBAR*CXBAR)
      DADZ = CXBAR/(CXBAR*CXBAR + CZBAR*CZBAR)
      DCANG = SQRT(DADX*DADX*DCXBAR*DCXBAR + DADZ*DADZ*DCZBAR*DCZBAR)
      DCANG = DCANG*180./PI
      DCMDCX = CXBAR*CXBAR/(CFMAG*CFMAG)
      DCMDCZ = CZBAR*CZBAR/(CFMAG*CFMAG)
      DCM = SQRT(DCMDCX*DCXBAR*DCXBAR + DCMDCZ*DCZBAR*DCZBAR)
      DCM = DCM/CFMAG*100.
      DCXBAR = DCXBAR/CXBAR*100.
      DCZBAR = DCZBAR/CZBAR*100.
      SIGCX = SQRT(SIGCX)/CXBAR*100.
      SIGCZ = SQRT(SIGCZ)/CZBAR*100.
      OPEN(2,FILE='LPT1',STATUS='OLD')
      WRITE(*,1030)PT,N0,N45,N60,CFMAG,ANGLE,DCM,DCANG
      WRITE(*,1035)CXBAR,CZBAR,DCXBAR,DCZBAR,SIGCX,SIGCZ
C       DO 250 JJ = 1,3
C       DCX0(JJ) = SQRT(DCX0(JJ))/CXBAR*100.
C       DCZ0(JJ) = SQRT(DCZ0(JJ))/CZBAR*100.
C 250 WRITE(*,1036)JJ,DCX0(JJ),JJ,DCZ0(JJ)
C       DO 260 JJ = 1,3
C       DCX45(JJ) = SQRT(DCX45(JJ))/CXBAR*100.
C       DCZ45(JJ) = SQRT(DCZ45(JJ))/CZBAR*100.
C 260 WRITE(*,1037)JJ,DCX45(JJ),JJ,DCZ45(JJ)
C       DO 270 JJ = 1,3
C       DCX60(JJ) = SQRT(DCX60(JJ))/CXBAR*100.
C       DCZ60(JJ) = SQRT(DCZ60(JJ))/CZBAR*100.
C 270 WRITE(*,1038)JJ,DCX60(JJ),JJ,DCZ60(JJ)
      WRITE(2,1030)PT,N0,N45,N60,CFMAG,ANGLE,DCM,DCANG
C       WRITE(2,1035)CXBAR,CZBAR,DCXBAR,DCZBAR,SIGCX,SIGCZ
C       DO 280 JJ = 1,3
C 280 WRITE(2,1036)JJ,DCX0(JJ),JJ,DCZ0(JJ)
C       DO 290 JJ = 1,3
C 290 WRITE(2,1037)JJ,DCX45(JJ),JJ,DCZ45(JJ)
C       DO 300 JJ = 1,3
C 300 WRITE(2,1038)JJ,DCX60(JJ),JJ,DCZ60(JJ)
C       WRITE(2,1039)
C       DO 310 I = 1,3
C 310 WRITE(2,1046)I,C0(I),I,DC0(I)
C       DO 320 I = 1,3
C 320 WRITE(2,1047)I,C45(I),I,DC45(I)
C       DO 330 I = 1,3
C 330 WRITE(2,1048)I,C60(I),I,DC60(I)
      CLOSE(2)
      END
C
C
      SUBROUTINE LSQ (N0,N45,N60,CF00,CF45,CF60,CFX,CFZ,A,B,D,DENOM)
      IMPLICIT DOUBLE PRECISION (A-H,O-Z)
      DIMENSION CF00(3),CF45(3),CF60(3)
```

```
      PI = 4.*ATAN(1.)
      COS45 = COS(PI*.25)
      COS60 = COS(PI/3.)
      SIN60 = SIN(PI/3.)
      A = N0 + N45*.5 + N60*.25
      B = N45*.5 + N60*SQRT(3.)*.25
      D = N45*.5 + N60*.75
      E = 0.
      F = 0.
      DO 2000 I = 1,N0
 2000 E = E + CF00(I)
      DO 2010 I = 1,N45
      E = E + CF45(I)*COS45
 2010 F = F + CF45(I)*COS45
      DO 2020 I = 1,N60
      E = E + CF60(I)*COS60
 2020 F = F + CF60(I)*SIN60
      DENOM = A*D - B*B
      CFX = (D*E - B*F)/DENOM
      CFZ = (A*F - B*E)/DENOM
      RETURN
      END
C
```